

Optimization of Small Unmanned Ground Vehicle Design using Reconfigurability, Mobility, and Complexity

Hannah Lyness

CMU-RI-TR-23-24

*Submitted in partial fulfillment
of the requirements for the degree of
Doctor of Philosophy in Robotics*

The Robotics Institute
Carnegie Mellon University
Pittsburgh, PA 15213

Thesis Committee:

Dr. Dimitrios Apostolopoulos (Chair), Carnegie Mellon University
Dr. John Dolan, Carnegie Mellon University
Dr. Aaron Johnson, Carnegie Mellon University
Dr. Corina Sandu, Virginia Polytechnic Institute and State University

Abstract

Unmanned ground vehicles are being deployed in increasingly diverse and complex environments. With modern developments in sensing and planning, the field of ground vehicle mobility presents rich possibilities for mechanical innovations that may be especially relevant for unmanned systems. In particular, reconfigurability may enable vehicles to traverse a wider set of terrains with greater efficiency by allowing them the benefits of multiple configurations. However, reconfigurability is not without its costs including increased size, weight, cost, and complexity. In this work, we present a method for evaluating the positive and negative impacts of reconfigurability to enable the optimization of unmanned vehicle design. We start with the formation of definitions and metrics for reconfigurability, mobility, and complexity, drawing from a wide range of robotic applications. Next, we analyze the combination and optimization of these functions to find ideal physical parameters for a given objective. After that, we delve into the application side of this topic with a case study in reconfigurable vehicles and the design of a novel manually reconfigurable tracked vehicle. Finally, we evaluate this vehicle and validate the optimization method experimentally and through mission scenarios.

Acknowledgments

I would like to express my appreciation for my advisor, Prof. Dimi Apostolopoulos, for all the help over the past few years carving this path. I hope you realize how many students you have inspired through your teaching. Your passion is contagious.

Thank you to my Thesis Committee, Prof Corina Sandu, Prof John Dolan, and Prof Aaron Johnson. I appreciate the different perspectives that each of you brought to the table and the encouragement you gave me over the years.

I am also thankful for Prof. David Wettergreen, Prof. Howie Choset, and Dr. Eugene Fang for their guidance as my research committee.

I am extremely grateful for CMU Robotics Club's shop, storage space, and community. I conducted most of the assembly of the modular vehicle here using essentially every machine in the shop. The officers were also kind enough to let me find nooks and crannies to store many aspects of my research.

I would also like to thank Rich Pantaleo, Matt Glisson, and Wil Hamilton from NREC for the design advice. I appreciate how approachable you three were and your design experience was very valuable.

I also owe Nishant Pol many thanks for answering all of my electronics questions and providing advice for devices and strategies.

On the logistics side, I would like to offer my gratitude to Graham Papciak and Ryan Danko for allowing me to use the water jet so often. Additionally, Tim Angert's advice and encouragement in the FRC shop was greatly appreciated.

I would like to express my thanks to the many other researchers that kindly gave me their time throughout my process. Paul Malchodi kindly granted me interviews so I could get a better sense for the industry of small tracked robots. Every member of the ISTVS community has been extremely welcoming and valuable for my understanding of the field.

I'd like to also recognize Dr. Myunghee Kim and all of Dr. Steve Collins' Experimental Biomechatronics Lab for my first experience with academic research and showing me what it takes to earn a doctorate.

Finally, I'd like to thank my coworkers, teammates, friends, and family for their support through this marathon.

Contents

Abstract	i
Acknowledgments	ii
Table of Contents	iii
List of Figures	v
List of Figures	viii
List of Symbols	ix
Outline	xi
1 Introduction	1
2 Defining and Quantifying Reconfigurability for Unmanned Ground Vehicles	8
3 Distilling and Modeling Mobility for Unmanned Ground Vehicles	25
4 Combining Varied Markers of Complexity for Unmanned Ground Vehicles	46
5 Optimizing Reconfigurability, Mobility, and Complexity	54
6 Reconfigurable Vehicle Design	62
7 Reconfigurable Vehicle Testing and Validation	76
8 Conclusion	92
A Test Vehicle Design and Iteration	95
B Additional Mobility Information	105
C Terminology Listing	108

Bibliography **a**

List of Figures

1.1	Three examples of unmanned ground vehicles with varying configurations from the DARPA Sub-T Challenge.	1
1.2	Seoul National University’s BioRobotics Lab’s Magic Ball Origami Wheel Robot navigating under an obstacle.	3
1.3	Mars rover Spirit immobilized in martian soil [11].	4
1.4	Overall flow of the primary thesis contribution.	7
2.1	Robotics papers with the term ‘reconfigurable’ sorted by application.	10
2.2	Usage of the term ‘reconfigurable’ divided by if the source made a distinction between ‘reconfigurable’ and ‘self-reconfigurable’, if the source used the term to refer to a manual process, or if the source used the term to refer to an automated process.	11
2.3	Number of papers with each definition of ‘reconfigurability’ sorted by publication date.	12
2.4	Percentage of papers per year with each definition of ‘reconfigurability’.	13
2.5	Illustration of scaling individual elements of reconfigurability cost.	17
3.1	Illustration of multi-dimension velocity and acceleration characteristics with the SAE-defined axes system.	25
3.2	Idealized rigid wheel and terrain parameters.	26
3.3	Examples of scenarios where vehicle movement is limited (engine power, friction, and soil strength).	26
3.4	Examples of materials with different angles of friction (left: dry loam, right: sand).	29
3.5	Side view of a vehicle moving up a slope against resistances due to aerodynamics, gravity, rolling resistance and drawbar pull.	30
3.6	Information flow diagram for vehicle optimization based on terrain.	37
3.7	Left: Aerial View of Keweenaw Testing site obtained using Google Maps [157]. Right: Aerial View soil distribution at test site generated in MATLAB from .tif file in the NG-NRMM dataset [156]. Soil abbreviations refer to USCS classifications which are detailed in the ASME International’s USCS standard [158].	38

3.8 Left: Image of Keweenaw Research Center where black pixels are those with drawbar pull over 0 and white pixels are those with drawbar pull 0 or less. Right: Keweenaw Research Center with untraversable areas (white) filled. . . . 39

3.9 Left: Drawbar pull depicted by intensity of pixels with inaccessible regions removed with the shortest path through traversible terrain shown in red. . . . 39

3.10 Mesh view of Meteor Crater with shortest paths plotted for candidate vehicles with 20, 30, and 40deg slope climbing capacity. The map is downsampled to 1/300th of original density for ease of visualization. . . . 41

5.1 Plot of proposed mobility metric versus proposed reconfigurability and complexity metrics. . . . 56

5.2 Ideal variables found with NSGA-II (gray lines) and Mixed Variable GA (green lines). The optimal NSGA-II solution given the weighting of [0.2, 0.6, 0.2] is in red and the Mixed Variable GA solution is in blue. . . . 58

5.3 Parallel coordinate plots for the same set of variables with different weights. From left to right, the weights are: [0.2, 0.6, 0.2], [0.2, 0.2, 0.6], and [0.6, 0.2, 0.2]. . . . 59

5.4 RMCVO user Interface. . . . 60

5.5 Optimal variables for [0.2, 0.2, 0.6] weighting with classic GA and 1000 iterations. . . . 61

6.1 The 510 PackBot. Image credit: [120]. . . . 63

6.2 Kegresse’s motor-sledge design from his 1914 patent. . . . 65

6.3 Two reconfigurable wheel-track designs. . . . 66

6.4 Kaist’s DRC-HUBO (left) and Tartan Rescue’s CHIMP (right) [263, 264]. Kaist won first place in the DRC Finals using a hybrid of walking and rolling on its knees. CHIMP earned third place through a combination of walking and rolling on four tracks located on its feet and elbows. . . . 67

6.5 The University of Utah’s Hex-A-Ball (left) and Kåre Halvorsen’s MorpHex (right) [267, 268]. . . . 68

6.6 Seventh and final version of the modular tracked vehicle. . . . 70

6.7 Example of attachment via machine screws from the exterior of the vehicle. . . 70

6.8 Electrical diagram for the system. The motor controller provided power distribution for both the motors and encoders, as well as a means of measuring current draw. . . . 71

6.9 A comparison of the middle (300 mm) and longest (400 mm) track contact length conditions. . . . 72

6.10 A comparison of the two available track widths (2 in and 3 in). . . . 72

6.11 Comparison of the smallest (4.75") and largest (7") sprocket conditions. The small sprocket has a longer sprocket mount to allow it to be the same height as the large sprocket. . . . 73

6.12 comparison of the 1.27 cm slack, 0 kg, and 2.3 kg track tension conditions. For each condition, the block that supports the top roller is moved to deform the spring based on the prescribed track tension. . . . 73

7.1 Soil preparation process. . . . 77

7.2 Plot of sinkage versus track width. . . . 79

7.3	Plot of sinkage versus track tension.	79
7.4	Plot of sinkage versus ground sprocket diameter.	80
7.5	Plot of sinkage versus track contact length.	80
7.6	Aerial view of test sites showing drawbar pull where lighter colors are higher drawbar pull.	84
7.7	Parallel coordinate plots for the same set of variables with different weights. From left to right, the weights are: [0.2, 0.6, 0.2], [0.2, 0.2, 0.6], and [0.6, 0.2, 0.2].	86
A.1	Version 1 of the modular tracked vehicle design.	95
A.2	Version 4 of the modular tracked vehicle design.	96
A.3	Version 5 of the modular tracked vehicle design.	96
A.4	Side view of track tensioning system.	97
A.5	Water jet and manually milled components.	97
A.6	Top view of the completed vehicle.	98
A.7	Side view of the completed vehicle.	98
A.8	Close-up view of old tension system (left) with bolts and nuts and new tension system (right) with shafts and shaft collars.	99
A.9	Illustration of the change in vertical distance as a result of the addition of one track link (0.5 in on each diagonal leg)	99
A.10	Plot of left and right motor current draw over the course of one traverse of an obstacle course. The blue line shows an expected variation in current as the vehicle drives over different obstacles. The orange line shows the current for the motor that becomes completely unlinked from the track throughout the trial.	100
A.11	Left and right motor alignment for 10 trials at 10 lbs.	100
A.12	Plot of 10 trials with the 10 lb track tension condition. There is no clear trend from trail 1 to trial 10, which indicates that the driveline is not loosening up over the course of the trials.	101
A.13	Side view of fifth wheel assembly CAD with key components labeled.	101
A.14	Example designs for self-contained reconfigurable track links based on the hobby links used for this vehicle.	103
A.15	Left: Separately Actuated Arms Design, Center: Lead Screw Linkage Design, Right: Expanding Track Design.	104
B.1	Wong's illustration of a simplified Ackermann-steered car. Image credit: [132].	105

List of Tables

2.1	Ground vehicle reconfigurability parameters.	18
2.2	Sample reconfigurability constant values.	19
2.3	Comparison of reconfigurability with the proposed and other definitions.	23
3.1	Prior terramechanics research in small and tracked vehicles.	27
3.2	Diversity of normal pressure equations.	28
3.3	Sample mobility constant values.	41
3.4	Comparison of reconfigurability with the proposed and other definitions.	44
4.1	Sample complexity constant values.	49
4.2	Comparison of complexity metric with the proposed and other definitions.	52
5.1	Comparison of various platforms based on the proposed metrics of reconfigurability, complexity, and mobility.	55
5.2	Table of Aggregated Reconfigurability, Mobility, and Complexity Value.	57
5.3	Selection of optimal vehicle based on outer gains.	59
5.4	Overall reconfigurability cost based on gains.	60
6.1	Reconfigurable Ground Mobility Systems Summary.	69
6.2	Comparison of different connection types for manual reconfigurability rated from 1 to 10 with 1 being poor and 10 being excellent.	74
7.1	Maximum slope results for 36 test conditions.	82
7.2	Mobility metric for reconfigurable vehicle configurations.	83
7.3	Mobility Metric Values.	85
7.4	Metric comparison for reconfigurable vehicle configurations.	86
7.5	Sample mission performance.	89
7.6	Scaled sample mission performance.	90
B.1	Mobility index elements.	107

List of Symbols

Symbol	Description	Units	Page
A	Surface Area in Contact with Ground	Area [m ² , ft ²]	27
A_{cov}	Coverage Area	Area [m ² , ft ²]	37
b	Average Unloaded Tire/Track Width	Length [m, in]	34
b_s	Track Shoe Width	Length [m, in]	107
BF	Bogie Factor	Unitless	107
c	Soil Cohesion Coefficient	Pressure [kPa, psi]	29
C	Proposed Complexity Metric	Decimal	48
c_a	Coverage Area Weighting	Constant [unitless]	37
c_{act}	Actuator Count Weighting	Constant [unitless]	48
c_{BF}	Bogie Factor Coefficient	Constant [unitless]	107
c_C	Overall Complexity Weighting	Constant [unitless]	56
c_{DOF}	Degrees of Freedom Weighting	Constant [unitless]	48
c_{DP}	Drawbar Pull Weighting	Constant [unitless]	37
c_e	Equipment Weighting	Constant [unitless]	18
c_{lp}	Path Length Weighting	Constant [unitless]	37
c_m	Monetary Weighting	Constant [unitless]	18
c_M	Overall Mobility Weighting	Constant [unitless]	56
c_{nl}	Number of Linkages Weighting	Constant [unitless]	48
c_R	Overall Rec. Cost Weighting	Constant [unitless]	56
c_t	Transition Time Weighting	Constant [unitless]	18
CPF	Contact Pressure Factor	Unitless	35
d	Average Unloaded Wheel Diameter	Length [m, in]	34
DCF	Deflection Correction Factor	Unitless	35
DP	Drawbar Pull	Force [N, lb _f]	30
DP_{avg}	Terrain Average Drawbar Pull	Force [N, lb _f]	37
E_{rec}	Total Equipment Contribution	Mass [kg, lb]	18
EF	Engine Factor	Unitless	35
GF	Grouser Factor	Unitless	35
H	Thrust	Force [N, lb _f]	30

Symbol	Description	Units	Page
h_s	Average Tire Section Height	Length [m, in]	35
i	Slip Coefficient	Percentage	31
L_p	Terrain Average Path Length Increase	Decimal	37
l_s	Track Shoe Length	Length [m, in]	34
l_t	Track Length	Length [m, in]	34
M	Proposed Mobility Metric	Decimal	37
M_{rec}	Total Monetary Cost Contribution	Currency [USD or other]	18
MI	Mobility Index	Unitless	35
MMP	Mean Maximum Pressure	Pressure [kPa, psi]	34
n_a	Number of Axles	Count [unitless]	35
n_{act}	Number of Actuators	Count [unitless]	48
n_{bh}	Number of Bogies on Ground	Count [unitless]	34
$n_{DOF,i}$	Number of Degrees of Freedom	Count [unitless]	48
n_{nl}	Number of Linkages	Count [unitless]	48
n_{rec}	Number of Reconfigurabilities	Count [unitless]	18
n_{wa}	Number of Wheels per Axle	Count [unitless]	34
n_{wg}	Number of Wheels on Ground	Count [unitless]	35
n_w	Number of Wheels (Total)	Count [unitless]	34
p	Track Pitch	Length [m, in]	34
P	Engine Power	Power [kW, hp]	107
PC	Pull Coefficient	Ratio [unitless]	31
RC	Proposed Reconfigurability Cost Metric	Decimal	18
T_{rec}	Total Transition Time Contribution	Time [s]	18
TF	Transmission Factor	Unitless	35
TRF	Track Factor	Unitless	107
VCI_x	Vehicle Cone Index (x Passes)	Stress [Pa, psi]	35
W	Total Vehicle Weight	Force [N, lb _f]	27
WF	Weight Factor	Unitless	35
WLF	Wheel Load Factor	Unitless	35
δ	Average Tread Deflection Track Pitch	Length [m, in]	34
ϕ	Soil Friction Angle	Angle [rad]	29
σ	Normal Stress	Stress [Pa, psi]	29
τ	Shear Stress	Stress [Pa, psi]	29
R	Resistance	Force [N, lb _f]	30
TEF	Traction Element Factor	Unitless	35

Outline

Chapter 1 sets the stage for this document by presenting introductory material. Basic definitions and conventions are presented in this section, as well as significance and thesis statement.

The core chapters are divided into two sections: a more theoretical exploration of metrics and optimization, and an application-focused section documenting the creation of a manually reconfigurable ground vehicle.

The former section consists of four chapters that explain the fundamental principles related in this work and all follow a similar pattern. An introduction orients the chapter, prior work in the area is explained, and then the proposed method of quantifying that concept is demonstrated. Concepts relating to reconfigurability are presented in Chapter 2. Mobility metrics are explained in Chapter 3. And finally, techniques for classifying complexity are described in Chapter 4. Different methods for combining and optimizing these metrics are explained in Chapter 5.

The later section covers reconfigurable vehicle design including current state of the art, design of a new system, and evaluation of this system. Prior mechanisms for reconfigurable ground mobility systems are explained in Chapter 6 including past and current alternative mobility systems like reconfigurable wheels, morphing wheel-tracks, and combined walking-rolling robots. This chapter also summarizes these different forms of reconfigurability and relate them to the previously described metrics. Finally, this chapter outlines the design and fabrication of a modular test vehicle designed for terramechanics testing. Chapter 7 presents the methods, results, and conclusions of examining modularity on this small tracked vehicle and validates the proposed optimization method through full mission simulations.

The Conclusion (Chapter 8) presents takeaways from this research as a whole and opportunities for further exploration.

Chapter 1

Introduction

1.1 Motivation

The domains of robotics are constantly expanding. No longer constrained to the lab or factory, robots are being developed for increasingly diverse environments. Ground robots are commissioned to work in fields, mines, pipes, and other planets. With these environments come more challenges including reliable perception, rugged mobility, and reliable control. These robots must be able to operate in dynamic, dangerous, or unknown terrain in a predictable and repeatable manner.

In terms of mobility, no single platform is optimally suited for all types of soil and topography. Even for one specific application or environment, different mechanisms and configurations are employed. For example, in the Defense Advance Research Project Agency (DARPA) Subterranean (SubT) Challenge involving mapping, navigation, and searching, different teams used different combinations of legs, wheels, and tracks in varying numbers and sizes to all accomplish the same mission [1]. The tracked vehicles were able to spread their weight out over a larger surface area but suffered from larger internal resistance. The articulated wheeled vehicles were able to traverse obstacles but have added complexity in these additional mechanisms. And finally, the legged robot was able to traverse the largest obstacles but struggled to gain traction on the slick, muddy sections.



(a) A six-wheeled vehicle with articulated chassis designed by the Robotika team [2].



(b) A BIA5 OzBot Titan [3] tracked robot used by Team CSIRO [4].



(c) Team Explorer's custom four-wheeled robot [5].

Figure 1.1: Three examples of unmanned ground vehicles with varying configurations from the DARPA Sub-T Challenge.

Perhaps mechanical reconfigurability would allow a vehicle the benefits of multiple configurations. This is the key proposition at the heart of this work. It is possible that a vehicle could

be more effective and efficient in diverse environments when granted the ability to transform between different forms. Reconfigurability could enable a robot to access a wider variety of terrain or move more quickly throughout a landscape.

However, as with any additional feature, the incorporation of reconfigurability has some consequences. For example, AZIMUT robot is a four-tracked vehicle capable of reconfiguring to accommodate wheel- and leg-like locomotion [6]. A typical vehicle with four tracks would likely need four motors for actuation. However, because this vehicle has more modes of movement, it has 12 motors. In addition to motors, the vehicle needs 8 additional motor controllers and larger batteries to enable the same run time. Besides the cost and weight that these components add, this also adds complexity to the system. The software must be able to measure and manipulate three times as many actuators. And there are three times as many actuator components that can fail. On the other hand, these additional motors may be able to serve as redundant manipulators in the case of damage. And the added capability that this vehicle possesses may enable it to replace two vehicles that could not reconfigure, which could ultimately save weight and cost.

The desire for increased automation in manufacturing, the DARPA challenges, planetary navigation, and the pursuit of safe self-driving vehicles have all accelerated the course of ground vehicle control. Over the last 70 years, the state of the art has shifted from careful "tortoises" integrating light and touch sensors, to full-speed autonomous cars amassing millions of miles of travel. For unmanned vehicles, intricacy can affect cost, weight, volume, ease of assembly, controllability, and repairability. In certain scenarios this complexity may outweigh the additional reachable terrain or faster travel speeds. The crux of this work is to quantify these benefits and costs to determine ideal vehicle parameters. Our thesis question is then: **when is it worthwhile to integrate reconfigurability into a ground vehicle's mobility system?**

1.2 Background

For this work, we use mobility as the primary lens for performance. For this reason, we focus on the reconfigurability of mobility systems as opposed to perception systems or control schemes. With mobility as the parameter we want to maximize, use reconfigurability cost and complexity as values that we want to minimize. Reconfigurability cost includes the downsides that are specific to reconfigurability and would not otherwise be present if the vehicle did not reconfigure. Complexity is especially relevant for unmanned systems as they must be able to operate independently often for prolonged periods of time. So our three core components of our optimization system are reconfigurability cost, mobility, and complexity, which are addressed in more detail in Chapters 2, 3, 4, respectively. A brief outline of these concepts and fundamental principles is provided here. 6 details the study of reconfigurability in robotics including historic and current examples of reconfigurable systems.

1.2.1 Reconfigurability

Reconfigurability can be found everywhere from computer programming to manufacturing. At the most basic level, reconfigurability describes a system's ability to change between different configurations. In every field, one can imagine different goals that would be better satisfied by different systems.

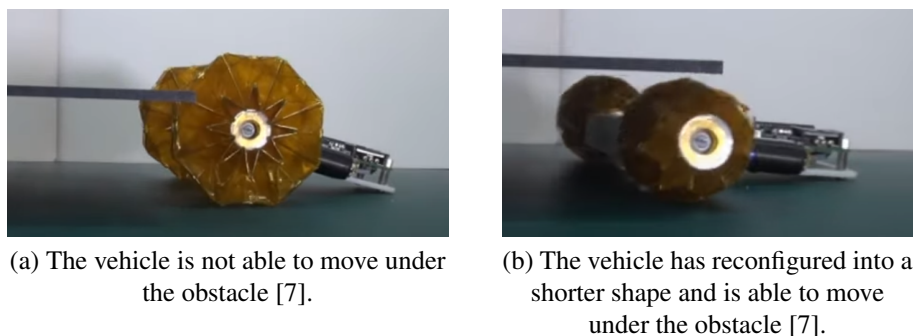


Figure 1.2: Seoul National University's BioRobotics Lab's Magic Ball Origami Wheel Robot navigating under an obstacle.

For example, a rover with large-diameter wheels could overcome gaps and traverse ground quickly. But a rover with small wheels could fit under certain obstacles and would require less torque to rotate. A vehicle equipped with variable wheel diameters, like that pictured in Figure 1.2, would allow the benefits of both to be realized.

Flexibility for multiple conditions is often baked into ground vehicle design. Increasingly, modularity and reconfigurability are also added with the expansion of automation. Unmanned vehicles are not beholden to interfaces and orientations that have become customary for human drivers.

The benefits of reconfigurability are evident both in the ability to complete diverse tasks and in optimizing different parameters at different times. However, quantifying reconfigurability and using it as a design parameter is not straightforward. In each scenario, reconfigurability looks different, and inherently adds complexity to the system. An intuitive quantification and connection to complexity and design objectives would benefit both the analysis and design of robotic vehicles. Chapter 2 presents a summary of current academic trends in reconfigurability, as well as a novel metric for vehicle optimization.

1.2.2 Mobility

In many off-road scenarios, the limiting factors on performance are not engine power, weight distribution, or friction, but the strength of the material that the vehicle moves over. Though the vehicle may be able to move its wheels (or tracks, or legs), the ground beneath it fails so the vehicle is unable to progress over it. Terramechanics, a field that came into existence less than 70 years ago, is the study of the relationship between implements or vehicles and the ground they interact with [8]. Since its inception, vehicle design, performance evaluation, virtual training development, and path planning have relied on these principles.

In the field, regions of lower soil strength are then untraversable by a vehicle. This limits the vehicle's use and adds uncertainty to a mission. According to the US Army Research and Development Center, "soft-soil immobilizations are among the most difficult to predict, yet militarily, could be the most disastrous" [9]. NASA's Mars rover Spirit also demonstrated the dangers of off-road navigation. Though it operated for more than 20 times as long as it was planned to, Spirit's wheels were immobilized several times during its operation. In May of 2009, Spirit became immobilized for a final time and remained there until communications ended with it eight months later and the rover was eventually retired [10].

Off-road mobility prediction is challenging because of the breadth of parameters and interconnectivity between physical phenomena. Analytical models are not able to succinctly combine all these effects into a usable quantity. Soil parameters are often unknown and imply homogeneity throughout the landscape, which is seldomly the case. This is a major assumption and shortcoming of finite element analysis (FEA) or discrete element models (DEM), in addition to the large computational power needed [12]. Furthermore, semi-empirical and parametric equations for characteristics like drawbar pull have mostly been developed on an as-needed basis for only a subset of vehicles. Originally these were wheeled and then tracked several-ton military vehicles. Only recently has attention been paid to smaller ground vehicles [13].

Estimating a vehicle's performance with respect to all criteria of terramechanics requires a combination of analytical and empirical calculation, or element-wise modeling. Each year, improvements are made to these equations and simulation models. This work outlines a single, common metric for describing vehicle mobility that can be adjusted based on environment. Though incapable of describing the entire workspace of terramechanics and limited by the underlying assumptions of its deriving equations, this value succinctly estimates the abilities of a vehicle.

1.2.3 Complexity

Complexity science abounds in fields from business to computer science. In complexity theory, a complex system can be broadly described as "any system featuring a large number of interacting components (agents, processes, etc.) whose aggregate activity is nonlinear (not derivable from the summations of the activity of individual components) and typically exhibits hierarchical self-organization" [14]. By this definition, a single physical robot is not a complex system, it can be fully divided into subsystems and components, it does not exhibit self-organization, and there is generally one planning system or coordinated plan, in the case of a decentralized planner. Instead, we adopt Dr. Simon's informal definition as "one made up of a large number of parts that have many interactions" [15]. Regardless, metrics of complex systems including number of elements, connectivity of elements, and hierarchy of subsystems are all relevant to physical systems. In addition, collections of large numbers of autonomous vehicles may interact in accordance with principles of complexity theory [16].

Complexity has always been an important metric for robotics, especially with the increasingly diverse missions that robots are tasked with. In some scenarios, it might be necessary to have separate platforms depending on the terrain. In other cases, one platform may be successful in both environments. Many applications may benefit from one device that is able to transform between modes. But with this added performance variability comes additional actuators, linkages, and controller complexity.

Intricacy is also a major inhibitor of adoption [17]. History has shown that increasing ca-



Figure 1.3: Mars rover Spirit immobilized in martian soil [11].

pabilities or flexibility does not always lead to market success. Every field has tools for quantifying the complexity of a system, problem, process, or product. This work, documented in Chapter 4, primarily focuses on the complexity of the product without regard to the difficulty in design or manufacturing. Complexity is also examined both by the number of mechanisms and the connections between them, which can each be a source of failure. Especially when dealing with mechanized and even automated systems, compound mechanisms can be especially risky, both from a structural and control perspective. In order to tailor this work to a variety of different applications, weights are given to each section of this proposed complexity metric to put value to these different perspectives.

1.2.4 Optimization

Optimization algorithms can drive efficient vehicle design. Beginning as early as 1960, Schmit and collaborators demonstrated systematic synthesis for vehicle design [18] which paved the way for multidisciplinary design optimization (MDO), which is still in use today. In 1995, Eltze and Pfeiffer determined optimal leg dimensions for a six-legged robot using inverse kinematics and an SQP [19]. Genetic algorithms have been implemented to steer modular linked robots [20] and terramechanics have been used as a basis for rapidly evaluating candidate configurations [21]. Recently, multibody physics simulation engines have been used to derive ideal vehicle parameters [22, 20].

1.3 Application Scope

In this dissertation, we focus on the mobility systems of tracked small unmanned ground vehicles (SUGVs). The majority of these efforts are applicable to both remote and autonomous systems.

For this work, "small" is considered between 5 and 60 kg. This size scale includes compact throwable surveillance vehicles like Roboteam's IRIS [23] up to medium-sized unmanned vehicles like Qinetiq's TALON [24]. This class of vehicles was selected because of the relevance to autonomous vehicles, applicability to terramechanics, and understudied nature in the field. Though mechanisms present on vehicles of other scales are mentioned in Chapter 6, the relationships developed are not validated for microrobots, ultralight robots, and larger unmanned vehicles.

Tracked vehicles were targeted as opposed to wheeled vehicles as they are largely less studied, especially in this weight class (shown in Table 3.1). As wheeled vehicles are far more ubiquitous, it makes sense that the majority of terramechanics work has been in this field. Yet tracked vehicles are clearly relevant for robotics including pipe inspection, surveillance, and search and rescue. Though reconfigurability can exist in many aspects of a robot, this thesis will only focus on reconfigurability of the system that allows a robot to move over terrain.

There are substantial use cases for planetary, military, and commercial ground vehicles that benefit from minimizing vehicle size and/or weight. Planetary rover designs, for example, have shrunk from multi-hundred kilogram vehicles [25] to sub-5-kilogram designs [26], reflecting engineering improvements as well as the challenge of moving weight through space.

1.4 Thesis Statement

Mobility, complexity, and reconfigurability can be quantified and optimized to improve the design of small unmanned ground vehicles.

1.5 Research Approach

Now that unmanned vehicles are becoming more and more informed about their environment, mechanical automation presents the opportunity for increased performance and flexibility. In this work, we seek to enable vehicle designers to evaluate candidate reconfigurable vehicles based on both complexity and mobility.

We split our efforts into two main thrusts:

1. A theoretical exploration of current and improved methods for evaluating reconfigurability, mobility, and complexity in unmanned ground vehicles.
2. An application-focused examination of reconfigurable vehicle design and testing.

In order to tackle the first element, we take a look at current usage of these three concepts in robotics literature. From there, we develop our working definitions to eliminate ambiguity and construct quantifiable metrics leveraging this broad background. The main principles at the basis of our metrics are:

- **Mission Specificity:** We wanted a way to capture the limitations of a given environment or project within the metrics. We do this in two ways. First, each vehicle parameter is limited by the user in the form of minimum and maximum values. Second, the mobility metric takes in terrain data about the environment of interest. In this way, the mobility metric is relevant to the mission environment. This also enables measures of performance including coverage, average drawbar pull, and path length, which reflect common robotics tasks including mapping, collection, and recovery.
- **Adjustable Prioritization:** Tuning is incorporated into our system in two places: within the metrics themselves, and in their combination. This allows the user to assign importance to elements that are more important to them and devalue less vital aspects.
- **Meaningful Numerical Comparison:** This work involves the integration of diverse variables and performance estimations. In order to ensure lateral comparisons, we scale all elements and subelements of the metric between 0 and 1. Unlike units are neither combined nor weighed against each other. This makes the overall value more readable and comparable.

After formulation, we use these metrics to evaluate a wide range of existing reconfigurable systems. Then we identify differences between these evaluations and those garnered from existing metrics to point out the added detail that can be expressed through our metrics. The outputs of this initial thrust of effort are: formalized definitions, metrics, and an optimization framework for integrating reconfigurability, mobility, and complexity into ground vehicle design.

On the application side, we first survey the state of the art in reconfigurable ground vehicle mechanisms. We then design and create a novel manually reconfigurable tracked vehicle. This vehicle has four degrees of variability that can be changed: track width, track contact length,

sprocket diameter, and track tension and is tested on sinkage and slope climbing ability. We use this robot to verify the proposed metrics and verify the analytical and empirical calculations of mobility through physical testing. This testbed also provides an ideal example to flex the metrics in mission-level use cases. Three scenarios are constructed and vehicle performance is examined in these full use cases to validate the optimization framework.

1.6 Contributions

1. Primary: A quantifiable system for comparing the mobility benefits of reconfigurability along with the various costs for small, tracked unmanned ground vehicles that enables design optimization (Chapter 5). A graphic of this contribution, dubbed "Reconfigurability, Mobility, and Complexity Vehicle Optimization (RMCVO)", is provided in Figure 1.4.
2. Formalized definitions and novel quantitative metrics for reconfigurability (Chapter 2), mobility (Chapter 3), and complexity (Chapter 4).
3. Design and implementation of an unmanned, manually reconfigurable tracked vehicle for terramechanics testing and best practices for implementing reconfigurability in small, tracked unmanned ground vehicles (Chapter 6).
4. Comparison of mobility performance with different characteristics using the custom manually reconfigurable tracked vehicle (Chapter 7).

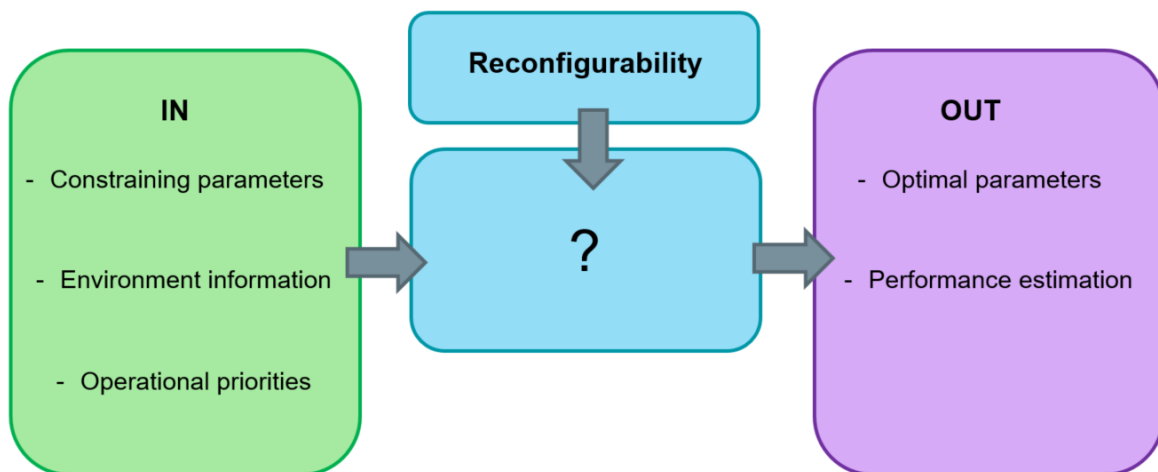


Figure 1.4: Overall flow of the primary thesis contribution.

Chapter 2

Defining and Quantifying Reconfigurability for Unmanned Ground Vehicles

2.1 Introduction

Reconfigurability is desirable in fields from management to engineering. It can offer a system increased skills, evolvability, and survivability [27]. A reconfigurable system can achieve more tasks than its static counterparts, though often at the expense of complexity. As a mission changes, reconfigurability also allows a system to respond to these changes and can keep a system relevant for longer. Finally, reconfigurability offers better chances of graceful degradation. If a device is able to reconfigure to a simpler state when in peril, it could still maintain some useful functionality even in the face of unexpected dangers.

As computing speed, power distribution, sensors, and actuators improve, robots are becoming a more viable choice for a wider variety of applications. Flexibility is especially valuable to operate in these various conditions. A history of reconfigurability in robotics through 2010 can be found in [28], and summary of technologies divided by type can be found in [29], [30], [31], and [28]. Additionally, the ASME/IFTOMM International Conference on Reconfigurable Mechanisms and Robots (ReMar) is held every three years, or so and conference proceedings from 2012 and 2015 are available in *Advances in Reconfigurable Mechanisms and Robots I* [32] and *Advances in Reconfigurable Mechanisms and Robots II* [30], respectively. Major areas of application are presented here as a reference for the space.

Modular and reconfigurable robots are considered highly viable for space applications, where most specialized assembly and manufacturing is not possible after deployment and projects are in service for decades. Flexible robots have been proposed for tasks including satellite inspection, planetary locomotion, and even planetary manufacturing as they offer advantages in terms of compactness, robustness, and adaptability [33], [34], [35].

The end effector of the Mars 2020 Rover is one application where minimizing weight and

Portions of this chapter were submitted in a manuscript to the ASME Journal of Mechanisms and Robotics in 2023.

volume is paramount. In 2014, Honeybee Robotics presented their innovations for sampling and collecting martian rock and regolith. One of their tools consists of a hollow drill bit. This bit serves to not only burrow into the material, but it can also capture the material inside its void. This second purpose is achieved by rotating an inner tube with a slightly different bore from the outer tube. The sample shears at the bottom of the drill bit and is captured by the system as the rotating inner tube causes it to rest on a flange at the bottom of the outer tube [36].

In manufacturing, flexible systems allow factories to retain capital equipment even when production changes [37]. Using the same facilities and equipment saves time and money throughout product evolution. Reconfigurable systems have been developed for MEMS assembly [38], [39] up to large systems for aerospace [40].

For these reasons, reconfigurability is a common theme in robotics. Yet the term ‘reconfigurability’ seems to have many different interpretations, from a system with elements that can be manually repositioned to a swarm of self-organizing robots that can change form on their own. This chapter works to create formalized definitions pertaining to reconfigurability so that a mechanism’s abilities can be quantified and compared.

2.2 Background

Fukuda and Nakagawa are widely regarded as the inventors of the class of robots consisting of many similar units that can connect and disconnect from each other on their own. In their first paper on the subject, they defined “a cell system of living creatures to a robot system with some intelligence analogous to the biological gene. Such a system called the dynamically reconfigurable robotic system (DRRS), which can reorganize its shape and structure dynamically by employing limited available resources for a given task and the strategic purpose, has many applicabilities in many fields, such as maintenance robots, more advanced working robots, free-flying service robots in space and more evaluated Flexible Automation, etc” [41]. Over the years, the descriptor ‘dynamically’ was replaced with ‘self’ to describe a robot that could alter its own configuration.

In parallel to this, Schmitz, Khosla, and Kanade were spearheading a different usage of the term for use in manipulation. They borrowed Wurst’s definition of a modular manipulator as “a robotic manipulator assembled from discrete mechanical joints and links into one of many possible manipulator configurations” [42] and “extend[ed] the concept of modularity throughout the entire manipulator system to include not only the mechanical hardware, but also the electrical hardware, control algorithms, and software as well”[43]. They dubbed their system the Reconfigurable Modular Manipulator.

In 1988, Dr. Toshio Fukuda and his team pioneered the area of reconfigurable robotic systems with the Cell Structured Robotic System (CEBOT) [41, 44]. This system consisted of separate self-contained joint elements that could operate independently and be combined into a single system through a centralized planner. Yim and Chirikjian advocated for unit-modular reconfigurable systems, where each reconfigurable element is identical [45], [46]. This offers benefits for ease of design, manufacturing, redundancy [45], and reduced cost [47].

For an unmanned system, redundancy can be especially vital. [48] differentiates static from dynamic redundancy where static redundancy is present at all times, for example combining multiple sensors and dynamic redundancy is only activated as needed, which is the case for reconfigurability. Modular multi-robot systems can demonstrate static redundancy, as well

[49].

Robotic prostheses and exoskeletons are also prime examples of the utility of adjustability in a robotic system. Adjustability is necessary in order to fit different users and is often implemented at the expense of added weight and bulk [50].

Programmatically, reconfigurable systems can be expressed using finite-state machines, Petri nets, and process algebras [51]. Dr. Siddiqi used Non-Homogeneous Markov Chains [27] to show the different states of a reconfigurable system and the transitions between them. Markov chains are used to depict a system with different states and define the probability of moving from one to another. In this case, non-homogeneous simply means that these probabilities change with time.

To explore the space of reconfigurability in robotics, all papers from IEEE Transactions on Robotics (2004-2020), IEEE Transactions on Robotics and Automation (1989-2004), IEEE/ASME Transactions on Mechatronics (1996-2020), and Proceedings of the IEEE International Conference on Robotics and Automation (ICRA) from 1984 to 2022 that contained the word ‘reconfigurable’ were collected. In total, 283 articles were considered after omitting irrelevant articles such as those with only ‘reconfigurable’ in the author description or a completely different usage of the term. A table of these documents is provided in C.

Papers were grouped according to primary application: ground, manipulation, control, manufacturing, marine, assistive, micro, sensing, space, and other. Where available, the actual target platform was considered. For example, a paper about the control scheme for a robot designed for satellite inspection was classified into the ‘space’ category. The ‘control’ and ‘planning’ categories were reserved for papers that were not specific to a certain platform or subfield. Figure 2.1 shows a breakdown of the articles by application.

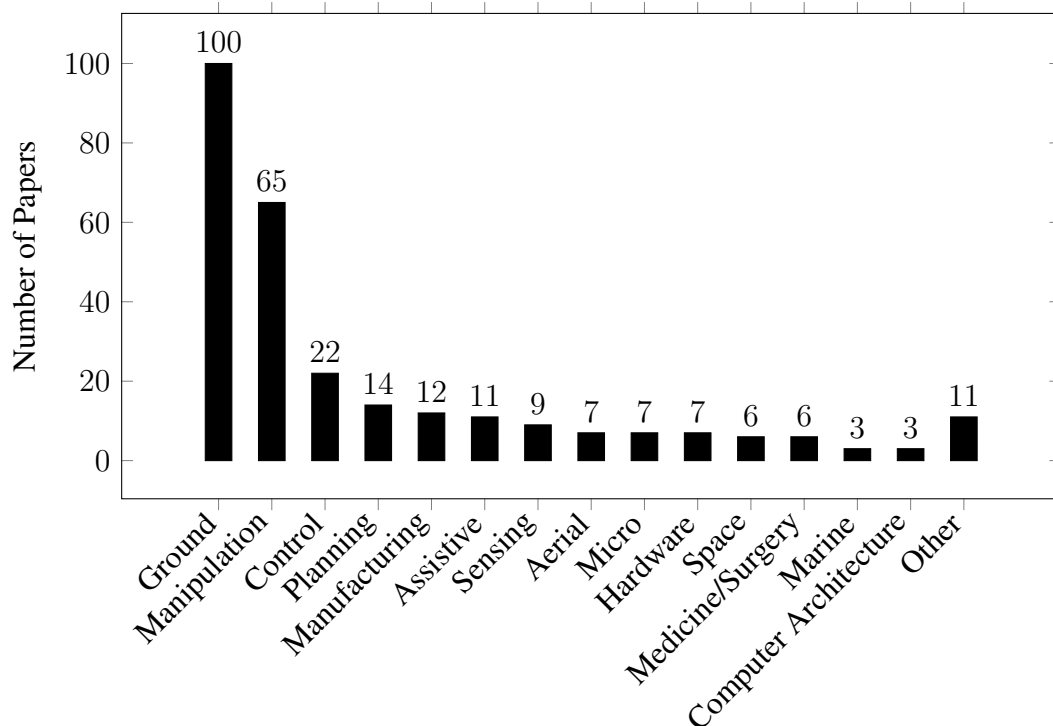


Figure 2.1: Robotics papers with the term ‘reconfigurable’ sorted by application.

From this plot, it is evident that mobile ground vehicles and manipulators were the most

common application for reconfigurability. Yet both of these applications had a wide variety of forms. For example, the ‘ground’ category encompassed wheeled vehicles that could have additional attachments and self-reconfigurable ground platforms that are only able to move by small amounts through inching techniques.

Section 6.2 summarizes key innovations of reconfigurable mobility systems for wheeled, tracked, walking, sliding, and hybrid vehicles.

Murata and Kurokawa provide the clearest delineations with four distinct classes of modular robotics: modular robots with fixed configuration, manually reconfigurable modular robots, self-reconfigurable modular robots and self-replicable modular robots [52].

In order to form working definitions for this work, the same articles described in the previous section are used. Sources were then grouped by their usage of the word ‘reconfigurable’ based on Yim et al.’s division between ‘manual’ and ‘automatic’ reconfiguration [53]. As shown in Figure 2.2, 39% of these articles made a distinction between ‘self-reconfigurable’ and ‘reconfigurable’. Of the half that did not make the distinction, 47% of these used ‘reconfigurable’ to mean automatically reconfigurable by the robot itself, and 53% referred to a robot that needed manual adjustment to reconfigure. (When an article provided examples of reconfigurable robots that were only automatic, it was assumed that that paper maintained the same distinction for reconfigurable as the papers it cited.)

40.9% of all papers also used this term to refer to self-contained independent systems that could join up with other self-contained independent systems like it (like the CEBOTs). In fact, sources like [54] and [55] integrate this into the definition of self-reconfigurable. Though robots fitting this description make up a large fraction of the research in reconfigurable robotics, they exclude vehicles with attributes like a transformable chassis or automatic tire pressure adjustment.

Papers pertaining to manipulation show a great deal of variation in definition, compounded by the fact that ‘configuration’ refers to a manipulator’s pose, as opposed to the attachment of components to one another. Some sources used the word to refer to a system that had interchangeable joint modules that could be taken apart and reassembled by a user manually (fitting the ‘manual’ designation in this study). Others had non-essential automatic reconfigurabilities like variable compliance, in line with the ‘automatic’ category of this comparison.

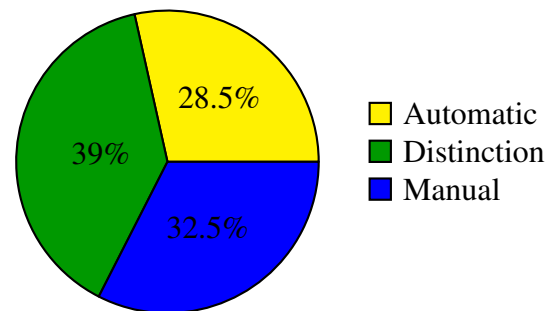


Figure 2.2: Usage of the term ‘reconfigurable’ divided by if the source made a distinction between ‘reconfigurable’ and ‘self-reconfigurable’, if the source used the term to refer to a manual process, or if the source used the term to refer to an automated process.

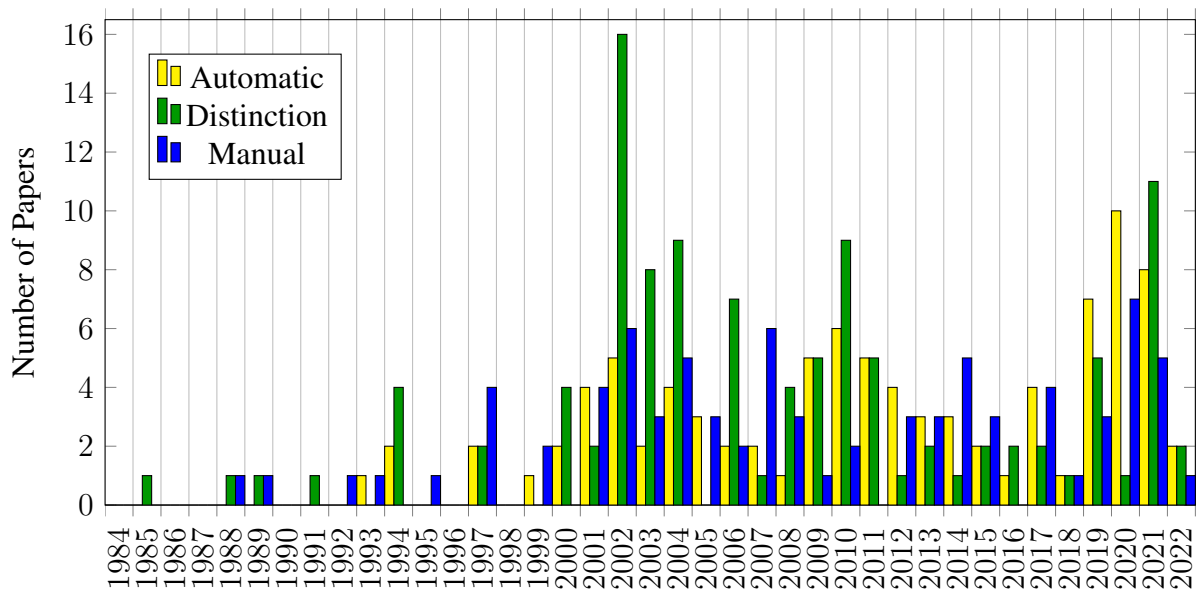


Figure 2.3: Number of papers with each definition of ‘reconfigurability’ sorted by publication date.

The years 1984, 1986, 1987, 1996, and 1998 had no papers with instances of the term ‘reconfigurable’ from the sources that were examined. The year 2002 had the greatest number of papers in a single year that contained this term with 27 total papers, 16 that differentiated between manual and automatic transformation, 6 that implied manual transformation, and 5 that implied automatic transformation.

There were a few key events that likely affected the popularity of this term and approach. Reconfigurability in robotics largely started in 1988 with Schmitz, Khosla and Kanade’s reconfigurable modular manipulation system (RMMS) [43] and Fukuda and Nakagawa’s dynamically reconfigurable robotic system (that would eventually become CEBOTS) [41].

In 1991, the first commercially available reconfigurable computer was created. This technology enabled 6 of the articles explored in this work. In 1998, the U.S. National Research Council put out "Visionary Manufacturing Challenges for 2020". The top priority item was "adaptable and reconfigurable systems" [56]. This likely influenced the 11 papers on reconfigurable manufacturing systems that came in the ten years following this publication.

In order to see the favoring of different understandings of reconfigurability throughout time, the data for each year is plotted as a percentage of that year in Figure 2.4.

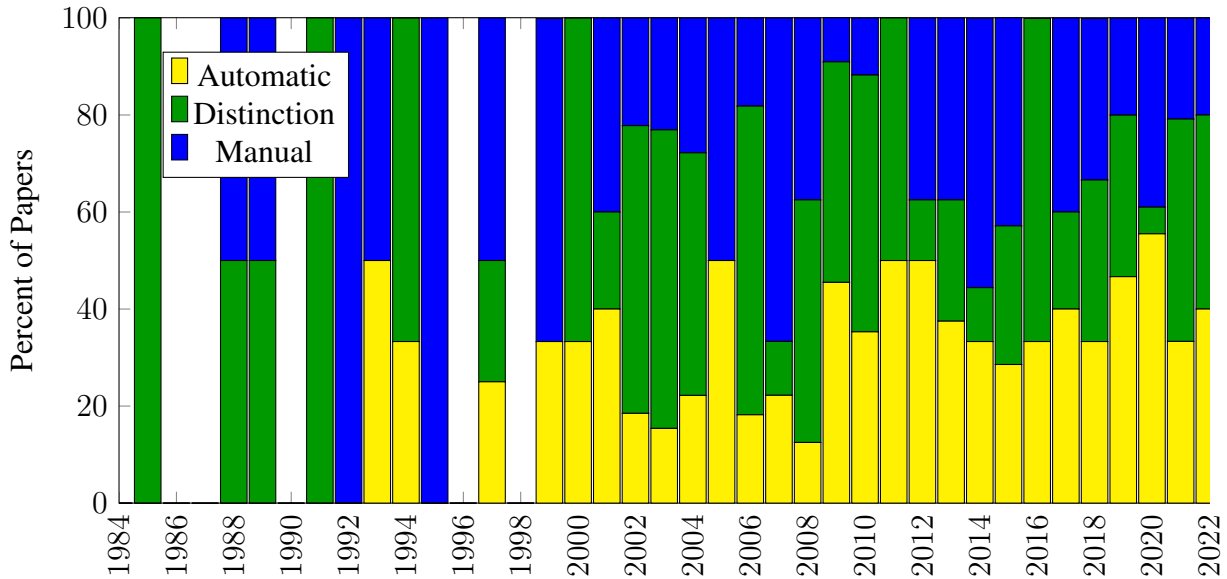


Figure 2.4: Percentage of papers per year with each definition of 'reconfigurability'.

From Figure 2.4, there seems to be a cyclical nature to the percentage of "automatic" classifications in the sources presented but perhaps a wider selection of journals would provide more statistical power to this result. From these articles, it is evident that there is not an overwhelming trend in time with the popularity of the three different divisions for the use of the terms throughout time. Therefore, explicit definitions are constructed and presented next.

2.3 Proposed Metric

We propose a cost metric that involves reconfiguration time, monetary cost, and the amount of required external material. This value is purposely a cost, as opposed to a measure of ability. Other metrics exist for describing how much a vehicle can reconfigure including Reconfigurability Index and Coefficient of Variation [27].

2.3.1 Working Definitions

In addition to this metric, the following definitions are presented:

Static Versatility

A characteristic of a system or subsystem to be used for multiple purposes that it would not otherwise be capable of without reorientation, modification, addition of other components, or subtraction of other components.

Here, we define a statically versatile mechanism as one that is able to accomplish different tasks as is, without alteration. Such a mechanism is multipurpose but differs from the other definitions in that its multiple purposes can be accessed without internal or external change. Oftentimes it is not possible to make a single mechanism versatile enough to achieve different tasks. In this case flexibility, modularity, or reconfigurability is necessary.

Flexibility

The ability of a system or subsystem to be modified for performance value or abilities other than those that the system was originally designed for.

Flexibility is a broad term used across domains that describes the ability to easily change [57, 58, 59]. In engineering, this can mean that a product is developed with the understanding that it may need to be modified to fit new markets or missions. This characteristic can be especially important in manufacturing when the product can change after the manufacturing infrastructure is built [60].

Though physical flexibility (as in compliant attributes) is also a valuable avenue for robotic exploration (often called soft robotics), this work will use the term ‘flexibility’ to apply solely to simplicity of change.

Manual Reconfigurability

The ability of a system or subsystem to be modified in a way that increases performance or adds an ability through the modification, addition, or subtraction of components by an external entity.

Manual reconfigurability offers slightly more drastic means of modification and can bring huge benefits for both designers and manufacturers [61] [62].

There is also a slight distinction to be made between systems that can be manually reconfigured without the swapping of parts and those that require components to be interchanged. In general, it is desirable to have fewer additional components, especially in a setting where space or weight is limited. On the other hand, removable and replaceable components can make the system itself lighter, simpler, and easier to repair. We will use the term ‘self-contained manual reconfigurability’ to refer to manually reconfigurable systems that do not require the addition or subtraction of components.

Self-Reconfigurability

The ability of a system or subsystem to modify itself in a way that increases performance or adds an ability.

Flexibility and manual reconfigurability are stepping stones, of sorts, to self-reconfigurability, where a system can transform without external intervention. In 2006, Afreen Siddiqi distilled a definition of a reconfigurable system as one "that can reversibly achieve distinct configurations (or states) through the alteration of system form or function, in order to achieve a desired outcome within acceptable reconfiguration time and cost". She goes further to include both the extent to which a vehicle can reconfigure and the ease with which it can do so in her definition of reconfigurability [27].

Dr. Yim et al. propose a classification for self-reconfigurable systems based on architecture. They specify lattice, chain/tree, and mobile as the three primary divisions [63] and have recently added divisions for hybrid and truss [47]. In their taxonomy, lattice architecture refers to a system with a regular, three-dimensional shape. Reconfigurability is conducted locally, and so planning complexity does not have to be proportional to number of elements. Chain or tree architecture applies to a system where each element is connected in a string or tree. Systems

with mobile architecture are capable of moving in space and can take the form of either lattice or chain/tree systems. Truss architectures capture designs where link lengths or node degrees change. These authors also divide reconfigurability into deterministic or stochastic reconfigurability, depending on if the pose of each element is known at each time (deterministic) or not (stochastic) [63].

Though some sources describe self-reconfigurability only in terms of modular reconfigurability, we will keep this as a subset of self-reconfigurability. Modular self-reconfigurable robots (MSRRs) typically refer to systems where an entire robot is doing the reconfiguration, as opposed to just one subsystem or element. ‘Metamorphic’ is a subset of self-reconfigurability that involves re-organization of identical, or ‘homogeneous’ modules [64]. Dissimilar modules are called ‘heterogeneous’ [65] or ‘hybrid’ in earlier literature [66]. Modular self-reconfigurability differs from swarm robotics in that the robots physically connect to one another during operation.

Since this body of work primarily focuses on mechanisms and not control schemes, the distinction between a system that transitions without direct command and one that does so by remote control is not of primary interest. However, it is worthwhile to distinguish ‘automated reconfigurability’ from ‘autonomous reconfigurability’ where automated reconfigurability can be initiated remotely while autonomous reconfigurability requires on-board sensing and logic to determine when to reconfigure.

Modularity

The term ‘modularity’ has divergent and specific definitions depending on application. Like reconfigurability, modularity can imply something that can be manually or automatically altered.

Karl Ulrich and Steven Eppiner separate modularity into three categories: slot, bus, and sectional architecture [67]. In this division, slot architecture allows for the substitution of like components. Bus architecture allows for the attachment of various components with a like adaptor. Finally, sectional architecture is the most variable and allows for components to attach to each other without a defined base structure. There are abundant examples of systems made up of units with a building block nature of the individual elements that allows for a wide range of sizes, shapes, and orientations.

In 1998, Dai and Jones coined the term ‘metamorphic mechanisms’ to describe mechanisms "whose primary function may be just to change structure" in order to enable a change in behavior based on a change in geometry [68]. There is a more physical connotation to ‘metamorphic’ as compared to ‘reconfigurable.’ To this day, this phrase is used to describe the articulation of bodies that are traditionally fixed, for example an articulated chassis or manipulator base.

For simplicity, the terms ‘modularity’ and ‘metamorphism’ are largely avoided in this work and used synonymously with ‘reconfigurability’.

Example

To demonstrate the difference between these terms, a car tire is considered. For a baseline, an early vulcanized rubber pneumatic tire is used. Compared to its solid predecessors, this tire offered a great deal more shock absorption but lacked a strong outer tread layer or radial support, which limited performance in adverse weather and longevity.

In a simple condition that increases performance, an all-season tire can be used, which has excellent performance on wet and dry ground and temperatures above 45 degrees. An all-season tire is versatile because it is a single entity that can perform acceptably in various conditions. Besides the materials innovations, this tire requires addition production methods in order to include the tread and radial supports. However, this tire has higher friction, durability, and fuel efficiency.

The modern car wheel system is an example of a flexible mechanism. Most cars are designed in a standard way to accept multiple different kinds of tires. Though the car may come with all-season tires standard, this offers the consumer the option to later change out the tire to change dimensions or tire characteristics.

Tires are an example of a manual reconfigurability. They can be switched out and replaced with other tires of different widths, diameters, and surface characteristics. For example, a winter tire can offer better performance at colder temperatures. This is not a self-contained reconfigurability like tire pressure, since it requires the swapping of components.

A tire that is able to change between all-season and winter characteristics automatically would be an example of a self-reconfigurable mechanism. Such tires are not mainstream yet for consumer vehicles, but CTIS offers the ability to change pressure for military and agricultural vehicles and some experimental self-reconfigurable tire examples include [69] and [70].

2.3.2 Metric Definition

The metric proposed here exclusively describes the negative consequences of reconfigurability that are not likely to be captured in performance metrics like coverage or speed. Though added reconfigurability could add other costs like weight, volume, number of components and control of components, we will assume that the effect of these is realized in other performance metrics, for example mobility and complexity.

For this work, we define n_{rec} as the number of features of the vehicle that satisfy our definition of either manual or self-reconfigurability. We omit symmetric reconfigurabilities (for example if both left and right track can be widened, this just counts as one reconfigurability). In this way, the value is completely different from degrees of freedom, which are typically captured in complexity metrics.

In order to compare these different values, the proposed metrics require acceptable values from the user that are used to normalize the raw numbers. The user must provide minimum acceptable and most desirable values for each of the three elements in alignment with the Department of Defense's threshold and objective values [71]. Each value is then scaled between 0 and 1 with 0.2 being the threshold value. Since this metric is a cost, 0.2 corresponds to 80% of the way to 0. 80% was chosen as the threshold value in alignment with the business principle that for non safety-critical criteria, the 80% solution is usually sufficient and that remaining 20% has diminishing returns [72, 73]. Finally, the user must provide weightings for the three aspects of reconfigurability cost based on their specific requirements. These weights must sum to 1 for standardization.

We define t_{rec} as the time it takes for a given reconfiguration to occur, measured in seconds. If the transition in one direction takes a different amount of time than reversing it, t_{rec} is the average of these values. If this value is not known, then 0.14 seconds for each percent of reconfiguration is utilized as an average for self-reconfigurable vehicles and 50 seconds per kilogram of vehicle weight for manually reconfigurable vehicles. For example, for a vehicle that can extend a dimension 50%, t_{rec} on its own is assumed to be 7 seconds and a 20-kg

manually reconfigurable vehicle would have a t_{rec} of 1000 seconds. These values were found using the average values for the 14 ground vehicles organized in Table 2.1 by name. In cases where the system is capable of multiple forms of reconfiguration, the mechanism with the largest impact on the vehicle was used for the time and extent values in this table. There is a differentiation in methodology here between the manual and self-reconfigurable vehicles since the manually reconfigurable vehicles present a larger opportunity for full subsystems to be exchanged, which is less meaningfully expressed as an extent. Mass is a relevant factor in manual reconfigurability time as higher mass makes it more difficult to manipulate the vehicle without the use of hoisting systems. Whereas in the self-reconfigurable vehicles, the system itself is doing the reconfiguration and mass of the vehicle does not correlate to transition time as greatly.

For the full system, T_{rec} is calculated as the maximum of all the vehicle's individual t_{rec} scaled by the threshold and objective values. This assumes that the vehicle can actuate different reconfigurabilities at the same time, otherwise the sum of the t_{rec} values is used. In order to scale the individual times by the desired values, the following rearrangement of the point-slope form of a line can be used.

$$t'_{rec} = \min \left(\max \left(\frac{0.2(t_{rec} - t_{rec,o})}{t_{rec,t} - t_{rec,o}}, 0 \right), 1 \right) \quad (2.1)$$

Figure 2.5 shows a visualization of this process. The candidate point is placed to the right of the threshold for ease of illustration, but it is worth noting that for some implementations, the threshold value is the absolute lowest acceptable value for the system (for example rover size to fit in an existing spacecraft). In these circumstances, it would be more reasonable to scale the value between 1 as the threshold and 0 as the objective. The 0.2 to 0 scaling methodology rates solutions that are outside of the threshold value to account for the conditions where no solutions meet the thresholds. This would be more common in research than production, as requirements may still be in flux and not actually represent hard cutoffs. Values are capped at 1 so that the overall value of RC is also capped at one. The metric is also limited by 0 on the lower end so that superior performance in one of the three metrics does not overpower the others.

We assign m_{rec} as the monetary cost of the reconfigurability mechanism. For a prospective vehicle where parts are not selected and a monetary estimate can not be found, a value of 0.35 times the base cost of the vehicle can be used. The value 0.35 was found to be the average of the cost of a reconfigurability divided by the base cost [27]. The total monetary contribution to the reconfigurability cost, M_{rec} , is defined as the sum of the costs of all the reconfigurabilities scaled between the threshold ($m_{rec,t}$) and objective ($m_{rec,o}$) monetary costs. The scaling is performed in the same manner as the transition time.

We denote the mass of the required ex-

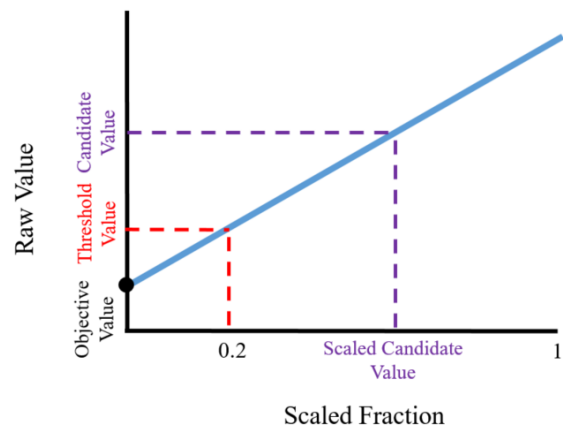


Figure 2.5: Illustration of scaling individual elements of reconfigurability cost.

Table 2.1: Ground vehicle reconfigurability parameters.

System	t_{rec} [sec]	Reconfig. Type	Total Mass [kg]	Reconfig. Extent	e_{rec} [kg]
ATHLETE [75]	8.5	Self	850	0.5	0
Azimut [6]	2	Self	63.5	0.7	0
EHR [76]	13	Self	150	1.3	0
El Dorado II A [77]	300	Manual	23.8	0.75	0.02
MAMMOTH Rover [78]	30	Self	75	1.3	0
MARS mini [79]	1470	Manual	13.14	1	9.3
NeWheel [80]	20	Manual	11.3	1	4.86
Polybot [53]	30	Self	3.6	1	0
Sample Return Rover [81]	10	Self	10	0.93	0
SUGV [82]	1	Self	13	0.18	0
VAL Modular Vehicle [83]	240	Manual	7.5	1	0.8
Wheel-Track [84, 85]	55	Self	24	5.7	0

ternal components as e_{rec} . This value is not the mass of the mechanism itself, but rather the mass of required tools or replaceable components that is necessary for the transformation. The weight of the vehicle with the additional mechanism would be taken into account in a separate performance function, for example mobility. A self-reconfigurable vehicle would have no external material. Based on [74], it is ideal to simplify design to limit the additional tooling and equipment as much as possible. A self-contained manually reconfigurable vehicle would only have any needed specialized tools. And a manually reconfigurable vehicle with swappable components would have the specialized tools plus the extra components. If no data exist to drive this value, 0.24 times the original vehicle weight is used as the average e_{rec} for a manually reconfigurable vehicle. This value is the average of the manually reconfigurable vehicles explored 2.1. Total equipment cost, E_{rec} is determined just as M_{rec} where the individual e_{rec} contributions are summed before being scaled.

The reconfigurability cost of the entire vehicle is a sum of each of the different cost values multiplied by a constant for each reconfigurability.

$$RC = c_t T'_{rec} + c_m M'_{rec} + c_e E'_{rec} \quad (2.2)$$

where c_t , c_m , and c_e are weighting constants for time, monetary cost, and extra components, which should sum to 1 for continuity and the prime designation indicates scaled value. This sum is a unitless value and does not represent a physical quantity, but rather an estimate of cost above objective due to the reconfigurability. Prospective designs should be compared only with the same constants.

We assume that these three values (transition time, monetary cost, and extra materials) are all values that we want to be strictly minimized. There may be a case where it could be desirable to spend all of a given budget, or have a transformation take exactly a certain amount of time. Because this entire sum is treated as a cost, especially when considering against mobility, such

Table 2.2: Sample reconfigurability constant values.

System	c_t	c_m	c_e
Development - Lab	1	0	0
Development - Field	0.5	0	0.5
Production - Vehicle-deployed	0.25	0.5	0.25
Production - Person-deployed	0.25	0.25	0.5
Production - Civilian	0	0.75	0.25

goals would be missed. It would be possible to rewrite the individual costs in a way that captured these desires, such as using the absolute value of the difference between the goal and actual values.

2.3.3 Choosing Constants

The constants in this equation serve to shape the output based on the specific priorities of the vehicle designer or evaluator. However, a metric involving empirical or subjective constants can be unwieldy and unhelpful if there is no intuition for these values. A few example constant combinations are listed in Table 2.2.

If there is no operational urgency or importance on reconfiguration time, then the total acceptable time for a reconfiguration would be infinite. This makes the T_{rec} term 0, which is essentially equal to having the c_t term be 0, indicating that transformation time is not a priority. On the other hand, for industrial systems, ease of transformation is one of the key parameters for reconfigurable design [86]. In the lab setting, the amount of additional equipment does not need to be factored in since tools could be stored in the environment and would not need to be transported.

As explained in [87], metrics such as cost and development time are more relevant for entrepreneurship than innovation. In a research and development setting, monetary cost may not be a design driver at all, in which case c_m would be 0. On the other hand, a design for a consumer product may prioritize this attribute most. However, in a consumer setting, cost is commonly the deciding factor among similar designs [88]. Again, in a research setting, additional tools and components may not be a major hindrance. However, for a robot that is going to be transported or carried regularly, this could be a major factor in decision making.

2.4 Metric Implementation

To compare the proposed metric with other definitions, a variety of vehicles are considered and compared against existing definitions for reconfigurability. R_{MK2} is defined as a reconfigurability that is manually adjusted (i.e. satisfies Murata and Kurokawa's Class 2), and R_{MK3} is a reconfigurability that can be adjusted on its own (i.e. satisfies Murata and Kurokawa's Class 3). R_{Yim} is defined based on Yim, et al.'s requirements of separate autonomous modules for self-reconfigurability [63]. For comparative purposes, the constants for field-based research denoted in Table 2.2 are used for all compared vehicles, along with the following threshold and objective values: $t_{rec,t} = 15$, $t_{rec,o} = 2$, $e_{rec,t} = 10$, $e_{rec,o} = 2.5$. A summary of these results

can be found in Table 2.3.

2.4.1 ATHLETE

All-Terrain Hex-Limbed, Extra-Terrestrial Explorer (ATHLETE) [75] was designed by the Jet Propulsion Laboratory and collaborators from the National Aeronautics and Space Administration, Stanford University, and Boeing Company. The vehicle is a testbed for lunar cargo movement strategies. It features six legs, each with six degrees of freedom including drive wheels. The robot is designed to roll over firm terrain and step across loose terrain. Since it is self-reconfigurable, $R_{MK2} = 0$, $e_{rec} = 0$, and $R_{MK3} = 6$. It is not comprised of identical, self-reconfigurable modules, so R_{Yim} is also 0. Based on video footage, the time it takes to change its height to the greatest extent is 8.5 seconds, which equates to 0.1 when scaled. Since the reconfigurabilities can take place simultaneously, this is used as our T_{rec} . Therefore $RC = 0.5 * 0.1 + 0.5 * 0 = 0.05$.

2.4.2 AZIMUT

The AZIMUT platform [6] is capable of wheeled locomotion or tracked locomotion, can operate with tracks of varying angles of attack, and can change its track contact area. The vehicle can also actuate the angle of the wheels/tracks in the z axis, but this is a method of steering, not really a different configuration. These three reconfigurabilities are self-reconfigurabilities, though not modules relocating, so $R_{MK2} = 0$, $R_{MK3} = 3$, $R_{Yim} = 0$, and $e_{rec} = 0$. Based on the slowest specified configuration actuator, it can change from vertical to horizontal in 2 seconds. Since this is our $t_{rec,o}$, the contribution from time is 0 and the overall RC is 0. It is worth noting that an RC of 0 does not mean that reconfiguration is without cost or time. It does indicate that the costs are within acceptable limits as given by the objective parameters.

2.4.3 EHR

The Environmental Hybrid Robot (EHR) [76] was designed to take on the challenging environment of the Amazon rainforest. It is comprised of four large wheels with paddles on one side that can be angled based on a linear actuator and linkage mechanism. The vehicle can reorient on its own and does not involve other identical modules, so $R_{MK2}=R_{Yim}=e_{rec} = 0$ and $RC_{MK3} = 1$. The actuator can transition between its extreme dimensions in 13 seconds, which equates to 0.17 when scaled. Therefore $RC = 0.5 * 0.17 + 0.5 * 0 = 0.085$.

2.4.4 El Dorado II A

The El Dorado II A system [77] was designed to explore sideslip mitigation strategies for planetary exploration. This vehicle has four vertical members on both sides of the vehicle that can be used to adjust ride height on the left or right side independently. This device uses extruded aluminum members to achieve this variability. Since the system is manually reconfigurable, $R_{MK3}=R_{Yim}=0$ and $RC_{MK2} = 1$. The system is self-contained, so the only additional equipment is a tool to adjust the connectors on the vertical members. This weight is negligible compared to the weight of the vehicle and less than the objective value of 2.5 kg, so the component of reconfigurability cost due to equipment is 0. The time to reconfigure this vehicle is approximately 300 seconds based on the number and type of fasteners, which results in a scaled time contribution of 1. So the overall RC is 0.5.

2.4.5 MAMMOTH

The MAMMOTH Rover[78] utilizes 16 motors to actuate 4 legs and adjust its footprint, ride height, and weight distribution. No additional tooling is required for these changes, so $e_{rec}=0$. Transition time ($t_{rec}=30$) is calculated from video footage for the maximum horizontal change in length. This value gives a scaled time contribution of 0.43 and a RC of 0.215.

2.4.6 MARS mini

Another example of a manually reconfigurable vehicle is the MARS mini prototype [79]. This vehicle was comprised of extruded aluminum and could be outfitted with different numbers of wheels or body shape. $R_{MK3}=R_{Yim}=0$ and $RC_{MK2} = 2$. This vehicle was used as a platform to test concept before the MARS X iteration. Because of the purpose of this device, its added equipment was quite bulky, measuring almost as much the original vehicle itself. The e_{rec} is the minimum additional weight from the different configurations. The scaled value is 0.18 as it is close to the threshold value. It also requires significant time to reorient, more than the threshold of 60 seconds. The 1470 second transition time equates to a scaled value of 22.6, which is again capped at 1, making the overall $RC=0.59$.

2.4.7 NeWheel

From Data61 (CSIRO), Queensland University of Technology, and University of Queensland, the NeWheel [80] is a suite of vehicles all based around a central actuated wheel station. The wheel station can be connected in endless configurations depending on mission needs. Based on [89], this reconfiguration can take place in a matter of seconds if the proper mating hardware is preinstalled. Number of wheels and shape of the vehicle can be adjusted, so $R_{MK3}=R_{Yim}=0$ and $RC_{MK2} = 2$. In order to go from one wheel to four wheels, a t_{rec} of 20 seconds is used to remove the wheel and insert it and three others on a new base. This also requires an additional 1.66 kg of material, which is 75% of the original vehicle's mass but less than our objective value for this example, so the equipment contribution is 0. This gives a total RC of $0.5*0.28+0.5*0=0.14$. If the most used configuration is the 4-wheeled vehicle, then the e_{rec} would be smaller as the additional wheel stations would not need to be separately transported.

2.4.8 Polybots

Polybots [53] are a series of identical modules that can link and decouple on their own. This fits Yim, et al.'s definition for reconfigurability, so $R_{Yim}=1$ and $R_{MK3}=1$. Since there is no additional hardware needed, $e_{rec}=0$. These devices can reorganize in 30 seconds, which is a scaled value of 0.43 and an RC of 0.215.

2.4.9 SRR

The JPL Sample Return Rover (SRR) [81] is a 7.2-kg system capable of almost doubling its footprint going from storage to traversing mode. It can actuate this reconfigurability on its own, so $R_{MK2}=R_{Yim}=e_{rec} = 0$ and its articulated suspension system results in a R_{MK3} of 1. It can transition in 10 seconds, which is a scaled value of 0.12 and a RC of 0.06.

2.4.10 SUGV

The FLIR SUGV [82] has one self-reconfigurability to adjust the track angle of attack and, at the extreme position, the contact length. These two reconfigurabilities are achieved by the same self-actuated mechanism, so $RMK2=0$, $RMK3 = 1$, and $e_{rec}= 0$. Based on video footage, the vehicle can go from minimum contact length to maximum contact length in 1 second. As with the AZIMUT platform, this means that the RC is 0 and the costs due exclusively to reconfigurability are beyond that of our objectives.

2.4.11 VAL Modular Vehicle

In this Master's Thesis, Johnson used a modular ground vehicle from the Virginia Polytechnic Institute and State University Vibration and Acoustics Laboratory (VAL) to compare mobility performance [83]. Since this system is manually reconfigurable, $R_{MK2} = 1$, $R_{MK3} = 0$, $R_{Yim} = 0$. The user has the ability to put wheels or tracks on this vehicle by swapping out the sprockets on six wheel stations. Each wheel station is assumed to take 40 seconds to switch based on experimental data with a similar sprocket set up. The mass of the 60 rubberized track links, sprockets, and tooling is .8 kg, which is 11% of the original weight but less than the objective value. Therefore the RC is $0.5*1+0.5*0=0.5$.

2.4.12 Wheel-Track Robot by Gao, et al.

The wheel-track system developed by Gao, et al. [84] has two means of reconfigurability. The first is the wheel-track mechanism. The second is the center of gravity position that is adjusted by means of an actuated tail. Thus for this system, $n_{rec} = 2$. Since these changes can both occur without manual intervention, $R_{MK2} = 0$, $R_{MK3} = 2$, and the e_{rec} for both reconfigurabilities is 0. This vehicle is not composed of autonomous modular elements, so $R_{Yim} = 0$. Based on [85], the time it takes for the vehicle to transition between wheel and track mode is 55 seconds. We assume that the time it takes for the tail to reconfigure is negligible compared to this and can take place simultaneously. This brings the reconfigurability cost (RC) to $0.5*0.82=0.41$.

2.5 Discussion

Table 2.3 shows a comparison of the number of reconfigurabilities of the aforementioned vehicles with the proposed metric, RC (Equation 2.2) compared to other definitions. The purpose of this table is not to compare the merits of each vehicle with respect to one another. Each system was developed for entirely different environments and weight classes. But rather, the table shows the added information that can be expressed through the RC metric compared to the other measures of reconfigurability. n_{rec} (green cells in the above table) amounts to the sum of two of the definitions of modularity that involve reconfigurability as described by Murata and Kurokawa (gray cells in the above table).

Table 2.3: Comparison of reconfigurability with the proposed and other definitions.

System	RC	n_{rec}	R_{MK2}	R_{MK3}	R_{Yim}
ATHLETE [75]	0.05	6	0	6	0
AZIMUT [6]	0	3	0	3	0
EHR [76]	0.085	0	0	1	0
El Dorado II A [77]	0.5	1	1	0	0
MAMMOTH Rover [78]	0.215	4	0	4	0
MARS mini [79]	0.59	2	2	0	0
NeWheel [80]	0.14	2	2	0	0
Polybot [53]	0.215	1	0	1	1
Sample Return Rover [81]	0.06	1	0	1	0
SUGV [82]	0	1	0	1	0
VAL Modular Vehicle [83]	0.5	1	1	0	0
Wheel-Track [84, 85]	0.41	2	0	2	0

The proposed metric (blue cells in the above table) gives preference to reconfigurabilities that occur quickly, are inexpensive, and require less added external components, resulting in a lower cost. The manually reconfigurable robots (El Dorado II A, MARS mini, NeWheel, VAL Modular vehicle) all had higher RC values compared to the self-reconfigurable robots (ATHLETE, AZIMUT, EHR, MAMMOTH, Polybot, SRR, SUGV, Wheel-track). This is because they did not have additional tools or materials required and faster transition times. Overall, the reconfigurability cost gives more information than a simple summation of the numbers of reconfigurability that is not otherwise captured in other performance metrics. It gives a value that can be minimized for the purpose of optimizing vehicle design. The metric also has slightly more readability as it is scaled to desired values.

2.6 Conclusions

Since the 1980s, reconfigurability has been a topic of increasing interest to robotics fields including ground vehicles, manipulation, space, sensing, marine, and aerial applications. Physical transformation offers benefits in terms of increasing the abilities of a system, redundancy, and flexibility.

It is evident that there are different understandings of the word ‘reconfigurability’ both between and within different subfields of robotics. Hopefully the summary of contrasting definitions and explicit listing of different terms will make future work in this area more standardized. As with any definition, though, adoption provides more evidence of utility than isolated

demonstrations. The proposed definitions for reconfigurability aligns well with the most discriminating definitions from literature and reduces ambiguity.

The proposed metric allows users to evaluate how efficient a reconfigurable candidate vehicle is in terms of time, cost, and external material required. These are costs that are specific to reconfigurability itself, and not otherwise captured in metrics like complexity or mobility. This metric also has adjustabilities for mission requirements and priorities, making it versatile for different applications. Most significantly, the cost metric presented in this work frames the consequences of reconfigurability in a quantifiable and readable manner. This allows the metric to be used in multi-objective optimization systems where reconfigurability cost is a value between 0 and 1 that should be minimized. The purpose of this metric is to be used in combination with a performance measure like mobility in order to drive vehicle design with consideration for the drawbacks of reconfigurability.

Chapter 3

Distilling and Modeling Mobility for Unmanned Ground Vehicles

3.1 Introduction

A vehicle's movement can be described through many diverse parameters including speed, acceleration, sinkage, and, slip. Figure 3.1 shows the Society of Automotive Engineers (SAE) coordinate System used to assign direction to these values [90]. A vehicle can also be characterized in terms of performance characteristics. Bruzzone and Quaglia used ten qualitative criteria to rate the typical performance of each system: maximum speed, obstacle crossing capability, step/stair climbing capability, slope climbing capability, walking capability on soft terrain, walking capability on uneven terrains, energy efficiency, mechanical complexity, control complexity, and technology readiness [91]. For unmanned vehicles, improved mobility performance can decrease perception challenges, reduce time necessary to find a path, reduce path length, and lessen the chances that the vehicle becomes stuck and immobilized [92].

In an idealized case, where neither the vehicle nor terrain are deformable or yieldable, the vehicle's movement and performance can be found by examining the vehicle's characteristics and friction with the terrain.

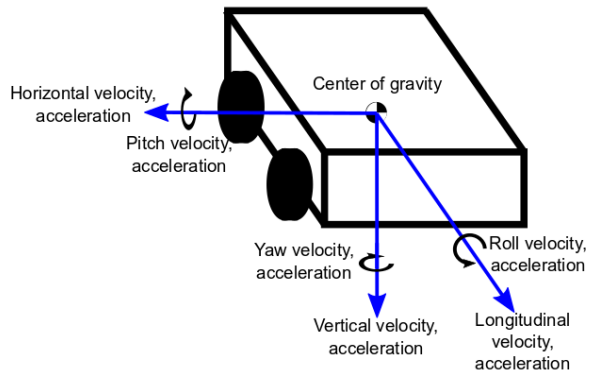


Figure 3.1: Illustration of multi-dimension velocity and acceleration characteristics with the SAE-defined axes system.

Portions of this chapter are being prepared in a manuscript for submission to the Journal of Terramechanics in 2023.

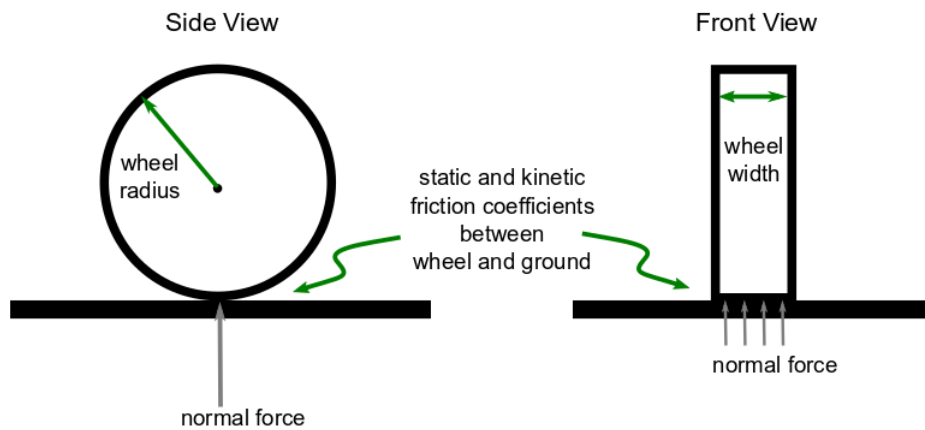
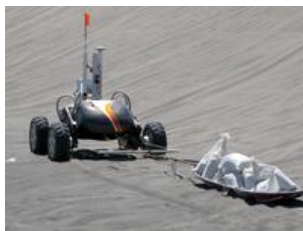


Figure 3.2: Idealized rigid wheel and terrain parameters.

Performance characteristics in this case are limited by the vehicle's engine, weight distribution, and friction coefficient between its wheels (or tracks, or legs) and the surface it moves on, as shown in Figure 3.3.



(a) Carnegie Mellon's lunar rover prototype Scarab attempts to drag increasingly heavy loads. Depending on the vehicle's engine size versus load, it may not be able to move [93].



(b) This vehicle does not have enough traction to traverse the slippery ice due to the limited friction between the tire and ice [94].



(c) failure due to soil shear is evident. Though the wheel may be spinning, the soil cannot provide the required normal force necessary to support the vehicle's forward movement [95].

Figure 3.3: Examples of scenarios where vehicle movement is limited (engine power, friction, and soil strength).

With a known measure of this coefficient of friction, a usable estimate of a vehicle's behavior on solid ground can be found. However, in a vast number of applications from planetary exploration to tactical military movement, the assumption of a rigid ground is highly unreasonable.

Terramechanics is the study of the interaction between soil and tools or vehicles. The term was coined in 1960 by Dr. Mieczyslaw Gregory Bekker, largely regarded as the father of the field [8]. At this time, the major applications for this field were agriculture, excavation and defense. Soon, planetary exploration and sea bed plowing also benefited from pioneering work by Bekker and Reece [96]. Recently, unmanned vehicles are becoming smaller and smaller,

and, as noted earlier, some of the relationships developed in the early years of terramechanics are inaccurate for this scale [97] [98], [99], [100].

Table 3.1: Prior terramechanics research in small and tracked vehicles.

Small Vehicles	Small Tracked Vehicles	Tracked Vehicles
Pressure-sinkage relationship [98], [101]	NRMM validation [102]	Pressure distribution [97], [103]
Stress distribution [100], [104]	Modular System [105]	MMP [106]
DEM evaluation [12]	Design [107] [108]	VCI [9]
Design [98]	Towing Capacity [109]	Thrust [97], [110]
Reconfigurable vehicles [111]	Empirical Analysis [108]	Wheels vs. Tracks [112], [113], [114], [115]

The size of military ground vehicles has also become more diverse. Unmanned ground vehicles are mostly under 100 kg. Though full-scale unmanned vehicles were made in the first decade of 2000, they were not integrated into any military's normal fighting force [116]. This may change, however, as robotics technology is becoming more cost-effective [117]. Currently, unmanned ground vehicles are being used for surveillance, reconnaissance [118], equipment transport [119], and bomb disposal [120].

3.2 Background

3.2.1 Analytical and Semi-Empirical

Normal Stress

Ground pressure is often used as a quick check to predict whether a specified terrain has enough strength to support a given vehicle. In general, the percent of off-road terrain that a vehicle can reach is inversely related to ground pressure [114], [121].

One method of categorizing pressure is to take the nominal ground pressure, or

$$\sigma = \frac{W}{A} \quad (3.1)$$

where σ is the normal stress (or pressure), W is the vehicle weight and A is the nominal surface contact patch.

However, pressure under a vehicle is neither constant throughout the vehicle's contact area nor at different depths beneath the soil. The vehicle's geometry and loading create areas of higher and lower pressure and, in addition, the normal stress in the soil varies non-linearly. Similar to stress concentrations under a human's foot, vehicle construction results in uneven loading under the vehicle. A wheeled vehicle will have higher pressure near the center of

the wheel's contact patch and a tracked vehicle will have higher pressure near the bogies that support the track.

When dealing with stresses in the soil, it is necessary to understand the pressure in locations other than a global maximum. Over the past century, the equations for normal stress have evolved greatly to include factors about the vehicle, as well as location and soil parameters. The following table documents just a few of the many versions of stress pertaining to soils. A fuller history of the various equations describing normal stress can be found in Gareth Meirion-Griffith's doctoral thesis [122]. Additionally, an overview of more than two dozen terramechanics models and their uses can be found in Rui He, et al.'s "Review of terramechanics models and their applicability to real-time applications" [123]. The details and coefficients of these equations are not reviewed in this document, but their general forms and empirical nature are evident.

Table 3.2: Diversity of normal pressure equations.

Author	Year	Expression	Citation
Nominal	-	$\frac{W}{A}$	-
Bernstein	1913	$kz^{0.5}$	[124]
Goriatchkin	1936	kz^n	[125]
Bekker	1956	$(\frac{k_c}{b} + k_\phi)z^n$	[97]
Reece	1964	$[ck'_c + \gamma bk'_\phi](\frac{z}{b})^n$	[126]
Wong/Reece	1967	$(ck'_c + \gamma bk'_\phi)(\frac{z}{b})^n(\cos\theta - \cos\theta_s)^n$	[127]
Griffith	2012	$\hat{k}z^{\hat{n}}D^{\hat{m}}$	[122]

A related parameter to describe vehicle performance is maximum sinkage. This can be used as an estimator of how well a vehicle will be able to float on a given terrain's surface and affects its interaction with obstacles. Maximum sinkage for a tracked vehicle using Bekker's equations can be estimated with the following equation:

$$z_{max} = \left(\frac{\sigma}{k_c/b + k_\phi} \right)^{\frac{1}{n}}. \quad (3.2)$$

As before, σ is the ground pressure, b is contact width, and k_c , k_{phi} and n are descriptors of the soil.

Shear Stress

In reality, soil behaves neither purely elastically nor purely plastically and varies with type and moisture. Largely, the field of terramechanics treats soils as plastic media because the question of maximum achievable thrust is of interest for vehicle performance estimation. In this case, the Mohr-Coulomb failure criterion [128] is most often used to describe the maximum shear stress that a material can provide with a given normal stress:

$$\tau = c + \sigma \tan \phi. \quad (3.3)$$

This equation relates both characteristics of the soil (c is the coefficient of cohesion and ϕ is the internal angle of friction) and characteristics of the loading (σ is the normal stress discussed in the previous section). Coefficients c and ϕ can be found using various tools and techniques. One of the most common tools is the Bevemeter, which has the ability to measure the torque required to pull a plate with known dimensions and variable weight through a soil [110] and can be used to find these constants from equation 3.4. Dr. Sally Shoop also showed that an instrumented wheel on a small wheeled testbed can provide reasonable constants that can be applied to much larger vehicles (a difference of 10% between predicted and measured traction for a vehicle about 8 times as heavy as the test vehicle) [104].

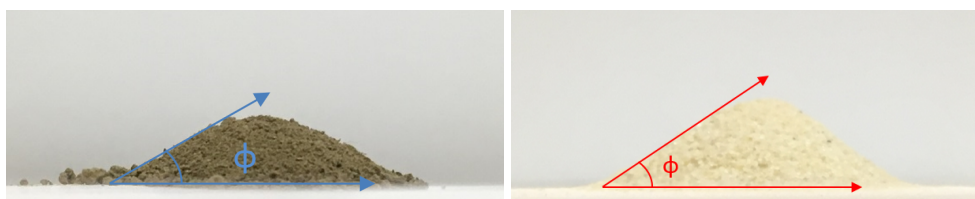


Figure 3.4: Examples of materials with different angles of friction (left: dry loam, right: sand).

For a perfectly cohesive soil, such as saturated clay, the angle of friction goes to 0. Here, the vehicle loading has no effect on the maximum shear stress, which is only a function of the cohesion coefficient. On the other hand, a perfectly non-cohesive material like dry sand, has a cohesion coefficient of 0. In this case, the maximum stress is only a function of the normal pressure, so the heavier the vehicle, the proportionally higher the maximum shear stress of the material.

Drawbar Pull

To go from strain of a material to shear force, one can simply multiply by the contact area of the two touching surfaces [106]:

$$H = \tau A. \quad (3.4)$$

In this equation, H represents thrust and A represents the contact surface area. It is worth noting that this contact surface area is often an approximation or simplification of the actual area in contact with the ground. [129] shows the variety of contact areas even for one single

tire on a soil with various amounts of moisture. This shape can be approximated as the area between two super ellipses but for empirical determination of characteristics like drawbar pull, this shape is usually abstracted to length, width and a measure of how far the implement deflects [106].

For legged vehicles, Yeomans et al.'s formula can be used to find maximum thrust that the soil can provide. The equation is based on the Mohr-Coulomb failure criterion. The equation is as follows:

$$H = (c + dg\gamma \tan\phi)\pi\left(\frac{w}{2}\right)^2. \quad (3.5)$$

In the real world, a variety of forces act on the vehicle that limit its thrust besides just the strength of the soil. The diagram below shows some of these resistances in the right plane. Effects normal to this view are omitted here as we assume the vehicle is moving straight ahead. Lateral forces that result from acceleration during turning are discussed in Subsection B.2.

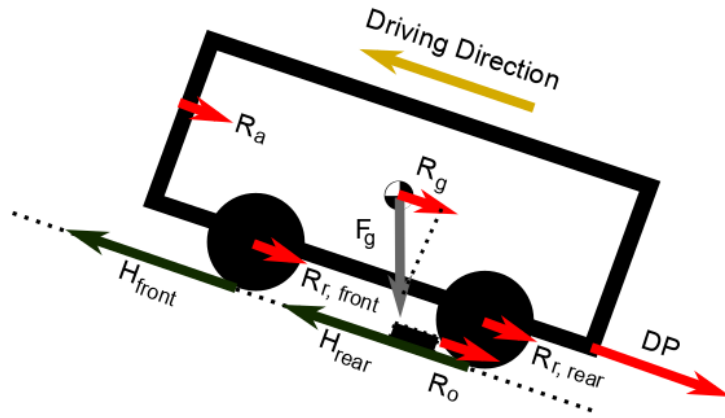


Figure 3.5: Side view of a vehicle moving up a slope against resistances due to aerodynamics, gravity, rolling resistance and drawbar pull.

Summing the forces at the center of mass in the driving direction yields:

$$ma = H - R_g - R_a - R_c - R_b - R_r - R_o - DP \quad (3.6)$$

where H is the thrust from the front and rear wheel, R_g is the resistance due to gravity, R_a is aerodynamic resistance, R_c is compaction resistance, R_b is bulldozing resistance, R_r is rolling resistance and DP is drawbar pull. If the vehicle is at static equilibrium, there is no acceleration and the left side of Equation 3.6 is 0. An equation for drawbar pull can then be derived as the difference between the thrust and the sum of the other resistances:

$$DP = H - \sum_{i=1}^{n_{res}} R_i \quad (3.7)$$

where each R_i is a different resistance and n_{res} is the total number of resistances acting on a system in an appreciable quantity. This number represents the maximum force that the vehicle

could bear before failure. In order to compare the relative strength of vehicles with different weights, the drawbar pull coefficient (PC) is used where W is the vehicle's weight:

$$PC = \frac{DP}{W}. \quad (3.8)$$

Drawbar power is the product of drawbar pull and the forward speed of the vehicle. Because the vehicle's thrust relies on a shear force on the soil, slip is likely. Slip (i) is defined as a fraction (sometimes given instead as a percent) of how much the actual speed of the vehicle (V) has been reduced relative to the theoretical speed (V_t) of the vehicle, which can be calculated as $V_t = r\omega$ where r is the wheel radius and ω is the rotational speed of the wheel. Slip is sometimes discussed in terms of a reduction in travel (TR) [130]. The equation for slip is shown below in Equation 3.9 [106]:

$$i = \frac{V_t - V}{V_t} = 1 - \frac{V}{V_t}. \quad (3.9)$$

Therefore, drawbar power can be written as:

$$P_d = (DP)V = (H - \Sigma R)V_t(1 - i). \quad (3.10)$$

Janosi and Hanamoto developed the following equation involving shear slip (j) and unitless constant (k_{slip}) to account for slip [131]:

$$\tau = [c + p \tan(\phi)](1 - e^{-j/k_{slip}}). \quad (3.11)$$

One of the most common resistances that vehicles must overcome is the resistance due to gravity from driving on a slope. This resistance can be represented as R_g and found using the angle of the slope that the vehicle is driving up (θ_s):

$$R_g = W \sin(\theta_s). \quad (3.12)$$

This resistance can be positive or negative depending on if the vehicle is traveling in the direction of the slope or against it. Again, in this equation, W is vehicle weight.

A ground vehicle must also overcome the force of aerodynamic resistance, which is expressed as:

$$R_a = \frac{\rho}{2} C_D A_f V_r^2. \quad (3.13)$$

This resistance is correlated to the density of the fluid that the vehicle is moving through (ρ), the size and shape of the vehicle (C_D is the drag coefficient and A_f is the frontal surface area) and the vehicle's speed relative to the wind speed (V_r). For vehicles moving slower than 48 km/hr or 30 mph, air resistance is rarely significant, so it is largely omitted from off-road vehicle calculations[106].

Another one of the main resistances that a vehicle must overcome is the force of compaction. This is the force necessary to press down the soil directly under the vehicle's wheel or track. Compaction under a wheel is equal to [106]:

$$R_c = b_{ti} \int_0^{\theta_0} \sigma r \sin\theta d\theta \quad (3.14)$$

where b_{ti} is the width of the wheel, θ_0 is the contact angle and r is the wheel radius. This can be expanded to:

$$R_c = \frac{1}{(3-n)^{(2n+2)/(2n+1)}(n+1)b_{ti}^{1/(2n+1)}(k_c/b+k_\phi)^{1/(2n+1)}} \left(\frac{3W}{\sqrt{D}} \right)^{(2n+2)/(2n+1)} \quad (3.15)$$

where D is the wheel diameter and n , k_c and k_ϕ are soil parameters. This equation can be found using Bekker's pressure-sinkage relationship (3.2 and substituting $\left[\frac{3W}{b_{ti}(3-n)(k_c/b+k_\phi)\sqrt{D}} \right]^{2/(2n+1)}$ for z_r . This latest relationship which comes from balancing the forces in the vertical direction. In this equation is it worth noting that b is the smaller of the two dimensions in contact with the ground. As opposed to b_{ti} , b could be the length of the contact area for a very wide wheel.

Using Bekker's pressure-sinkage relationship for a deformable wheel to solve for sinkage ($z = \left(\frac{p_i+p_c}{k_c/b+k_\phi} \right)^{1/n}$) and a vertical force balance to solve for the approximate length of the contact patch ($l_r = \frac{W}{b_{ti}(p_i+p_c)}$) compaction resistance for a deformable wheel can be expressed as [106]:

$$R_c = \frac{b_{ti}(p_i+p_c)^{(n+1)/n}}{(n+1)(k_c/b+k_\phi)^{1/n}} \quad (3.16)$$

The variables are the same for this equation, with the addition of p_i and p_c , which are the inflation pressure and pressure due to the tire carcass, respectively.

Finally, compaction resistance for a tracked vehicle can be written as [132]:

$$R_c = \left(\frac{1}{(n+1)b^{1/n}(k_c/b+k_\phi)^{1/n}} \right) \left[\frac{W}{l} \right]^{\frac{n+1}{n}} \quad (3.17)$$

Again, W is weight, D is the wheel diameter, l and b are the length, and width, respectively,

of one contact patch, and n , k_c and k_ϕ are soil parameters.

As a vehicle moves, it also pushes some material to the sides of its wheels or tracks. This is apparent after a vehicle has moved through especially highly cohesive soils, when there are two mounds on either side of the vehicle's compacted paths. This phenomenon is called bulldozing and can be found through the following integration:

$$R_b = \int_{-r \sin \theta_f}^{r \sin \theta_f} [\gamma N_\gamma f(x) + c N_c + q N_q] f(x) dx. \quad (3.18)$$

It should be noted that Bekker developed the majority of his work (including Equations 3.14 and 3.18) for multi-ton military vehicles and mentioned that their utility is limited to vehicles with wheels over 0.5 m in diameter.

Equations for rolling resistance due to tire flexing have been explored by Bekker and Semonin, among others [133]. As a first approximation, the effect of resistances including the deflection of the tire and internal resistance is often calculated using an experimental coefficient of rolling resistance (f_r) and is proportional to vehicle weight [21]:

$$R_r = f_r W. \quad (3.19)$$

There are some empirical methods for calculating rolling resistance depending on the type of tire, typically as a function of the square of the vehicle speed [132]. For a car, rolling resistance typically varies between 0.13 to 0.1 depending on the terrain [134].

Finally, each obstacle presents resistance to the vehicle. The force that these objects impart to the vehicle varies by their characteristic and the wheel that they impact.

The resistance due to the front wheel overcoming an obstacle is [132]:

$$R_{oF} = \frac{W(l_1 + x)(\mu_{alpha} - f_r)(f_r \sin \alpha + \cos \alpha)}{(\cos \alpha + f_r \sin \alpha)(h(-\mu + f_r) + l_1 + l_2 + x)}. \quad (3.20)$$

The resistance due to the rear wheel overcoming an obstacle is [132]:

$$R_{oR} = \frac{W(l_2 - x)(\mu_{alpha} - f_r)(f_r \sin \alpha + \cos \alpha)}{(\cos \alpha + f_r \sin \alpha)(h(\mu - f_r) + l_1 + l_2 - x)}. \quad (3.21)$$

In these equations, α is the contact angle expressed as:

$$\alpha = \sin^{-1} \frac{d_1 - 2h}{d_w} \quad (3.22)$$

and x is a parameter based on obstacle height (h_o) and wheel diameter (d_w):

$$x = 0.5\sqrt{d_w^2 - (d_w^2 - 2h)^2}. \quad (3.23)$$

A related parameter developed by Bekker is maximum traversable obstacle (H_{obs}) [135]:

$$H_{obs} = \frac{(N - 3)W_0 * \mu + (2W_0 - K'd/2)7 - (W_0 - K'd/2)}{K'(1 - \mu^2)}. \quad (3.24)$$

In 2011, Rajabi et al. explored slope climbing capabilities for straight and articulated tracks, developing a model for maximum theoretical slope [136].

Resistance due to steering is largely ignored for this work. Additional details on steering resistance can be found in B

3.2.2 Empirical Methods

Pressure

In the United Kingdom, the prevailing method for describing a vehicle's pressure is through the Mean Maximum Pressure (MMP). The MMP was established by Rowland in 1972 and the equation for wheels was modified by Larminie, Maclaurin and Priddy in 1992, 1997 and 2004, respectively [103, 137, 138, 9]. The equations below represent Priddy's modified MMP for pneumatic wheels (3.25), and Rowland's 1975 versions of MMP for tracks on rigid wheels (3.26), and tracks on pneumatic wheels (3.27):

$$MMP_{wheels, P} = \frac{W}{n_w m b^{0.8} d^{0.8} (\delta)^{0.4}} \quad (3.25)$$

$$MMP_{tracks \text{ with rigid wheels, R}} = \frac{1.26W}{2m(b_s l_s / pb)b(pd)^{0.5}} \quad (3.26)$$

$$MMP_{tracks \text{ with pneumatic tires, R}} = \frac{0.5W}{2mb(d\delta)^{0.5}}. \quad (3.27)$$

In these equations, W is the vehicle weight, m is the number of wheel stations per track, n_w is the number of wheels per axle, d is the ground wheel diameter or tire diameter, b is the ground wheel or tire width, l_s is the length of one shoe or link, δ is the tire deflection [139, 9].

MMP has been used in military applications as a first pass at estimating a vehicle's trafficable area and as benchmarks for acceptable designs [140]. Standards were created for the maximum essential and desirable Mean Maximum Pressures for different vehicles depending on their use and environment [121]. This metric is of particular interest as a rough first pass at performance. However, it was developed in the 1970s, when testing was mostly performed on military trucks, tankers, construction equipment and passenger vehicles, as opposed to smaller robotic ground vehicles [141].

The United States uses a different metric, the Vehicle Cone Index (VCI). Instead of simply a measure of soil strength for a vehicle to traverse it, the VCI represents the minimum soil strength necessary for a given vehicle to traverse a certain number of times (usually 1 or 50) [9]. This number of passes is given in the subscript after VCI. Equations 3.28 and 3.29 describe this parameter for wheeled and tracked vehicles, respectively:

$$VCI_{1,wheels} = \begin{cases} 11.48 + 0.2MI - \frac{39.2}{MI+3.74}DCF & MI \leq 115 \\ (4.1MI^{0.446})DCF & MI > 115 \end{cases} \quad (3.28)$$

$$VCI_{1,tracks} = 7.0 + 0.2MI - \frac{39.2}{MI + 5.6}. \quad (3.29)$$

The units for the associated equations are inches and pounds. DCF refers to the Deflection Correction Factor, which was conceived by Priddy to account for the deformation of tires. This coefficient is calculated as follows: [9]

$$DCF = \left(\frac{0.15}{\delta h} \right)^{0.25} \quad (3.30)$$

where δ is again the tire deflection and h is the average section height.

MI stands for Mobility Index and is calculated as follows:

$$MI_{wheels(Priddy)} = \left(\frac{(CPF)(WF)}{(TEF)(GFW)} + WLF - CF \right) (EF)(TF). \quad (3.31)$$

And for tracked vehicles, the MI is:[106]

$$MI_{tracks(Wong)} = \left(\frac{(CPF)(WF)}{(TRF)(GFT)} + BF - CF \right) (EF)(TF). \quad (3.32)$$

The definitions of each of these factors can be found in B.

3.2.3 Computational Methods

While the majority of the vehicle performance estimation methods discussed up until this point are analytic, semi-empirical, purely empirical or parametric, there are also computational strategies.

In 1986, U.K. researchers formalized relationships between weight, MMP, armor depth and penetrability in a BASIC program designed to help address the tradeoffs between protection and mobility [121].

Around the same time researchers in the United States began working on the Nepean Wheeled Vehicle Performance Model and Tracked Vehicle Performance Model (NWVPM and NTVPM) [142, 143]. In the past 30 years, this model has been continually improved and developed.

The NATO Reference Mobility Model (NRMM) is another computer-based estimator of vehicle performance developed by the U.S. Waterways Experiment Station (WES) and Tank-Automotive and Armaments Command (TACOM) [144]. Unlike Wong's methods, based on semi-empirical relationships, NRMM uses empirical characteristics including VCI to describe parameters like maximum speed [145]. As of 2017, efforts were being made to incorporate more analytical terramechanics relationships into the model [146].

Finally, terramechanics has been approached from using finite element (FEA) and mesh-free models. In FEA and DEM (discrete element methods) each vehicle and ground object is broken up into finite elements connected by imagined springs [132]. Alternatively, soil can be considered a continuum and vehicle interactions are examined holistically, as opposed to on an

element basis. A summary of these various computational methods is provided by Contreras et al. in "Soil Models and Vehicle System Dynamics" [145].

Recently, machine learning techniques have also been employed to better estimate vehicle and soil properties. Neural networks have been used to predict soil parameters given vehicle behavior [147]. Bayesian calibration has been used to estimate sinkage and drawbar pull given vehicle information and soil parameters [148].

3.2.4 Controllability

Unmanned vehicle control can be largely divided into three main strategies: teleoperation, following, and complete autonomy [149]. Though a given mission may use a combination of these modes, each offers both benefits and costs depending on familiarity with the tasks and environment.

Just as vehicle mobility prediction is complicated by terrain, structured environments, developed paths and off-road areas each offers different challenges for vehicle design and control [150]. The focus of this work is off-road navigation, though aspects are applicable to more intentional roadways, as well. David Silver's thesis provides a thorough analysis of recent trends in automated vehicle control [150]. Of particular relation to this thesis are efforts made to control vehicles in the face of diverse or high-slip terrain. Especially for completely autonomous systems, accurate localization is essential and is simplified with predictable and repeatable movements.

The movement or obscuring of perception systems is of particular importance for unmanned vehicles. Though videos can be smoothed and denoised in post processing [151], eliminating this step through a smoother ride would allow for faster decision making or the ability to add additional sensing. Terrain roughness can be estimated by examining 3D perception data from the oncoming ground [152] and the effect on the vehicle can be measured during traversal [153] using IMU data.

Kick up from other vehicles or itself can challenge perception systems. In 2017, NREC unveiled their perception solution for discerning dust clouds from obstacles in a convoy [154]. An articulated system that moves into a position that blocks part of the robot's field of view would also have negative implications for planning. However, variability in perception positioning may offer greater potential for the robot. For example, designs for the Mars 2020 rover include 23 cameras, some of which are on pan and tilt mechanisms or the articulated robot arm [155]. If mobility reconfiguration could enable one or more of these degrees of freedom, that would be one fewer actuator involved in perception.

3.3 Proposed Metric

The proposed metric describes mobility performance for an unmanned vehicle with weighting constants that the user can tune. It combines three primary attributes: coverage, drawbar pull, and path length. These three metrics were chosen based on their relevance to common autonomous behaviors including mapping and collecting samples. They are also familiar metrics for users of NRMM and the Nepean Wheeled Vehicle Performance Model (NWVPM). Figure 3.6 shows the primary inputs for the metric as well as the workflow for optimization.

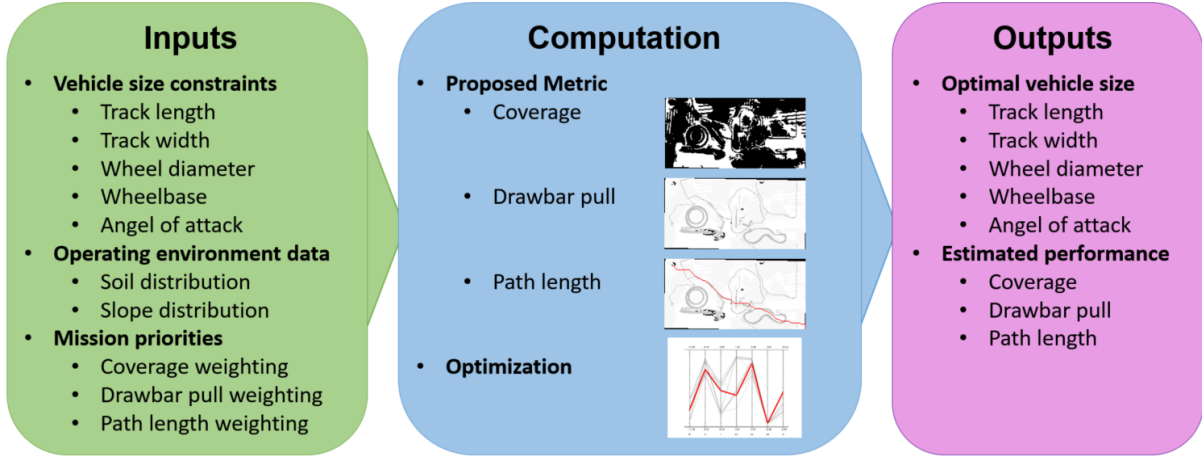


Figure 3.6: Information flow diagram for vehicle optimization based on terrain.

The equation for the proposed mobility metric (M) is:

$$M = c_a * A'_{cov} + c_{DP} * DP'_{avg} + c_{lp} * L'_p \quad (3.33)$$

where c_a , c_{DP} , and c_{lp} are the weights for coverage, drawbar pull, and path length, respectively. Just as in Chapter 2, the user must provide threshold and objective values for each section of this metric; a_{cov} , dp_{avg} , and l_p and the real vehicle values are scaled based on these. Unlike reconfigurability and complexity, mobility is a value that is meant to be maximized. So Equation 2.1 is rewritten as:

$$a'_{cov} = \min \left(\max \left(1 - \frac{0.2(a_{cov} - a_{cov,o})}{a_{cov,o} - a_{cov,t}}, 0 \right), 1 \right) \quad (3.34)$$

For the purpose of illustration, the dataset acquired for the NG-NRMM effort at The Keweenaw Research Center, in Calumet, Michigan in 2018 is utilized as our environment of interest[156]. This terrain and soil distribution are shown below.

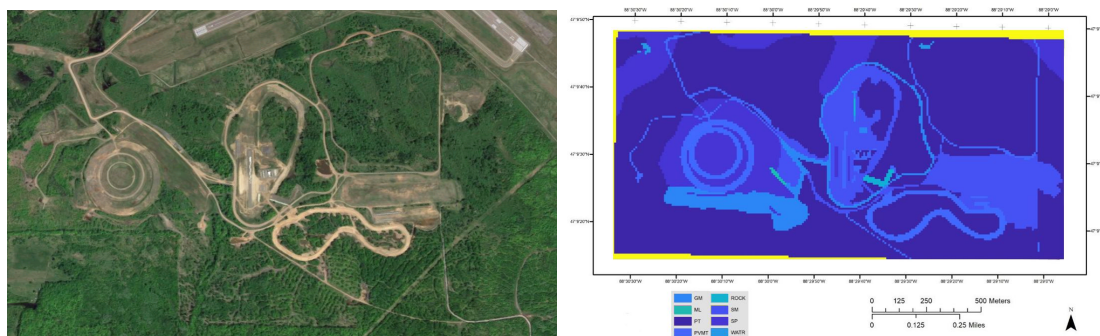


Figure 3.7: Left: Aerial View of Keweenaw Testing site obtained using Google Maps [157].

Right: Aerial View soil distribution at test site generated in MATLAB from .tif file in the NG-NRMM dataset [156]. Soil abbreviations refer to USCS classifications which are detailed in the ASME International’s USCS standard [158].

This dataset includes event information, reports, promotional videos, publications terrain data, test data, and vehicle data that are all free for download [159]. The data used for this work is from the terrain and soil information, which includes high resolution data about the terrain stored in Tagged Image Format (.tif) files.

Coverage is calculated by determining what proportion of the environment can be reached by the vehicle. In this implementation, a patch of terrain is determined accessible if the drawbar pull at that location is greater than 0. For NRMM, this value was displayed in GO/NO-GO maps. For this document, mobility of a tracked vehicle is documented, but equations for wheeled vehicles can also be substituted. Soil parameters were gathered from [132] [160], [161], and [162]. Drawbar pull is calculated using Equation 3.7 with 3.3 and equations 3.16 and 3.17 for compaction. Other resistances including aerodynamic resistance and rolling resistance are assumed to be negligible due to the low speeds that autonomous vehicles are expected to be navigating off-road [106].

Though the drawbar pull at a given location may be positive, it may not be reachable based on the traversability of the surrounding area. For example, a flat patch of packed clay may be inaccessible if it is encircled by steep slopes of sand. To account for this, a binary array is created representing crossability at each coordinate. An image is a good representation of this data structure where pixels of value 1 are pixels where drawbar pull is greater than 0 and pixels of value 0 are pixels where drawbar pull is 0 or negative. Then, the curves of accessible areas are found via Suzuki's border following algorithm [163] and the floodfill algorithm is implemented to fill areas of inaccessibility [164]. The image below shows pixel-based traversability and true reachability after filling in islands of reachability.



Figure 3.8: Left: Image of Keweenaw Research Center where black pixels are those with drawbar pull over 0 and white pixels are those with drawbar pull 0 or less. Right: Keweenaw Research Center with untraversable areas (white) filled.

The component of this metric documenting drawbar pull is a weighted average of the drawbar pull in the reachable areas. The values for drawbar pull at each coordinate found when calculating go/no go regions are used accounting for regions cut off by non-traversable areas. The metric is the sum of these values divided by the number of accessible pixels.

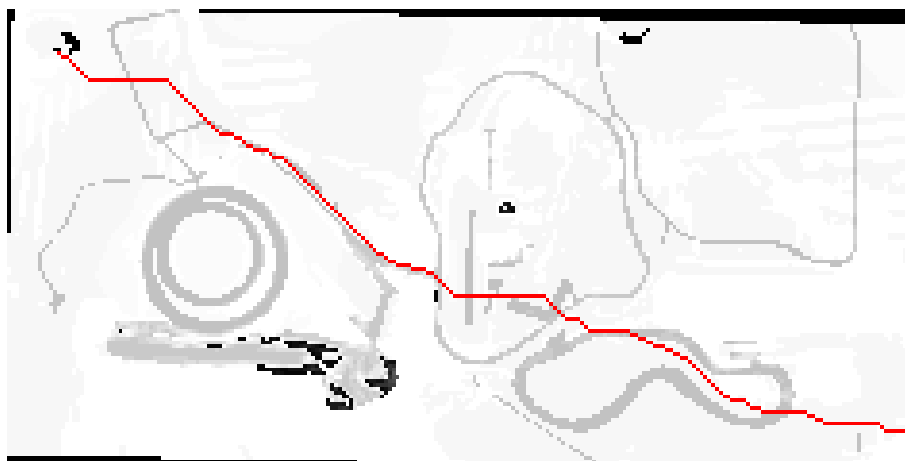


Figure 3.9: Left: Drawbar pull depicted by intensity of pixels with inaccessible regions removed with the shortest path through traversible terrain shown in red.

Speed-made-good has been another staple of NRMM calculations and is an area of focus for NG-NRMM [165]. included in this work from the lens of path planning. Average path length is calculated by measuring the increase in length between Euclidean distance between two test points and the shortest path that a vehicle could take in the given environment. To determine shortest path, the A* algorithm is utilized with Euclidean distance to the goal as the

heuristic, though other algorithms can be substituted[166]. Equation 3.35 represents this where $f(n)$ is the cost at node n , $g(n)$ is the sum of the cost from the start node to node n , and x and y are the coordinates of the node and the end node.

$$f(n) = g(n) + \sqrt{(x_e - x_n)^2 + (y_e - y_n)^2} \quad (3.35)$$

It was assumed that the vehicle could make point turns in all cases to get to adjacent points. Obstacles like rocks and trees were ignored. The robot was assumed to be able to travel to all neighbors in the graph. Since the distance between points was on the order of the size of the vehicles in question, this seemed like a fairly reasonable assumption. Pairs of points are successively chosen until the path length change converges to within 1%. This value is capped at 1 (i.e. a path that is double the original length) and subtracted from 1 such that each of the three elements of the metric is intended to be maximized.

In the absence of position-based soil and grade data, this metric can be distilled from an approximation of soil type distribution in combination with an estimate of grade distribution or a point cloud. For example, in 2008, the Yuma Proving Ground Middle East Desert vehicle endurance course (MEXC) was categorized by the Desert Research Institute and U.S. Army to give a distribution of ground cover [167]. Alternatively, for a point cloud data set, Delaunay triangulation can be used to create edges between the points [168]. The figure below shows a Delaunay triangulation mesh generated from a point cloud obtained from OpenTopography with various paths plotted with different vehicle parameters using the A* algorithm [169]. In this case, the edges of the graph are the edges of the triangle, and from each node, there are up to two nodes added to the open list at any one time. Therefore the time complexity is $O(2^h)$ where h is the depth of the solution path. The space complexity is the same as all open node costs and backpointers must be stored until the algorithm terminates. This algorithm was chosen because it is complete, ubiquitous, and straightforward to implement for this situation. It is not ideal for larger datasets and an algorithm like D* would be less space-intensive [170].

The point cloud data in Figure 3.10 taken is of meteor crater in Winslow, Arizona, USA to demonstrate the dramatic effect that slope climbing ability can have on path length. Even keeping other variables the same, assuming uniform distribution of soil, the vehicles with 30° and 20° slope climbing ability had a 22% and 97% longer path compared to the vehicle with 40° ability for this start and endpoint pair. For this work, it is assumed that a vehicle can turn in place such that it can reach any point in the graph from a neighboring point.

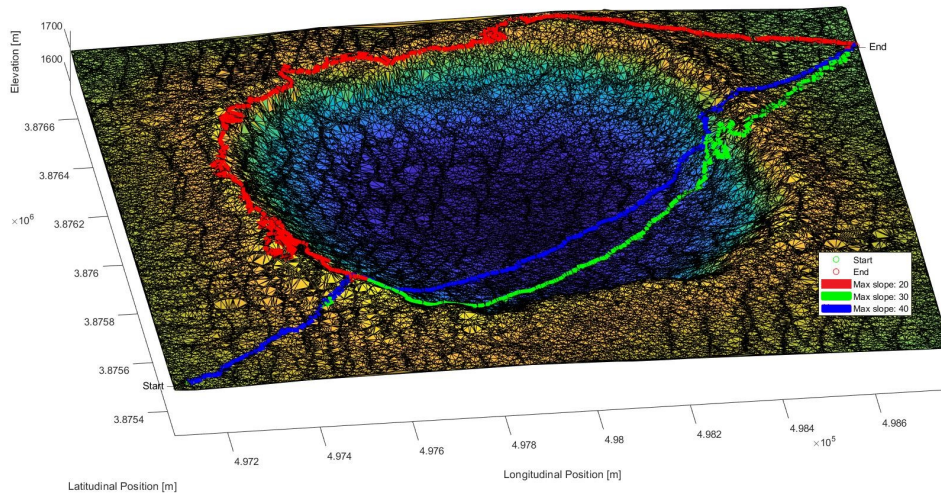


Figure 3.10: Mesh view of Meteor Crater with shortest paths plotted for candidate vehicles with 20, 30, and 40deg slope climbing capacity. The map is downsampled to 1/300th of original density for ease of visualization.

Each of the three components of the mobility metric is normalized, so they can be weighted and summed. However, it is also possible to treat this problem as a multi-objective problem and keep each of the three sections separate. In this case, it would be necessary to manually select from candidate optima or use pseudo weights to determine the best solution in a three-function setup.

3.3.1 Choosing Constants

For mapping missions, the greater percent of territory that the vehicle can cover, the lower the perception burden to map the environment [92]. Being able to physically traverse a greater fraction of the environment means that the vehicle does not need to rely on sensors to capture untraversable regions or extrapolate data from other sources.

For search and rescue missions, coverage and path length are the key elements of mobility [92]. These two features are linked in that a greater coverage means that the path length can be shorter for a greater percentage of the environment.

In transportation environments, drawbar pull is the primary defining factor of mobility [171]. Path length is also a key feature in order to perform the transportation efficiently, but this is not as impactful as drawbar pull.

Table 3.3: Sample mobility constant values.

System	c_a	c_{DP}	c_{lp}
Mapping	1	0	0
Searching	0.2	0	0.8
Transporting	0	0.8	0.2

3.4 Metric Implementation

To demonstrate the alignment and uniqueness of the proposed metric, eleven tracked vehicles are compared. For each vehicle, $c_A=0.5$, $c_{DP}=0.25$, $c_L=0.25$, $A_{cov,t}=0.75$, $A_{cov,o}=1$, $DP_{avg,t}=0.01$, $DP_{avg,o}=0.05$, $L_{avg,t}=1$, and $L_{avg,o}=0$. For comparative purposes, the maximum M and DP , and the minimum VCI and MMP among all configurations are given for each vehicle.

3.4.1 ATHLETE

ATHLETE is on the larger side of rovers explored in this work at 850 kg [75]. Its six wheels measure 0.5 m in diameter and 0.17 m wide, which is comparatively small for a vehicle of this size. The vehicle has a high ground clearance at 2.5 m, which aids its VCI measurement. It can access 66% of the terrain of interest, which scales to a A_{cov} of 0.73. The average path length increase is 31.5%, which scales to a L_p of 0.94. And the average DP is 0.016 kN, which scales to DP_{avg} 0.83. The overall mobility metric M is 0.81.

3.4.2 AZIMUT

AZIMUT features four tracks and a maximum combined track length of 1.2 m on each side [6]. It weighs 63.5 kg and features continuous tracks. Its VCI comes out to 13.4 psi and its MMP to 38.93 kN. It can reach 98% of the terrain of interest with a drawbar pull greater than 0. Its average path length increase on this terrain is 8% and its average drawbar pull on accessible terrain is 0.007. This sums to a M value of 0.93.

3.4.3 EHR

EHR possesses four large wheels measuring 0.56 m in diameter and approximately 0.25 m wide [76]. The vehicle has a very low MMP for its 150 kg weight due to these wide wheels. The EHR was designed to take on the challenging environment of the Amazon rainforest. It can traverse 66% of the terrain of interest. Its average path increase is 31.5%, and it has an average drawbar pull of 0.03. This results in a $M = 0.5 * 0.73 + 0.25 * 0.94 + 0.25 * 0.91 = 0.83$

3.4.4 El Dorado II A

The El Dorado II A features four 0.2 m wheels measuring about 0.1 m wide [77]. This 23.8 kg robot has a A_{cov} of 0.73, an L_{avg} of 0.94, and a DP_{avg} of 0.77, resulting in a M of 0.79.

3.4.5 MAMMOTH

The 75-kg MAMMOTH Rover spreads its weight over four 0.17 by 0.08 m wheels[78]. Its ground clearance can be as much as 0.68 m in its extended position. The vehicle can access 66% of the test terrain, has an average path length increase of 31%, and has an average drawbar pull of 0.003 kN. The coverage and drawbar pull values are slightly below threshold and the path length increase is over threshold, which brings the overall M to 0.79.

3.4.6 MARS mini

In 4-wheel configuration, the MARS mini weighs 9.3 kg [79]. The vehicle has 0.254 m diameter wheels measuring 0.0635 m wide. The vehicle has a drawbar pull of 0.07 kN in the sand and 0.62 kN on silty sand. A_{cov} for this vehicle calculates to 0.94, L_p to 0.98, and DP_{avg} to 0.94. The overall M is 0.95.

3.4.7 NeWheel

The NeWheel configuration considered for this metric is 6.5 kg and has four rigid wheels measuring 0.208 m in diameter [80]. The lack of deformation in these wheels decreases their contact area compared to the similarly sized MARS mini robot. This vehicle can reach 0.86% of the given terrain, has an average path length increase of 8.1%, and an average drawbar pull of 0.01. Its total mobility metric with the given constants is 0.89.

3.4.8 Polybots

The Polybots system can only articulate at the center and has incomparable locomotion to the other vehicles examined. When connected together, they can form a mobile tread, but because they cannot use traditional terramechanics equations, they are omitted from this analysis [53].

3.4.9 SRR

The SRR system has four 20-W motors actuating four 0.2 m diameter wheels [81]. It has the potential to reach 70% of the terrain of interest and has an average path length increase of 9.8%. The average drawbarpull in this area os 0.0033 kN, making the M 0.82.

3.4.10 SUGV

The SUGV [82] vehicle measures 13 kg, has a contact length of 1.28 m when fully extended, and has .17 m diameter sprockets. The track of this vehicle is continuous and approximately .1 m in width. A_{cov} is 0.98, L_p is 0.98, and DP_{avg} is 0.8, which results in $M = 0.5 * 0.98 + 0.25 * 0.98 + 0.25 * 0.8 = 0.93$

3.4.11 VAL Modular Vehicle

The VAL testbed can reconfigure between wheels and tracks. In track configuration, the vehicle is 7.47 kg with .1143 m diameter sprockets, 0.4 m track length, and 0.05 m track width. The vehicle can theoretically traverse 94% of the test field, has an average path length increase of 8.1%, and an average drawbar pull of 2.3 N.

3.4.12 Wheel-Track Robot by Gao, et al.

For its size, the wheel-track developed by Gao, et al. [84] has a wide track. It is able to traverse 94% of the test terrain, has an average path increase of 8.1%, and has an average drawbar pull of 3.4 N. The mobility metric is therefore $M = 0.5 * 0.95 + 0.25 * 0.98 + 0.25 * 0.77 = 0.91$

3.5 Discussion

Table 3.4 shows a comparison of the proposed metric with existing metrics. $M_{proposed}$ comes from Equation 3.33, DP comes from Equations 3.3, 3.7, 3.17, MMP comes from [9] and VCI comes from [9]. Soil properties were obtained from [106] and [160].

Table 3.4 demonstrates how the proposed metric can capture data from across a mission, instead of just a snapshot at a particular type of terrain. Cells marked with an asterisk represent vehicles that were too light to calculate a VCI. These vehicles yield a negative VCI, which has no physical meaning. Due to their unusual locomotion strategy, there is no representation for the mobility performance of the Polybots. They do not contain wheels, tracks, or legs, but together can form any of these shapes.

Depending on the soil, drawbar pull alone could be an overly conservative or overly optimistic assessment of vehicle performance. MMP and VCI also represent perceived performance on a given terrain, but lack direct traceability to measurable entities.

Table 3.4: Comparison of reconfigurability with the proposed and other definitions.

System	M	DP_{sand} [kN]	DP_{clay} [kN]	MMP [kPa]	VCI_1 [psi]
ATHLETE [75]	0.81	6.28	10.51	0.03	60.32
AZIMUT [6]	0.93	0.47	3.31	38.93	13.4
EHR [76]	0.83	1.11	6.08	0	7.66
El Dorado II A [77]	0.79	0.18	1.01	0	0*
MAMMOTH Rover [78]	0.79	0.55	1.27	0.02	0*
MARS mini [79]	0.77	0.07	0.62	0	0*
NeWheel [80]	0.76	0.05	0.47	0	0*
Sample Return Rover [81]	0.82	0.05	0.87	0	0*
SUGV [82]	0.93	0.1	3.84	6.1	3.13
VAL Modular Vehicle [83]	0.91	0.05	0.96	9.48	7.74
Wheel-Track [84, 85]	0.91	0.19	1.49	24.1	12.9

3.6 Conclusions

The metric presented in this work is customizable, enabling the user to tune the weightings to suit their priorities. The system was designed with autonomous systems in mind, including key variables of interest like coverage and path length. It is also inherently relevant to the environment of opportunity as it uses this data to drive each of the three elements of the objective. The metric is also readable by nature, using meaningful proportions of objective values as

comparison, as opposed to unitless values or incompatible functions. It is able to capture more information than existing metrics while still being quantitative and able to be optimized.

In the future, even more autonomous-specific parameters could be included including considerations for perception and odometry. Additionally, probability could be introduced like in [172] to increase the robustness of the calculations. Finally, more advanced physics-based simulations could be paired with this metric in order to drive more precise optimization. Combination of this metric and NG-NRMM systems [156], DEM simulation[12], or multibody simulation software would further increase the utility of this metric.

Chapter 4

Combining Varied Markers of Complexity for Unmanned Ground Vehicles

4.1 Introduction

In engineering, complexity is the measure of how interconnected or intricate a system is. Complexity can be used to describe the design problem, process, and product and typically includes size (in the broad sense), coupling, or solvability [173]. In computer science, complexity is typically thought of in terms of the time or resources required for an algorithm to run [174]. Since this thesis focuses on mechanical reconfigurability, the former definition is more relevant. However, computational complexity will be touched on in the form of control considerations.

High complexity is typically undesirable because it makes the system difficult to design, create, and/or analyze [175]. In the automotive industry, 64% of managers agreed or strongly agreed that complexity is a major cost driver [176]. Dieter and Schmidt advocate that mechanical design, user interface, and function should all be implemented in the simplest manner possible [88]. However, sometimes complexity is unavoidable or can add flexibility and adaptability [177] that can benefit consumers. TRIZ (or "TIPS" - "Theory of Innovative Problem Solving") highlights such trade-offs as examples of contradictions. These contradictions can be physical (e.g. the vehicle gets heavier as additional mechanisms are added) or technical (e.g. a software becomes more capable but harder to use) [178].

[179] proposes that good design has the minimum complexity for a given performance. And that suboptimal design is any design that does not meet minimum performance standards or that increases complexity without increasing performance.

Robotic mobility [180], grasping [181, 182], perception [183], and overall design [184] are all areas of robotics where mechanical simplicity is a key design driver. Steering is a common example where the increased number of degrees of freedom can result in increased maneuverability, increased controllability, and decreased required driving power during a turn [180]. These additional degrees of freedom come at the cost of additional actuators, which add to the volume, weight, and cost of the system.

However, the connection between complexity and off-road ability is not always proportional. In 2012, a study was conducted at the University of Vermont with evolutionary robots in

five different complex environments. Their findings showed that the ideal robot for the simplest environment had at least one degree of freedom higher than every other condition. The authors proposed that this may have been because of the limited possible movement in the simpler environments and the smaller number of possible configurations to achieve this limited movement [185].

4.2 Background

In 1999, Bashir and Thomson developed a simple method for estimating the complexity of a product ($C_{Bashir-Thomson}$) as:

$$C_{Bashir-Thomson} = \sum_{j=1}^l F_j j \quad (4.1)$$

where F_j is the number of functions at level j and l is the number of levels [186]. (In their work this value is named PC , but it has been renamed here to avoid conflict with pull coefficient.)

Tamaskar et al. cite seven different considerations for evaluating complexity: level of abstraction, system representation, structure/function, size (number of components and interactions), heterogeneity of components and interactions, network topology, dynamics involving different modes of operation, and off-design interactions. As a metric, they propose a weighted sum of a size metric $\Lambda \ln \lambda$ and coupling metric $\sum_{j=1}^c j \sum_{i=1}^n W_i \sum_{k=1}^m W_k$ where λ is the number of unique components, Λ is the total number of components, c is the number of cycles, j is the size of the cycle, W_i is the weight of link i , and W_k is the weight of a link not in a cycle [179].

In 2010, Summers and Shah created expressions to describe each of these forms of complexity for each stage of design. In their article, "Mechanical Engineering Design Complexity Metrics: Size, Coupling, and Solvability" they also present a comparison of 13 different previously existing metrics [173]. Their method for calculating the complexity of the size of the design problem relates to the number of primitive modules available in a specific representation (M^0), the number of relationships available between all available modules (C^0), the number of independent variables (idv), the number of dependent variables (ddv), the number of relations (dr), and the number of variables that describe the measure of goodness (mg) in the following equation [173]:

$$Cx_{size_{prob}} = (M^0 + C^0) \times \ln|idv + ddv + dr + mg|. \quad (4.2)$$

Similarly, their equation for the complexity of the design process uses these same variables [173]:

$$Cx_{size_{art}} = (M^0 + C^0) \times \ln|idv + ddv + dr|. \quad (4.3)$$

Finally, the measure of the size complexity of the final product also incorporates the number of unique process types P_{op} , the number of analysis operators (a_{op}), the number of evaluation operators (e_{op}), the number of synthesis operators (s_{op}), and the number of representing mapping operators (r_{op}) [173].

$$Cx_{size_{process}} = ((M^0 + C^0 + P_{op}) \times \ln|idv + ddv + dr + mg + a_{op} + e_{op} + s_{op} + r_{op}|). \quad (4.4)$$

Summers has also developed a measure of coupling complexity together with collaborators for any type of graph [173]. This method relies on recursively counting connections between nodes for each dividable version of the entire graph.

Complexity in solvability is largely determined by subject-specific coefficients or by examining the total number of degrees of freedom (DOFs) [173]. The Chebychev–Grübler–Kutzbach Criterion provides a way to estimate the number of degrees of freedom based on number of joints and the degrees of freedom of each joint [187]. For an open chain, that is a mechanism whose links do not form a loop, the total number of degrees of freedom (M in the literature but n_{DOF} here to not overload the variable M) is:

$$n_{DOF} = 6n - \sum_{i=1}^j (6 - f_i) \quad (4.5)$$

where n is the number of moving bodies, j is the number of joints, and f_j is the number of DOFs at that joint.

TRIZ defines complexity in terms of number of elements, interconnectivity, and difficulty of use [188]. The first two of these characteristics are relevant for unmanned systems and the final element could be reframed as difficulty of control.

4.3 Proposed Metric

To quantitatively present the complexity of a given design, we propose a metric that considers the number of actuators, number and size of linkages, and degrees of freedom. It is desirable to keep the number of actuators down both to reduce the monetary cost and lessen the control burden. Summers and Shah also point out the importance of separating both number of links and the length of the links since their connections, and therefore their contribution to complexity, can differ greatly [173]. These attributes are relevant to a wide variety of small unmanned vehicles and can be evaluated without a high degree of subject matter expertise. We combine these in the following equation:

$$C = c_{act} * N'_{act} + c_{nl} * N'_{linkages} + c_{DOF} * \max(n_{DOF,i})'. \quad (4.6)$$

In this equation, each c represents a constant from 0 to 1 for how important it is to minimize that aspect of complexity. These constants must sum to 1 for uniformity and to ensure that this combined sum is also constrained between 0 and 1, inclusively.

$N'_{actuators}$ is a scaled total number of the actuators in the system. This value is calculated in the same way as 2.3 using threshold and performance values for the number of actuators. $N'_{linkages}$ and $\max(n_{DOF,i})'$ are also calculated using the user's limits on number of linkages and number of degrees of freedom, respectively. Like the others, this metric is unitless, so its value lies in comparison while maintaining the constant values.

4.3.1 Choosing Constants

Constants for the complexity metric are primarily determined by the tradeoff of mechanical and programmatic risk appropriate for the mission. For example, a precision system operating in a lab setting with a very controlled environment may not be affected by external stresses on the actuators and linkages. In this case, it is ideal to bring down the length of the links and degrees of freedom in order to ease control and decrease aggregated error. Though design for assembly dictates that fewer components is ideal [189], the number of parts typically increases over iterations for electromechanical systems at the prototype or experiment phase [190].

When a system needs to sustain itself for a long time in the field or a foreign planet, it is paramount that it be as reliable as possible [191]. Such systems are also bound by the previous discussion of accumulated error in link lengths. Vehicles operating in an austere environment without need for precision control would benefit from fewer actuators and number of links, but link length would likely not impact mission success negatively by exacerbating error. A high-precision field robot would have the biggest impact by number of degrees of freedom of its longest link, but still need considerations for number of actuators and number of linkages since the vehicle could not easily be fixed in the field.

For consumer products, as examined in [88], cost is often the deciding factor. Since actuators and their associated control and power requirements are typically more expensive than links, this portion is most heavily weighted. However, equal weight is given to number of links and link length as an issue in either dimension would not likely be easily fixed by a consumer.

Example constant combinations are listed in Table 4.1.

Table 4.1: Sample complexity constant values.

System	c_{act}	c_{nl}	c_{DOF}
High-precision - Lab	0	0	1
High-precision - Field	0.25	0.25	0.5
Low-precision - Lab	0.5	0.5	0
Low-precision - Field	0.4	0.4	0.2
Production - Civilian	0.5	0.25	0.25

4.4 Metric Implementation

The same example vehicles presented in Chapter 2 are used as test cases for this metric. For this analysis, we use the low precision field variables with $c_{act} = 0.4$, $c_{nl} = 0.4$, and $c_{DOF} = 0.2$. We set the threshold and objective values for number of actuators to 8 and 4, the threshold and objective values for degrees of freedom for one link to 2 and 1, and the threshold and objective values for number of linkages to 4 and 2, respectively.

4.4.1 ATHLETE

The ATHLETE rover is highly articulated, with 36 total actuators [75]. When scaled using the threshold and objective values, this value becomes 1.6, which is capped at 1. The 36

motors are distributed between 6 legs, with each leg having an $n_{DOF,i}$ of 6. Therefore $C = 0.4 * 1 + 0.4 * 0.4 + 0.2 * 1 = 0.76$.

4.4.2 AZIMUT

AZIMUT has 12 actuators distributed on 4 legs [6]. 6 of these motors are used to articulate the tracks and 4 are used to actuate the tracks. Therefore, $n_a=12$, which scales to 0.4, $n_{nl}=4$, which scales to 0.2, and $n_{DOF}=3$, which scales to 0.4. This yields a cumulative $C = 0.32$.

4.4.3 EHR

The EHR features 8 total actuators, so $n_a=8$ [76]. Half of these actuators reorient the struts for the wheels and half of them rotate the wheels themselves. This means that each of the 4 linkages ($n_{nl}=4$) has two degrees of freedom ($n_{DOF}=2$). And the total $C = 0.4 * 0.2 + 0.4 * 0.2 + 0.2 * 0.2 = 0.2$. This value represents a system that exactly meets the overall threshold value of 0.2 but it may have violated certain individual thresholds.

4.4.4 El Dorado II A

El Dorado II A utilizes 4 motors to steer and 4 motors to move its wheels [77]. Therefore $n_a=8$, $n_{nl}=4$, and $n_{DOF,i}=2$. After scaling, this gives a total complexity of $0.4 * 0.2 + 0.4 * 0.2 + 0.2 * 0.4 = 0.24$.

4.4.5 MAMMOTH

MAMMOTH has 16 degrees of freedom ($n_d=16$) enabled by 16 motors ($n_a=16$), 4 on each (l_i) of 4 legs ($n_l=4$) [78]. These result in scaled values of 0.6, 0.2, 0.2, and 1, respectively, and a cumulative C of 0.5.

4.4.6 MARS mini

The MARS mini vehicle can have a variable number of motors depending on the configuration [79]. The maximum typical value n_a is 4. Using manual reconfigurability, the vehicle can also change the position of each of these 4 wheels. This yields a complexity of $0.4 * 0 + 0.4 * 0.2 + 0.2 * 0 = 0.08$.

4.4.7 NeWheel

The NeWheel system can also have a variable number of wheels, with the largest common variant having $n_a = 4$ [80]. Just like the MARS mini system, each wheel can be repositioned and the overall C is 0.08.

4.4.8 Polybots

An individual Polybot is a rather simple system with one rotational motor and one motor on each side to enable connection to other Polybots [53]. Examining a single Polybot, $n_a=3$, $n_{DOF,i}=3$, $n_l=1$, and $l_i=3$. Therefore the overall complexity is $0.4 * 0 + 0.4 * 0 + 0.2 * 0.4 =$

0.08. Though this vehicle exceeded the threshold value for number of degrees of freedom, this parameter was weighted less and the overall C was still less than 0.2.

4.4.9 SRR

Ignoring the manipulator portion of the Sample Return Rover, this vehicle has $n_a = 6$ accounting for 4 wheels and 2 active rocker systems [81]. These $n_l=2$ sides couple the left and right motors in such a way that the degrees of freedom of each linkage is $n_{DOF,i}=2$. Therefore the C is $0.4 * 0.1 + 0.4 * 0 + 0.2 * 0.2 = 0.08$.

4.4.10 SUGV

FLIR's SUGV can be deployed with various manipulators and payloads, which are omitted for the purpose of this comparison [82]. The base model has $n_a=3$ with 2 for the tracks and 1 for the front paddles. Each of the two links (left and right track) have $n_{DOF,i}=2$. Therefore $N_a=N_d=0$ and the overall C value is also 0.04. The vehicle has many points of adjustability, but almost no intermediate mechanisms between the motor and the part that interacts with the ground.

4.4.11 VAL Modular Vehicle

Each of the six wheels or sprockets on the VAL vehicle is powered by their own motor [83]. If each wheel station is a link, there are 6 links each with $n_{DOF,i}$ of 1. Therefore the C is $0.4 * 0.1 + 0.4 * 0.4 + 0.2 * 0 = 0.2$.

4.4.12 Wheel-Track Robot by Gao, et al.

In terms of complexity, the [84] vehicle has five motors ($n_a=5$), two for the track, two for the transformation structure, and one for the tail. Each expanding linkage is comprised of a specially formed four-bar linkage. The tail is one single member. The vehicle has five degrees of freedom (each wheel can move independently, each track can expand independently, and the tail can be positioned). The proposed complexity metric does not have a means of describing the complexity added by the expanding track. This results in an overall complexity value of $C = 0.25 * 0.05 + 0.25 * 0.1 + 0.22 * 0.2 = 0.1$ for the vehicle.

4.5 Discussion

The complexities for each system are documented in Table 4.2 compared to degrees of freedom, n_{DOF} (Equation 4.5), and Bashir and Thomson's complexity metric, $C_{Bashir-Thomson}$ (Equation 4.1). As previously stated, additional perception and manipulation payloads were removed from these comparisons.

Like our proposed reconfigurability and mobility metrics, the complexity metric only varies between 0 and 1. Here, vehicles with a complexity below 0.2 are closer to the ideal parameters established by the user. It is possible to still exceed some of the threshold values, but the weightings provided by the user should favor the aspects that the user most cares about. The vehicles with more than 12 motors (ATHLETE, MAMMOTH) also had the highest number of

links, which in turn drove up their complexity cost. The best scoring systems were the SUGV and Polybots, which each just have 3 motors. The Wheel-Track and Sample Return Rover also had low complexity metric values as they had comparatively fewer motors, links, link lengths, and degrees of freedom.

Table 4.2: Comparison of complexity metric with the proposed and other definitions.

System	C	n_d	$C_{Bashir-Thomson}$
ATHLETE [75]	0.76	36	151
AZIMUT [6]	0.32	12	54
EHR [76]	0.2	8	16
El Dorado II A [77]	0.24	10	38
MAMMOTH Rover [78]	0.44	16	70
MARS mini [79]	0.08	8	38
NeWheel [80]	0.08	8	38
Polybot [53]	0.08	3	16
Sample Return Rover [81]	0.08	6	28
SUGV [82]	0.04	3	16
VAL Modular Vehicle [83]	0.2	8	27
Wheel-Track [84, 85]	0.1	5	23

Degrees of freedom happened to correlate to the complexity metric for the most part, which makes sense as it is one element of the metric. However, this value alone does not capture how interconnected these degrees of freedom are. A vehicle with six single-link arms would likely be much easier to control than a vehicle with one six-linked arm as any error, uncertainty, or dynamic effects that happen to one part of the arm would affect the other parts of the arm, as well.

The Bashir-Thomson criterion correlates to some of the complexity metric values, but not all of them. The MARS mini and NeWheel platforms have higher $C_{Bashir-Thomson}$ values compared to the Wheel-Track systems primarily because they have more motors that must be powered, controlled, and measured. In the $C_{Bashir-Thomson}$ metric, each of these levels is summed. This is helpful from a software perspective, but may overestimate the mechanical implications of additional components. Components that are similar to existing subsystems can be readily added without the full burden of adding the original subsystem [47].

It is difficult to compare complexity metrics quantitatively since there is no unit for complexity. Bashir, Thompson, and others have come up with estimations of design effort based on product complexity that put effort in terms of time [192]. Though this would create a constant unit with which to compare metrics, it may not be as applicable to robotics since ongoing

actions after design like planning, control, and usability have a large influence on a design's effectiveness.

4.6 Conclusions

Our metric allows the user to specify acceptable limits on the number of actuators, number of linkages, and number of degrees of freedom, which are all relevant for robotics. The number of actuators affects power consumption and locomotion gaits. The number of linkages can affect redundancy and can present challenges for simultaneous control. Higher link length complicates inverse kinematics and can propagate errors. And degrees of freedom affect planning and control schemes. The three tunable constants allow a designer to tweak the metric to be most responsive to their design priorities. In this way, a single number can represent how complex a system is relative to the user's situation.

Chapter 5

Optimizing Reconfigurability, Mobility, and Complexity

5.1 Introduction

Chapters 2, 3, and 4 lay out three metrics for evaluating a vehicle. These elements can be combined to provide a single number that can be used to compare vehicles. For our work, mobility is the parameter that we want to maximize. Complexity and reconfigurability cost are both values to minimize. This chapter discusses the methods and challenges of combining disparate metrics with many design parameters.

5.2 Background

A concept-scoring matrix is a tool used to make design decisions based on a tradeoff of multiple criteria [67]. Typically, requirements are made for a system, subsystem, or component, and from these requirements, performance measures are extracted. These performance metrics are given weights based on their importance. Then, each prospective system, subsystem, or part is rated for each of the performance metrics. This rating is then multiplied by the respective weight and all these components are summed to generate one score for the vehicle. This is an effective way of discerning the tradeoffs between different designs. A weak point of this process is that the ratings can be subjective and limited by the number of possible ratings. (Ratings are typically whole numbers between 1 and 3 or 1 and 10, for example.)

Multiobjective optimization is a method for deriving ideal parameters based on multiple different objectives. Many optimization strategies have their history in economics with Edgeworth [193] and Pareto [194] providing the foundations for deriving the optimum solutions for problems with multiple priorities. Goal programming is one strategy pioneered in 1955 by [195] that involves building a series of objectives, assigning penalties for missing these objectives, and then minimizing the sum of these penalties. Evolutionary algorithms are a popular a posteriori method for multiobjective optimization used in fields ranging from computing to neuroscience. The most popular embodiment is a genetic algorithm where better points are successively found by selecting variables, evaluating their "fitness", and discarding the lower scoring variables.

Optimization is now utilized in almost every component of vehicle design and in engineer-

ing design processes such as [196]. Multi-objective programming techniques have been used to design planetary rovers using mass, power consumption, sinkage, and dynamic stability as objective functions [197]. A similar strategy has also been implemented on the parameters of a reconfigurable off-road rover with stability margin and traction as driving factors [198].

5.3 Methods

5.3.1 Element-wise Comparison

One of the simplest methods for evaluating a system is to compare its performance to other alternative systems. Table 5.1 shows the values of the proposed metrics (described in 2.3.2, 3.3, and 4.4) for the vehicles explored throughout the earlier chapters.

Table 5.1: Comparison of various platforms based on the proposed metrics of reconfigurability, complexity, and mobility.

System	RC	M	C
ATHLETE [75]	0.05	0.81	0.76
AZIMUT [6]	0	0.93	0.32
EHR [76]	0.085	0.83	0.2
El Dorado II A [77]	0.5	0.79	0.24
MAMMOTH Rover [78]	0.215	0.79	0.44
MARS mini [79]	0.59	0.77	0.08
NeWheel [80]	0.14	0.76	0.08
Sample Return Rover [81]	0.06	0.82	0.08
SUGV [82]	0	0.93	0.04
VAL Modular Vehicle [83]	0.5	0.91	0.2
Wheel-Track [84, 85]	0.41	0.91	0.1

It is important to remember that the RC and C values are costs while the M is a performance value. Interestingly, one of the highest scoring vehicles for mobility, the SUGV vehicle, has the lowest reconfigurability cost and complexity. This means that the vehicle achieved preferred coverage and drawbar pull while not exceeding the objective complexity requirements. The VAL rover, on the other hand, scored similarly in mobility with a M of 0.91, but had RC and C values over 0.2, which means that it exceeded the threshold values for these metrics. The NeWheel system had the lowest Mobility metric but also fairly poor reconfigurability cost and complexity cost.

This information is plotted in the following 3-dimensional graph with mobility metric on the vertical axis.

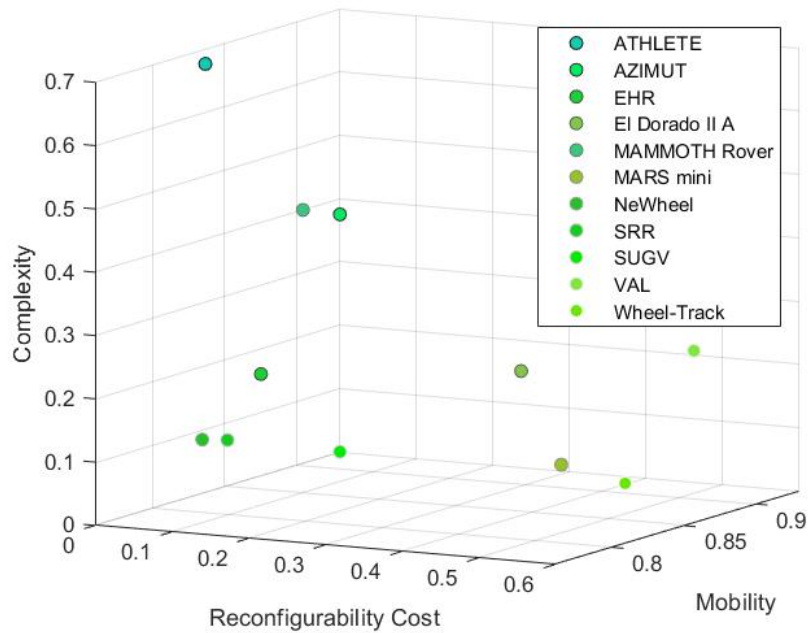


Figure 5.1: Plot of proposed mobility metric versus proposed reconfigurability and complexity metrics.

The 3-dimensional graph and table can be helpful if one of the variables is definitively most important. For example, if maximizing the mobility was most valuable, then only the designs with the highest mobility could be examined and then complexity and reconfigurability cost could be secondary considerations. But if all three parameters are important, such a graph is not easily interpreted.

5.3.2 Aggregated Analysis

We can combine the metrics for reconfigurability, mobility, and complexity into a single function. Three constants, c_R , c_M , and c_C are used to weigh the relative importance of each attribute reconfigurability, mobility, and complexity respectively. We choose weights that sum to 1 based on qualitative importance of each metric.

In order for these scaling values to prioritize the three elements as we specify, it is necessary to normalize the values first. Since our three metrics were made to scale to 0, it is not necessary to reportion them, but it is necessary to take the complement of the cost values (reconfigurability and complexity) so that the aggregated value is one that is intended to be maximized. Our new values are $R' = 1 - R$ and $C' = 1 - C$. Now the sum will reflect how closely our vehicle adheres to the threshold values that we set, where a value over 0.8 is likely to be over our threshold in the categories we value. For this analysis, we use $c_R=0.1$, $c_M=0.7$, and $c_C=0.2$.

Table 5.2: Table of Aggregated Reconfigurability, Mobility, and Complexity Value.

System	<i>AggregatedValue</i>
ATHLETE [75]	0.71
AZIMUT [6]	0.89
EHR [76]	0.83
El Dorado II A [77]	0.76
MAMMOTH Rover [78]	0.74
MARS mini [79]	0.76
NeWheel [80]	0.8
Sample Return Rover [81]	0.85
SUGV [82]	0.94
VAL Modular Vehicle [83]	0.85
Wheel-Track [84, 85]	0.88

As we observed in the element-wise comparison, the SUGV vehicle had the best cumulative score due to high marks in the three metrics. The AZIMT and Wheel-Track vehicles had the next highest cumulative scores. These vehicles had high M values, which was the metric that we rated most highly for this comparison. Most of these vehicles have values around the 0.8 mark, which is the value we selected for threshold performance.

5.3.3 Optimization Algorithms

Another way of reframing this problem is using optimization algorithms. For our purposes, we set up the problem as a seven-variable mixed optimization (weight, width, track length, diameter, reconfigurability dynamics, reconfigurability style, and reconfigurability extent) with three objective functions (reconfigurability cost, mobility, and complexity). The entirety of this system is dubbed "RMCVO" for Reconfigurability, Mobility, and Complexity Vehicle Optimization.

Since each metric is already scaled between 0 and 1, this problem could be structured as a single objective optimization problem with the summation process discussed in Section 5.3.2. However, the three are kept separate for this work to better illustrate the three separate components that come together for this optimization.

For weight, width, track length, and diameter, the minimum and maximum values for each dimension are set by the user. These variables are floats with precision to the tenths place. The options for reconfigurability dynamics are 0, 1, or 2. These represent no reconfigurability, manual reconfigurability, and self-reconfigurability. The options for reconfigurability style are integers 0 through 18, representing the styles documented in Table 6.1. Finally, extent of reconfigurability can vary continuously from 0 to 2, representing no reconfigurability or doubling a feature. Vehicles with 0 dynamic reconfigurability were constrained to tracked vehicles and their extent of reconfigurability was set to 0.

The reconfigurability dynamics, style, and extent determined the RC and C values through the empirical functions defined in Chapter 2. M was calculated based on the type of vehicle

(set by the reconfigurability style) and then the maximum drawbar pull at each pixel of terrain between the vehicle configuration(s) calculated following the process in 3.3.

A classic genetic algorithm (GA) [199] and the Non-Dominated Genetic Source Algorithm II (NSGA-II) [200] were selected because of their multiobjective and mixed variable abilities. The classic GA uses a $\mu + \lambda$ evolutionary strategy. The NSGA-II algorithm divides parent-offspring pairs into fronts before discarding less ideal pairs. It also has a parameter to encourage diversity to avoid local minima. There is no assurance that all the Pareto optimal points are found through this method, but all points found do not dominate one another.

Once a Pareto plot is obtained, it is still necessary to select the "best" point from a series of Pareto optimal points. It is possible to use pseudo weights to scale the objective values based on the weights after normalizing, perhaps by ideal and nadir points. However, since each metric was scaled between 0 and 1 with threshold and objective functions at the 80% mark, we do not scale the points in order to keep this meaning. Here, the ideal points are the minimum sum of products of the metrics (or metric complements as explained in 5.3.2 and their weights (c_R , c_M , and c_C)). Figure 5.2 shows a parallel coordinate plot of the design variables throughout both algorithms using a population size of 20. 20 was chosen as the population size through trial and error because it offered a good combination of allowing multiple different combinations without homing in too quickly within one iteration. The number of iterations were tested between 10 and 1,000. There was not a significant change in the number of Pareto optimal points found during 20 iterations compared to 1,000.

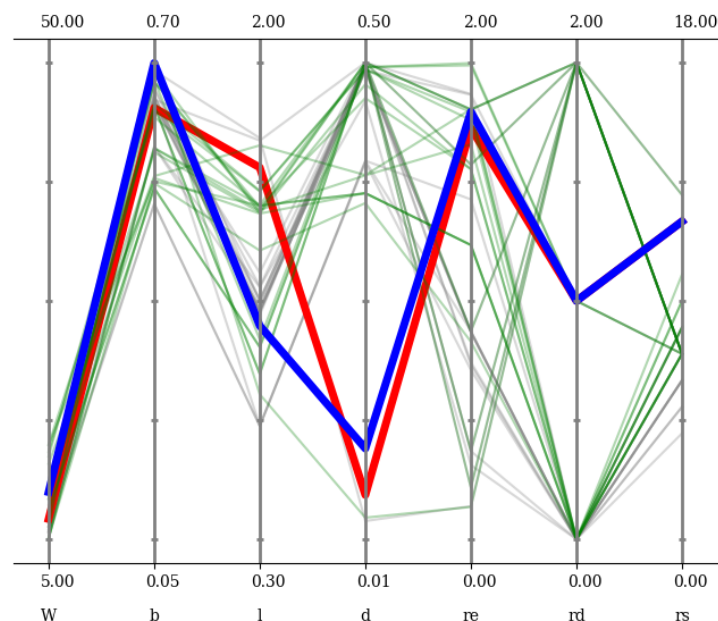


Figure 5.2: Ideal variables found with NSGA-II (gray lines) and Mixed Variable GA (green lines). The optimal NSGA-II solution given the weighting of [0.2, 0.6, 0.2] is in red and the Mixed Variable GA solution is in blue.

The two algorithms converged to fairly similar points. The NSGA-II was more aggressive based on its elitist methodology for carving away less favorable solutions. The traditional GA is more exploratory, which can be seen in the increased variation in the green lines in Figure 5.2. There were a few solutions where the traditional GA converged to what appeared to be a

local minima while the NSGA-II found a better solution.

As expected, the overall metric weightings had a significant impact on the final optimal solution selected. The figures below show the same plots for different sets of metric weightings:

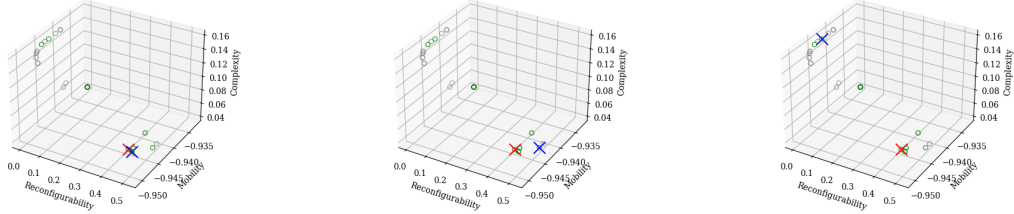


Figure 5.3: Parallel coordinate plots for the same set of variables with different weights. From left to right, the weights are: [0.2, 0.6, 0.2], [0.2, 0.2, 0.6], and [0.6, 0.2, 0.2].

The effect of the overall gains is easily understood as they are simple products of the three described metrics. We examine a sample tradeoff where one metric is maximized and the other two attributes are 10% less. As demonstrated in table 5.3, with this condition, a gain over 0.47 sways the chosen parameters. This is because even if another gain was given the full remaining 0.53 gain, it would not overcome the 0.47 times the 10% higher value.

Table 5.3: Selection of optimal vehicle based on outer gains.

R	M	C	Selected for Gain Ranges
0	0.9	0.1	$C_r > 0.47$
0.1	1	0.1	$C_m > 0.47$
0.1	0.9	0	$C_c > 0.47$

The gains in the individual metrics work similarly. For example, we will examine the effect of changing the individual gains of the reconfigurability metric on this overall value. Table 5.4 summarizes the impact for an example vehicle that using the MARS mini as a testbed and the gains proposed in 2.4. From Chapter 2, we know that this vehicle takes 1470 seconds to transform and has 9.3 kg of additional weight, which scale to time and equipment contributions of 1 and 0.18, respectively using the limits set in Section 2.4. Based on estimating the cost of the additional extruded aluminum and motors, the reconfigurability of this vehicle costs \$780 USD. We will set our threshold equal to \$1000 and our objective \$500, giving this vehicle a M_{rec} of 0.112.

Table 5.4: Overall reconfigurability cost based on gains.

c_t	c_m	c_e	RC
1	0	0	1
0.5	0	0.5	0.556
0.25	0.5	0.25	0.368
0.25	0.25	0.5	0.351
0	0.75	0.25	0.168

Since the time to reconfigure of this vehicle was so long, the combinations with a higher time weighting overpowered the other values and the RC was greater than 0.2 in all cases. However, when reconfiguration time was not prioritized at all (as the last row of Table 5.4), this overall metric met the 0.2 threshold value since both the reconfiguration equipment and monetary cost were within threshold limits.

RMCVO Information Flow

Prior to running the system, the terrain files must be obtained and stored locally to the folder with the RMCVO program. For these examples, soil and grade data was taken from the NG-NRMM dataset and transformed from .tif to .png files ahead of time. The coordinate system of these input files is then manually set in code.

Programmatically, the first module that is called is the user interface module. This program creates the window for interaction and gathers limits and priorities for the optimization. The user interface features text boxes for each required value as well as radio buttons to enable certain types of reconfigurability. The text boxes are prepopulated with reasonable numbers for the equations used in this work.

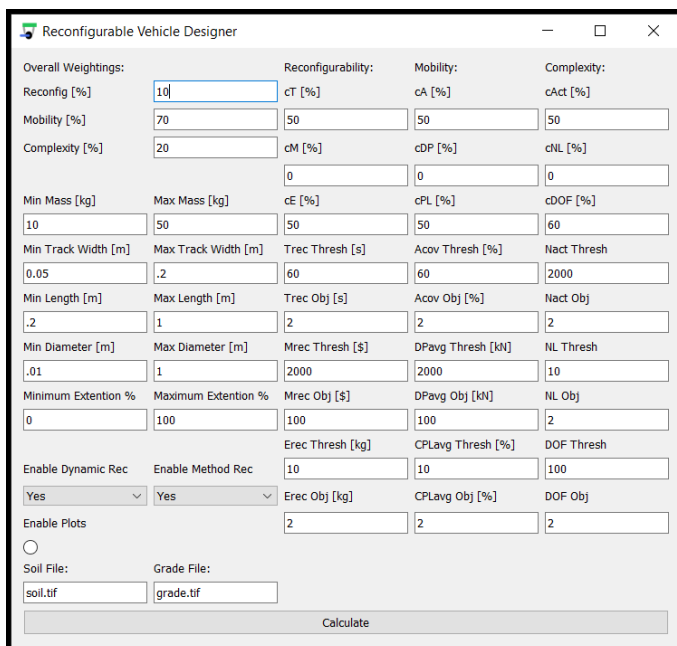


Figure 5.4: RMCVO user Interface.

This information is then fed into the optimization subsystem. The optimization script uses the Pymoo library [201] to set up the two algorithms. The optimization variables are established based on the user’s minimum and maximum values. The three objective functions also utilize the user’s inputs for weights. Complexity and reconfigurability cost are calculated in their own functions while mobility is calculated using a series of functions to set up the terrain-based calculation of drawbar pull depending on if the vehicle is wheeled, tracked, or legged.

In order to reduce computation time for the mobility calculations, a dictionary is maintained as the algorithm iterates through the soil and grade maps. With these two parameters as the keys, drawbar pull (and thus go/no go) is saved so that pixels with the same characteristics do not have to be recalculated. Similarly, path length increase is saved to a comma separated value file so that from iteration to iteration, path length increase can be looked up instead of recalculated if coverage is the same.

Finally, the solution is printed and plotted. The final outputs are the optimal variable values, estimated performance based on the metrics, and 2D and 3D plots of the solution and iterations. The plots below are examples of the optional piecewise plots of the variables:

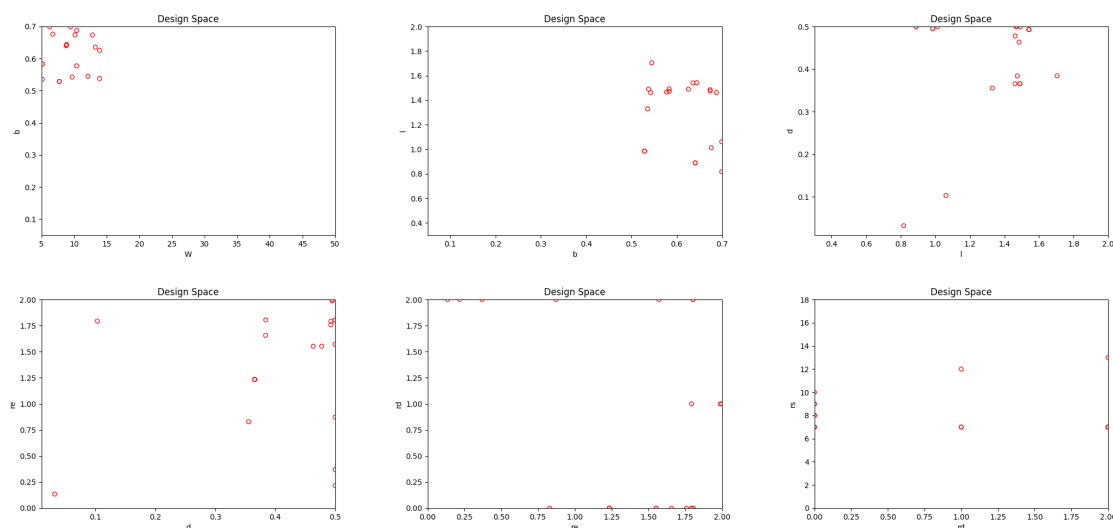


Figure 5.5: Optimal variables for $[0.2, 0.2, 0.6]$ weighting with classic GA and 1000 iterations.

5.4 Conclusion

Element-wise comparison, a weighted sum, and genetic algorithms offer three possibilities for optimizing a vehicle based on three separate conditions. Element-wise comparison offers the simplest strategy and can be useful when there are only one or two objective functions. In this circumstance, vehicle designers can make a judgement based on the highest performer in a specific attribute. When there are three or more variables, it can become harder to visualize and immediately pick out the best combination. A weighted sum offers another straight forward strategy for combining the multiple metrics into a single rating for a given vehicle.

Optimization algorithms offer the greatest ability to maximize desired goals while maintaining constraints. In this chapter, we presented an optimization system that takes in parameter limits and weights from the user and outputs an ideal set of vehicle parameters using genetic algorithms. This system allows for candidate configurations to be evaluated in a way that is most meaningful to the user without needing to build a full system or simulation.

Chapter 6

Reconfigurable Vehicle Design

6.1 Introduction

Modularity is not a new idea for small unmanned ground vehicles. Top military robotics developers including iRobot (now FLIR) and QinetiQ have created versatile products using the same base vehicle with optional add-ons including arms and sensor systems [82, 24]. BAE Systems has taken this idea one step further with their Ironclad platform, which is available with various sensor attachments and can even be combined with other Ironclad vehicles for increased carrying strength [203]. Milrem's THeMIS [204] and NIC Instrument's Zeus [205] also capitalize on the idea of modularity with swappable bases and easily-removable components.

Our reconfigurable vehicle was designed to have a large number of modular entities to get a sense for the relative effects of each parameter. There are four independent adjustable elements: track contact length, tread width, sprocket diameter, and track tension. Throughout the full sweep of these adjustabilities, the other variables including center of mass, and ground clearance were designed to remain constant. The vehicle chassis was built entirely in-house using equipment at NREC and CMU's Field Robotics Center.

This work was informed by an effort lead by Rich Pantaleo from NREC in which he examined obstacle performance for various suspension configurations on a sheet metal chassis that he designed. Similarly in 2012, Christopher Johnson used a modular platform to examine the differences in sinkage and obstacle performance for wheeled and tracked configurations [83].

6.2 Background

For over 100 years, vehicles have been deployed in off-road environments [206]. Agricultural, military and planetary applications all require vehicles to operate on diverse and non-cohesive terrain. In 1988, Hethering and Littleton described the unfortunate paradox of survivability that arises when increased armor weight leads to less mobile vehicles. In their opinion, the solution to this problem was either lighter armor materials, more efficient suspension, or wheel/track systems [207].

Portions of this chapter were presented in the ISTVS 20th International and 9th Americas Conference Proceedings[202] and the ISTVS Student Speaker Series on December 8th, 2021.

Versatility is a benefit for off-road autonomous vehicles, especially those in unknown environments like military surveillance, combat, bomb disposal and search and rescue. One of the pioneers in this realm, iRobot (bought by Endeavor Robotics and now part of FLIR Systems, Inc. [208]), has been somewhat eponymous with highly mobile and ruggedized teleoperated vehicles since the 1990s. Most of their vehicles feature secondary treads on actuated paddles that can be moved depending on the terrain. This reconfigurability is used for slightly more than just changing angle of attack and track length. It can also be used as a manipulator, of sorts, reorienting the body and conforming to obstacles. These paddles give the operator the choice of many different track shapes without having to change hardware or platforms.



Figure 6.1: The 510 PackBot.
Image credit: [120].

6.2.1 Wheel-Based Systems

Surface Area Variability

In the mid 1800s, inventors sought ways to increase the surface area of military vehicles and farming equipment. One idea was to have hinged panels or pivoting feet on the wheel that would allow for a longer interface area but the efficiency of a wheel, as opposed to a track. The "Dreadnaught Wheel" [209] or "Pedrial Wheel" [210] saw many different forms over the next century, from interlocking panels to a removable rigid wrap.

The Hankook Tire and Technology Group has been putting forth innovative future wheel concepts for the past few years. In 2014, they presented the "Boostrac" and "Alpik", which could change diameter and width, respectively [70]. Though these concepts are not quite ready for the marketplace, such out-of-the-box designs could be revolutionary for vehicle performance.

Over-tire tracks have been around for over 60 years [211, 212], with one of the most modern being the Track N Go quick track transformation system for passenger vehicles [213]. Recently, JWheelz has also created static width-increasing attachments for personal off-road vehicles [214].

In 2014, researchers at Seoul University developed a wheel based on the spherical water-bomb tessellated pattern that is able to expand by pulling its sides closer together. The wheels in their prototype were able to change between 28 and 68 mm excluding grousers. In order to pull a heavier load, the wheels automatically collapse to a smaller diameter [215].

Other methods of adjusting wheel shape include: pinned linkage systems [216, 217] and variable diameter pulleys [218, 219].

Pressure Variability

For years, farmers have capitalized on the decreased ground pressure that underinflated tires offered. Alternative technologies to the typical carcass tire include: spring-based spokes [220, 221, 222], foldable side walls [223, 224], deformable inner structures [225] and shape memory alloys [226]. In 2014, Goodyear unveiled a concept comprised of two coaxial tires with separate bladders. The main chamber has a slightly larger diameter and more shallow

grooves, intended for driving on the street. The secondary chamber features a shell with more aggressive grooves intended to provide traction over sand and mud [227].

A central tire inflation system (CTIS) is a great example of a field-ready reconfigurable technology. CTIS relies on pressure sensors mounted in each tire and a centralized control system that processes this sensor data, along with user commands. A single air tank and pneumatic control that connects to all four tires allows for each tire to be inflated or deflated as needed [228]. Currently, CTIS systems are used in the military, agriculture, and off-road materials transport. Recently, Continental and Toyota have expanded on this idea with increased tire sensing and adaptation [69, 229].

Suspension Variability

Suspension technology has evolved greatly from early thorough brace systems on horse-drawn carriages, which consisted of leather straps that supported the passenger area of the vehicle [230]. Suspension can reduce impact, putting less stress on structural components. Such systems can also lessen vibration, which is not only beneficial for manned vehicles but also for unmanned systems, especially those with cameras and other perception systems.

Bicycle suspension is a prevalent example of an easily-reconfigurable suspension system. Though the range of bike suspension is quite diverse, a coil-sprung telescopic fork is one of the simplest and most common methods for damping impacts to the front wheel. Most of these systems can be locked at a minimum and some can be further tuned by adjusting the spring rate to affect the preload. This allows riders to lock their suspension when riding on roads and hard paths so that no energy from pedaling is lost to compress the spring. Then when on rough, downhill sections, the user can unlock the suspension and be slightly less discriminating when choosing a line to bike on as abrupt bumps will be less devastating to the bicycle and rider. Suspension can even be adjusted automatically, using a system like Fox's Live Valve system [231]. Adaptive and active suspension systems have also been used in cars for decades [232].

Wheeled vehicles are not alone in using suspension. Tracked vehicles [233] and legged robots can both capitalize on elasticity to improve performance.

Wheel Shape Variability

Stair climbing is a common use for highly variable robots with unique mobility schemes. Applications from home assistance to search and rescue usually require negotiation of stairs or steps of some type. There have been many diverse designs for overcoming stairs including multiple wheels on each hub and shape-changing wheels. Eshcol Gross's 1986 patent [234] for a dolly with 3 idle wheels that rotate around a center axle may have influenced the design of wheel chairs like Ken Cox's Stairmaster Wheelchair [235]. Hankook's whimsical take on stair climbing is a wheel with individual segments that can retract radially to conform to a step [236]. [237] and [238] both created unique wheels that could reorient into spokes or "whegs" to aid in stair climbing.

Module-Based Wheeled Systems

As described in section Section 2.2, modular reconfigurable vehicles can offer benefits in terms of cost, size, and adaptability.

In 2002, Kawakami et al. developed a vehicle consisting of a static central chassis with independently mobile wheel modules that could connect to it [239]. The vehicle could perform as a single device or use each wheel module as a manipulator to conduct separate missions.

Recently in 2020, the MIT Media Lab demonstrated a series of wheeled vehicles with magnetic "shells" that they could interact with [240]. The robots, dubbed "HERMITS" after their likeness to hermit crabs are simple two-wheeled cubes that can roll into various manipulators and transporters. Current applications include manipulation, haptics, and story telling.

6.2.2 Track-Based Systems

Track Development

The creation of the gasoline-powered vehicle and spread of passenger automobiles accelerated the pace of invention in this area. Vehicles were soon outfitted with half-tracks [206] and a variety of track variations for off-road and high load applications.

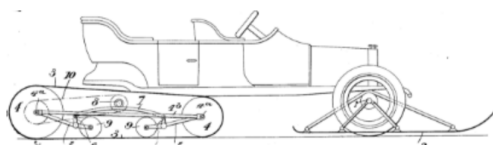


Figure 6.2: Kегresse's motor-sledge design from his 1914 patent.

Early deformable tracks more closely resembled a string of small tires than a continuous tube [241, 242]. Inflatable tracks first became outfitted with drive lugs in 1964 [243], which meant that motion was no longer limited by the friction between the wheel and the track. This style of track has largely been replaced with solid rubber continuous tracks or metal linked tracks with rubber padding, with the exception of a few specialty track manufacturers [244].

Track Variability

In terms of reconfigurability, some versions of Kubota Global's Mini-Excavator have a hydraulic system that is able to alter its width depending on the application [245]. A wide stance can aid in stability for heavy scooping maneuvers while the ability to reduce the track distance enables the vehicle to fit into narrow spaces. [246] implemented a similar idea for wheelchairs to ease in movement in tight areas.

Yim, et al. studied modular reconfigurable vehicles for space applications that could be arranged in a single, moldable, track formation [247].

Finally, Gehl's IdealTrax allow tractors the ability to automatically tension their tracks, eliminating the need for manual adjustment [248].

Multi-Track Designs

iRobot's unmanned military vehicles were some of the first vehicles to combine tracks and arms, which helps with surmounting stairs and large obstacles [249, 250]. Finally, in the fall of 2014, DCD Protected Mobility revealed their experimental four-tracked unmanned vehicle. Each track was also actuated and could lift the central body up at a range of heights [251].

AMOEBA-I was a 4-track vehicle used as an example platform to examine the space of all possible configurations for a reconfigurable linked robot [252]. Li, et al. were able to determine

which configuration was most favorable for each terrain condition including stairs, obstacles, and debris [253].

Module-Based Tracked Systems

Guanghua, et al. created a modular reconfigurable system specifically for off-road navigation in 2006 [254]. Each module was equipped with linkages that could rotate with respect to one another. This vehicle was capable of getting through tight holes by rotating modules relative to the others. It could also self-right itself through the same mechanism.

In this same year, S-bots demonstrated the ability to self-connect with up to 15 other modules through on board grippers [111]. Carnegie Mellon's Millibots operated with a similar chain structure, though each module was much smaller. This device showed promising results for stair climbing [105].

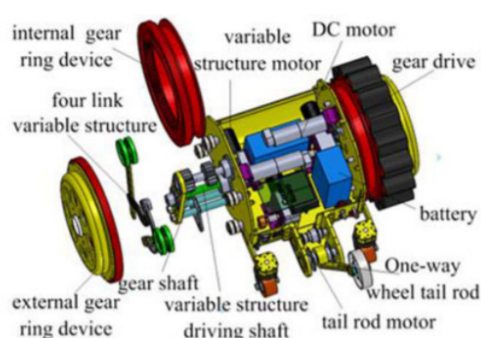
6.2.3 Wheel-Track Hybrids

Combined Wheels and Tracks

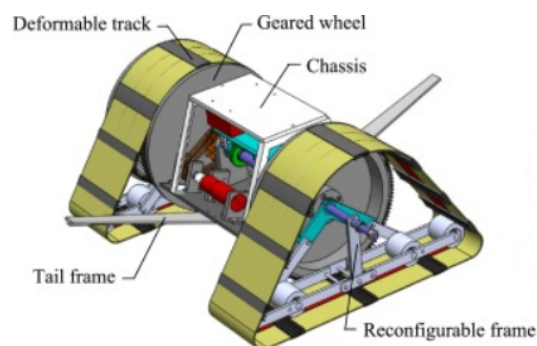
One of the first attempts to merge the benefits of both a wheel and track was the late 1800s "Dreadnaught Wheel", mentioned before. Northrup Grumman has iterated for many years on a device with both wheels and tracks on their Andros Robots designed for surmounting stairs and off road environments [255]. In 2014, the company now called Scewo started development on a wheelchair that could ascend stairs using a deployable track. The track conforms to the angle of the stairs while keeping the user upright [256].

Transforming Wheels and Tracks

In 2007, Elbit Systems debuted a two-wheeled vehicle with stretchable treads. These treads enabled the wheels to become tracks with folding supports that stretched the tread into a triangle shape [257]. A decade later, Gao et al. created a smaller version of this device that relies on a four bar mechanism and timing belt embedded in a stretchable track [84]. In 2018, Luo et al. created one based on a six-bar mechanism with a similar expanding tread [258].



(a) Gao, et al.'s reconfigurable wheel-track mobile vehicle [84].



(b) Luo, et al.'s reconfigurable wheel-track mobile vehicle [258].

Figure 6.3: Two reconfigurable wheel-track designs.

Mattracks also worked on a wheel-track system, but using a deflatable bladder to allow for a sprocket to interact with a tread [259]. This wheel was developed to allow vehicles better

traction in highly deformable terrain. In 2018, Carnegie Mellon University's National Robotics Engineering Center debuted a reconfigurable wheel-track installed on a traditional HMMWV. These mechanisms could transform from a circular wheel with a moving hub to a triangular track with a fixed hub while in motion [260].

6.2.4 Walking Hybrid Vehicles

Wheel-Based Walking

There is a fruitful sector of research for robots that combine rolling and walking. While rolling may be more efficient on road, many devices and spaces made for humans-whether stairs or cars-assume the ability to walk. Additionally, dramatic off-road environments may not provide enough surface areas for a wheeled or tracked vehicle. One of the first attempts at a combination of wheels and feet came at the turn of the 20th century with the Perdrial Wheel [210]. This device consisted of a hub with hinged feet. Some had active suspension to alter the shape of the rim, as well. According to a contemporary article, a vehicle outfitted with these devices "climbed over a nine-inch balk of timber,...ruts ten inches deep and very soft ground, with the greatest of ease" [261].

Leg-Based Rolling

The DARPA Robotics Challenge (DRC) brought brought more interest to walking robots or hybrid movers. Of the 24 teams that competed, many used a combination of walking and rolling on wheels or tracks [262].

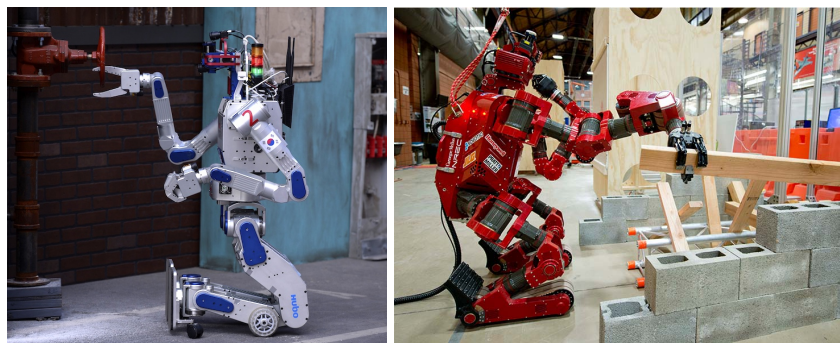


Figure 6.4: Kaist's DRC-HUBO (left) and Tartan Rescue's CHIMP (right) [263, 264]. Kaist won first place in the DRC Finals using a hybrid of walking and rolling on its knees. CHIMP earned third place through a combination of walking and rolling on four tracks located on its feet and elbows.

Another Boston Dynamics Robot, Handle, uses some of the control schemes and flexibility of walking robots again with the increased efficiency of wheels [265]. Instead of feet, Handle features two wheels and is capable of making tight turns, carrying loads of up to 45 kg and jumping several feet in the air. These recent developments show the difficulty of purely walking vehicles and the benefits of versatile mobility systems.

Reconfigurable Walking and Rolling

Other notable mentions in dynamically hybrid vehicles include unfolding designs from the University of Utah and Kåre Halvorsen's MorpHex, both pictured below. The University of Utah has created two folding vehicles, one disc (The Rolling Disc Biped) and one sphere (The Hex-A-Ball). The Rolling Disc Biped (RDB) unfolds to a biped that can walk by inching or flipping. In its disc shape, it can be propelled passively or by extending and retracting one of its links [266]. Halvorsen created a similar structure to the RDB in that it is a sphere that can unfold into a crab-like walking structure. His design also has a more active rolling mode facilitated by opening certain panels in succession while in a sphere shape.

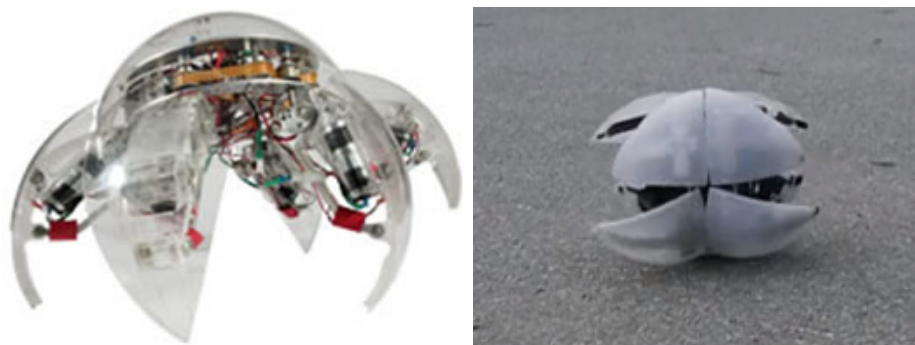


Figure 6.5: The University of Utah's Hex-A-Ball (left) and Kåre Halvorsen's MorpHex (right) [267, 268].

6.2.5 Sliding and Crawling Systems

Numerous researchers [269, 270, 271, 272, 273, 274, 275, 276, 277, 278] have created reconfigurable modules that can operate in various configurations through sliding and crawling. These novel mobility systems have been proposed for use in search and rescue where space is confined and adaptability may be required [270]. Castano, et al.'s CONRO and Yim, et al.'s Polybots demonstrated different locomotion strategies based on configuration including a sinusoidal snake-like gait, whole-body rolling gait, and various waling gaits [272, 273]. The University of Southern Denmark created a robot with telescoping links and pivoting joints [279].

Reconfigurable systems also offer promising possibilities for small-scale systems. Small sliding and swimming robots show potential for small applications where typical tools and vehicles are too large. Shape memory alloys and magnets offer a more compact actuation method that can be employed for connections that also propel the vehicle [280, 281].

6.2.6 Reconfigurable Systems Summary

Based on this survey, there exist 8 primary means of transforming a ground vehicle's mobility system: changing the contact area, changing the contact placement, changing the contact element pressure, changing the contact element shape, changing the suspension system, combining modules, using a different mobility mode, and transforming the mobility mechanism into a different mechanism. Table 6.1 shows a summary organized by vehicle type. Vehicle type categories are the same as those presented in [91] with the addition of the 'sliding' cat-

egory. For this work, a hybrid vehicle type is only indicated if the mobility system actually changes from one to the other, as opposed to having both and using one or the other.

Table 6.1: Reconfigurable Ground Mobility Systems Summary.

Vehicle Type	Reconfigurability	Modern Examples
Wheeled	Contact Area	[215], [213]-[219]
Wheeled	Wheel Locations	-
Wheeled	Tire Pressure	[228], [69]
Wheeled	Wheel Shape	[237], [238]
Wheeled	Suspension	[232]
Wheeled	Module Assembly	[239]
Tracked	Contact Area	[82], [24]
Tracked	Track Spacing	[245], [246]
Tracked	Tension	-
Tracked	Angle of Attack	[82], [24]
Tracked	Suspension	-
Tracked	Module Assembly	[33]
Legged	Contact Area	-
Legged	Foot shape	-
Legged	Suspension	-
Legged	Module Assembly	-
Wheeled-Legged	Use of wheel to/from use of leg	[239], [282]
Wheel-Leg	Wheel transform to/from leg	[267], [268]
Wheeled-Tracked	Use of wheel to/from use of track	[6]
Wheel-Track	Wheel transform to/from track	[257], [283], [284]
Legged-Tracked	Use of leg to/from use of track	[263], [264]
Leg-Track	Leg transform to/from use of track	-
Sliding*	Module Assembly	[269]-[278]

*Since reconfigurable sliding vehicles reconfigure primarily in the sense of modules joining and reforming, only this reconfigurability is considered.

6.3 Design

This vehicle was designed in SolidWorks 2018 [285] because of familiarity with the software, availability at CMU, and the ability to connect to the Project Chrono simulation software [286]. Where available, part files were downloaded from suppliers including McMaster-Carr [287], Vex [288], and Andy Mark [289]. LynxMotion provides links to user-created models of some of their parts [290], but these were not accurate enough for the design and simulation, so

they were reverse modeled, instead.

The diagram below (Figure 6.6 shows the final vehicle CAD. Minor adjustments were made after construction and are outlined in Section A.4. To decrease the overall width of the vehicle, a 90° gearbox was added to the motor assemblies. To reduce weight, the sprocket mounts were cut down based on FEA performed in SolidWorks. More material could easily be removed from these parts, but they also function as mild protection of the bearings from debris. A center platform was added to mount the battery and electronics. Motor shrouds were designed to protect the motor, encoder, and gearbox from inbound debris like sand.

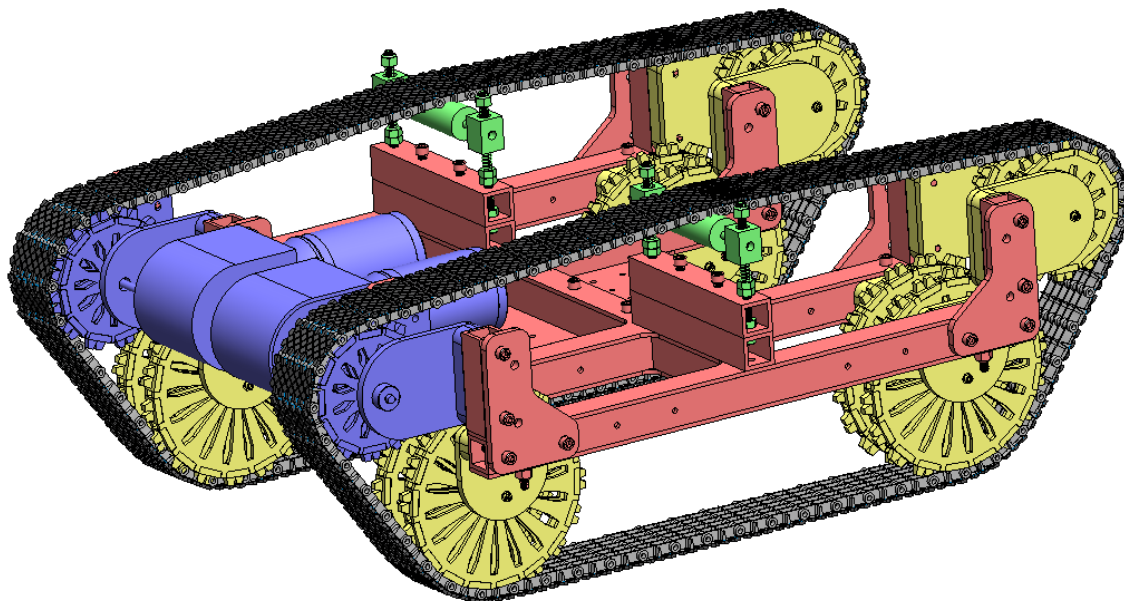


Figure 6.6: Seventh and final version of the modular tracked vehicle.

The motors and sprockets attach to the vehicle's frame through bolts that attach from the outside for more convenient access, as shown in Figure 6.7.

A VEX Mini CIM 12 V brushed DC motor with 10:1 VersaPlanetary gearbox and 1024 CPR VersaPlanetary encoder was selected for its torque-speed combination at maximum efficiency [288]. It was important for experimentation that the vehicle was limited by soil shear, and not motor torque, whenever possible.

An Arduino Mega [291] was selected for its ability to connect to a large number of inputs and outputs and sufficient computing power for testing. A Basicmicro dual motor controller was used in order to keep torque relatively constant throughout trials [292]. The motor encoders and a shunt resistor allowed for monitoring of the sprocket position, and motor current, respectively.

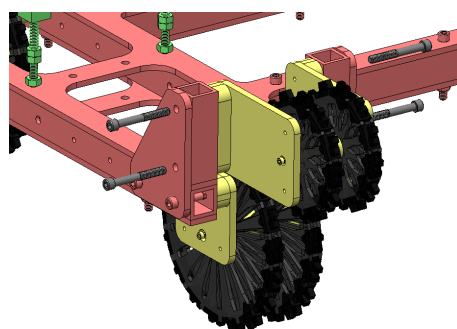


Figure 6.7: Example of attachment via machine screws from the exterior of the vehicle.

The electrical diagram for the system is presented below. In addition to these components, cameras monitored the robot's position externally.

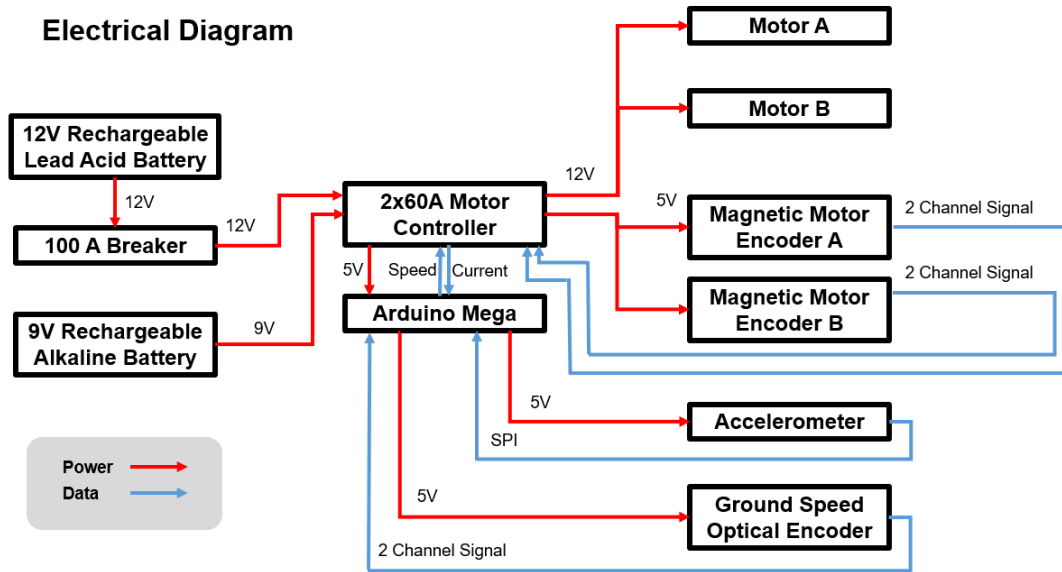


Figure 6.8: Electrical diagram for the system. The motor controller provided power distribution for both the motors and encoders, as well as a means of measuring current draw.

For each experiment, torque was controlled by feeding back the current measurement at the motor controller. We assumed that the $\tau = i * k_T$ where τ is torque, i is current, and k_T is the torque constant. A simple proportional controller was set up to maintain torque 10 times per second:

$$v_{cmd} = v_{base} + k_p * (i_{meas} - i_{des}) \quad (6.1)$$

where v_{cmd} is commanded velocity, v_{base} is base velocity, k_p is a proportional constant, i_{meas} is measured current, and i_{des} is desired current. Velocity is commanded since that is the typical format of the motor commands.

6.4 Configurations

In order to change the vehicle's track contact length, we drilled holes to allow the sprocket modules to attach to various points along the vehicle's side rails. Track links could be added or subtracted as needed to get an adequate tension range at each length.

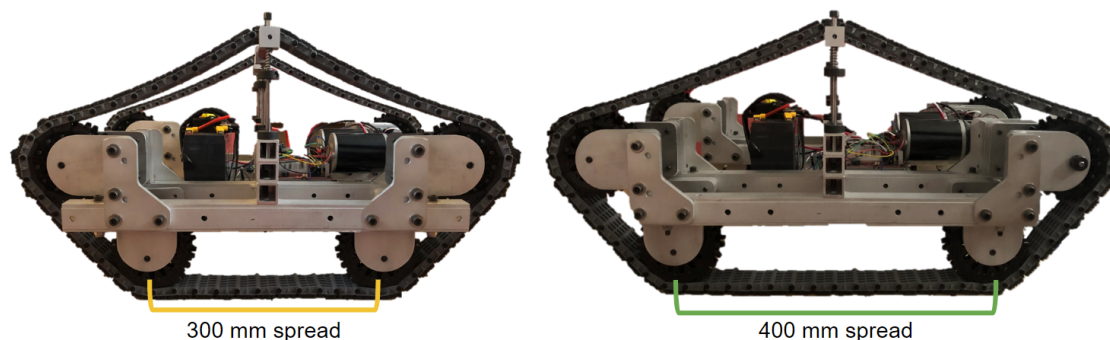


Figure 6.9: A comparison of the middle (300 mm) and longest (400 mm) track contact length conditions.

To change the track length, the entire track assembly is replaced. The arms of the chassis are fixed. There are removable spacers between the chassis and the sprocket mounts so that different sprocket axles could fit in to allow for the change in track width. Through initial testing, it was determined that the wider track could fit on the smaller track's sprockets, so these spacers were kept in for both configurations.

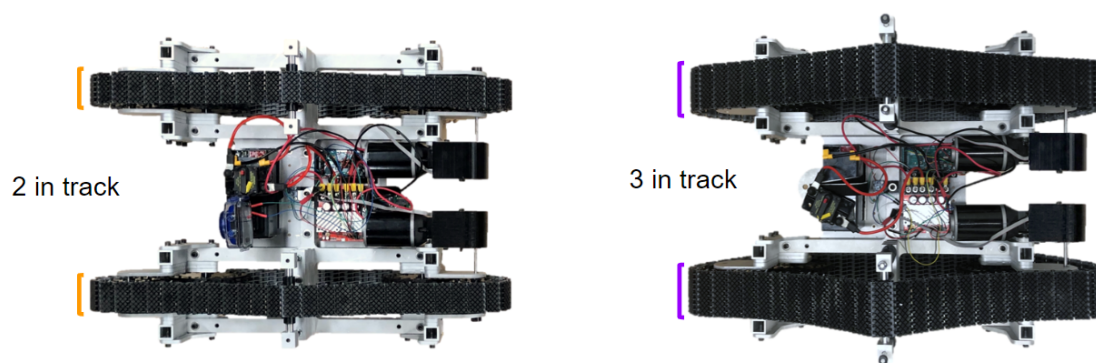


Figure 6.10: A comparison of the two available track widths (2 in and 3 in).

There are three different sprocket assemblies which could be used on this vehicle. In order to keep the ride height and center of mass constant, each sprocket fits with a different size mount. For example, the smaller sprocket has a longer mount so that the distance from the sprocket's point of contact with the ground to the vehicle body is constant.

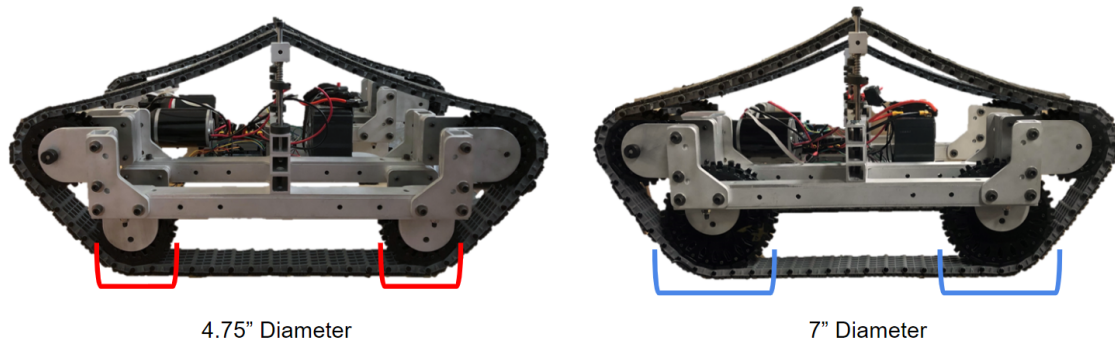


Figure 6.11: Comparison of the smallest (4.75") and largest (7") sprocket conditions. The small sprocket has a longer sprocket mount to allow it to be the same height as the large sprocket.

To adjust tension, the idle roller that supports the top point of the track can move up and down on a spring assembly. Tension is approximated using a spring that supports this roller. The force on the track is derived from the displacement of the spring times the spring constant. Two different springs were used to increase the range of track tensions.

Seven different track tensions were tested: 1.27 cm slack, 0 kg, 0.45 kg, 0.9 kg, 1.4 kg, 2.3 kg, 4.5 kg, 6.8 kg was also tested but turned out to be infeasible for the motors to overcome.

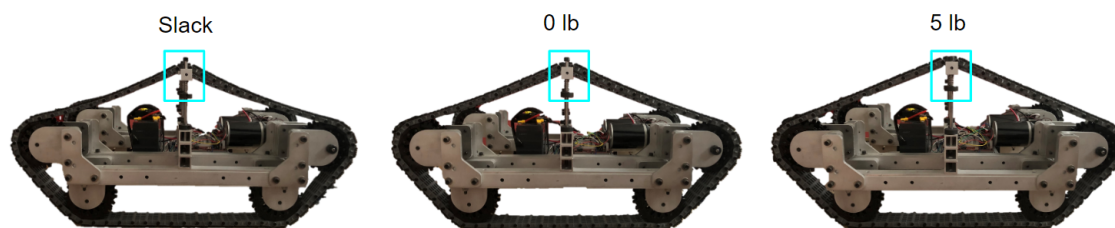


Figure 6.12: comparison of the 1.27 cm slack, 0 kg, and 2.3 kg track tension conditions. For each condition, the block that supports the top roller is moved to deform the spring based on the prescribed track tension.

6.5 Design for Reconfigurability

As discussed in Section A.5, working with this vehicle revealed key aspects of design for reconfigurability. There are three primary characteristics of a reconfigurable adjustability: number of distinct connections, size between adjustments, and connection type. The first two characteristics could also be expressed as reconfigurability extent and resolution for more continuous reconfigurabilities.

Number of connections and distance between these connections are often linked. In this work, where possible, three different adjustabilities were implemented to more definitively identify trends. The minimum and maximum values were chosen either based on available components (in the case of track width and sprocket diameter), predicted difference in drawbar pull (in the case of track length), and after preliminary experimentation (in the case of track tension). Based on theoretical predictions of drawbar pull, the sprocket diameter was not predicted to have an effect, indicating that a wider range of values is needed. However, there was noticeable difference in the predicted and experimental sinkage.

Connection type can be broadly categorized by the types of connections described in 2.3.1: slot, bus, and sectional. But within each of these categories, the precise mechanism can have a large influence on reconnection time and reliability. Table 6.2 shows a comparison of connection and fastener types. This table was gathered from observations throughout this work and [293, 294] and would benefit from full experimental study in the future.

Table 6.2: Comparison of different connection types for manual reconfigurability rated from 1 to 10 with 1 being poor and 10 being excellent.

Connection Type	Ease of Design	Ease of Manufacturing	Number of Parts	Connection Strength	Longevity	Speed	Cost
Bolt and nut	10	10	7	5	9	3	10
Bolt and locknut	10	10	7	7	1	1	9
Bolt, nut, and lock washer	10	10	5	6	3	2	8
Bolt and threaded material	9	7	7	4	2	5	10
Bolt with threaded insert	8	7	7	5	3	5	9
Set screw	10	10	7	3	3	8	10
Split hub clamp	10	10	7	7	10	8	7
Quick release pin	10	10	10	9	8	10	3
Clevis pin	10	10	7	9	3	9	8
Binding screw	9	7	7	6	10	2	9

6.5.1 Connection Strength

For any system with reassembly, connection strength is often at odds with other characteristics like durability and ease of connection. Especially for a field-deployable setting, connection strength can be vital, even in the face of vibration, impact, debris, or moisture. The through holes and threaded plates method that was used to support the sprockets offered a very strong means of attachment. The two treads both used the same attachment method, so this connection strength was not affected by reconfigurability. The track tensioning mechanism used oversized clamping shaft collars, which did not seem to slip throughout any of the testing.

6.5.2 Connection Durability

A major lesson learned from the creation of the manually reconfigurable tracked vehicle was that even strong connections can degrade with use. This robot used tapped 6061 Aluminum and 1/4-20 bolts for many of the reconfigurabilities. The thinnest tapped material was 0.25", giving the bolts 5 threads to grip. However, all the holes were tapped by hand, which meant that some were not perfectly parallel with the hole. Overtime, Aluminum dust on the bolts could be

observed as the bolts wore away at the threads in the Aluminum. This threaded system could be improved using a stronger material or helicoil inserts.

Taking on and off the track did affect the integrity of some of the plastic pins that retain the plastic rod that connects adjacent shoes. These pins came with the track system and did not sit as close to the track toward the end of testing due to their deformation. The shaft collars for the tension system exhibited some wear from the springs vibrating against them over time.

6.5.3 Ease of Connection

Changing the sprocket diameter and sprocket spacing were both time-consuming processes for this system. This was primarily due to the number of connection points (8 for each sprocket). The through holes and threaded plates were quicker than a nut and bolt system, but slower than a pin system. It is also worth pointing out that some holes were "reused" for both the ground and idle sprockets. Though this reduced the total number of bolts needed for each sprocket, it likely cost time in the long run. This is because when one ground sprocket needed to be replaced, removing these bolts made the idle sprockets also unsupported. This is an example of the subtlety in reconfigurability design and the difference, perhaps from design for assembly.

No effort was made to alter the off-the-shelf track system. The locking brads were fairly difficult to change without a box cutter or thin blade, but with these tools, reconfigurability was fairly quick.

The track tensioning system only required 4 bolts to be loosened and tightened in order to change the tension of both tracks. One thing that would have improved the system is perhaps physical stops for the required measurements. As is, the user has to alternate between tightening the bolts and measuring the spring or track distance until the required condition is met.

6.6 Conclusion

As explored in Chapter 2, the applications of reconfigurability in robotics is highly diverse. Even within only the mobility system of ground vehicles, this chapter demonstrated a wide range of vehicles and designs. It is also apparent that there are many platforms reconfigurabilities that have yet to be tried, particularly for tracked and legged vehicles.

We also presented a vehicle that allows for the variation of four different properties through manual reconfigurability. The system has two options of track width, three options of track contact length, three options for sprocket diameter, and a wide range of tension options. Creation of this vehicle shed light into principles of design for reassembly, which are seldom discussed in typical mechanical design. In particular, we identified the common tradeoff between connection strength and speed of reassembly.

The design of this vehicle required fairly simple manufacturing methods. Iterations on the vehicle after fabrication improved the vehicle's long-term operation and sensing abilities. Perhaps in the future, this system could be modified to include other modularities like body averaging suspension variability, track spread, or weight distribution. Alternatively, continued refinement of the existing reconfigurabilities could reduce or eliminate transformation time through quicker mechanisms or automation.

Chapter 7

Reconfigurable Vehicle Testing and Validation

7.1 Introduction

The overall goal of experimental testing was to examine the vehicle's performance on a variety of criteria while adjusting just one modularity at a time. In this way, it would be possible to determine any benefits provided by this modularity. The vehicle was tested in the field, as well as through equations in order to provide a more clear picture of performance since there is a lack of theoretical predictions for some values for this weight scale and some variables (for example tension) do not appear in many of the equations at all.

This chapter is divided into three main components: a physical testing section, a metric evaluation section, and a metric validation section.

7.2 Field Testing

7.2.1 Methods

A set of tests was designed to examine how experimental drawbar pull, maximum slope, maximum step, contact area, and sinkage related to their theoretical derivations and how they were affected by vehicle configuration. Throughout all tests and trials center mass and lateral track spread were kept constant. Each trial had a specified longitudinal sprocket spacing (200 mm, 300 mm, or 400 mm), sprocket diameter (4.75 in, 5.75 in, or 7 in), track width (2 in or 3 in), track tension (0 lb, 1 lb, or 2 lb), and ground material (hard ground or sand).

Soil Preparation

For soft ground testing, the soil was reset and prepared between each trial. The same procedure was used for each test.

Most terramechanics equations assume that the soil is a continuum and not a series of objects. In order for this assumption to hold, we desired that the average dimension of the soil grains did not exceed 5% of the smaller width of the contact patch [122]. For this reason, and its abundance, sand was selected as a soft ground material throughout testing.

Unless otherwise stated, the soft ground testing was performed outside, and not in a controlled lab environment with calibrated soil. This decreases the power of the measurements taken since the soil properties can not be assured to be consistent. However, care was taken to ensure that the soil was as consistent in size and type as possible and prepared in accordance with terramechanics testing procedure. Furthermore, the comparisons between configurations still hold since they were all conducted on the same terrain. To ensure that the boundaries of the testing area did not affect the forces in the soil, Terzaghi's bearing capacity theory was used [295].

Between each test, the soil was loosened, leveled, and compacted as in NASA Glenn Research Center's Drawbar Pull Procedures for Off-Road Vehicle Testing [130]. In order to loosen the soil, a blade was dug in to a depth of approximately 4 inches, angled, and removed. This churned up the soil as shown in Figure 7.1a.

The soil was then lightly leveled using a 3 ft Aluminum beam and box level. The level was moved across the surface in perpendicular directions. Any ruts were filled in with surrounding sand between passes.

Where prescribed, a 10.2 kg tamp was used to compact the sand from a height of 8 cm. This tamp is twice as heavy as the one prescribed in [130], but also has twice the surface area to amount to the same pressure. To ensure that the tamp was dropped from a height of 8 cm each time, a coin was taped to the tamp at a distance of 8 cm from the bottom of the tamp. The tamp was lifted until the coin just brushed the surface of the sand and then dropped.

The tamping process left a slight lip at the edges of each impression (seen in Figure 7.1c, so where relevant, the surface was also lightly smoothed after this procedure so that track prints could be seen more easily while not compacting the soil further.

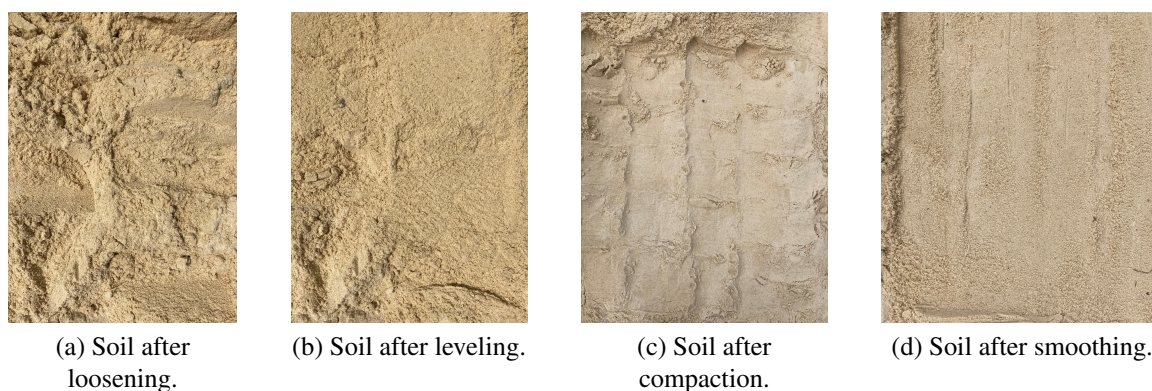


Figure 7.1: Soil preparation process.

Soil moisture was measured using a Delta-T SM150T Soil Moisture Kit [296] ($\pm 3\%$ accuracy) and by measuring the change in weight for a measured volume of soil when all the water had evaporated. Weight was measured with a VIVOHOME High Precision Electronic Digital Refrigerant Charging Weight Scale [297] (capacity: 220 lbs, 100 kg, resolution: 0.2 OZ/ 0.01 LBS/ 5 G, accuracy: $\pm 0.05\%$). These values were used to determine soil coefficients using Kumari's study of moisture effects on soil strength in sand [298].

Conditions compared in text or illustration are from the same day of testing to limit difference in performance based on temperature or humidity.

Sinkage Methods

Pressure and sinkage are good indicators of soft soil performance. As discussed in Subsection 3.2.1, there are many equations for determining pressure based on sinkage. To determine maximum sinkage in the field, two static methods were employed, each test condition was repeated six times.

First, the depth of the vehicle's impact was measured manually using a method similar to that described in [299] except using a level and calipers instead of two measuring sticks. The level was placed on the ground across the ruts, then the caliper plunger was used to measure the depth from the top of the level to the bottom of the rut for all four sprockets. In this method, there is a necessary degree of steadiness to ensure that the caliper does not plunge into the sand and the horizontal measure is level and also does not dig into the sand.

The second method used was backing out sinkage from contact patch. Since the geometry of the vehicle is known, if the difference in contact length between the vehicle with some sinkage and no sinkage is known, geometry can determine the distance between them. Since the track is flexible, this estimate is still the maximum sinkage.

Maximum Slope Methods

Assuming tip over is not reached, maximum traversible slope is directly related to drawbar pull as slope is one of the resistances that acts against the overall thrust of the vehicle. Using Equation 3.7 and Equation 3.12, the maximum slope should be proportional to drawbar pull, assuming the same thrust.

Experimentally, the vehicle was placed on slopes of increasing angle in multiples of 5 degrees until it could no longer progress 30 cm moving with a motor speed of 1200 RPM. The motors were capped at a current draw of 15 A each. From the last successful setting, the angle was then increased in increments of 1 degree to fine-tune the result. Angle was measured using the M-D Building Products 92500 SmartTool Gen3 Digital Level [300] (angle accuracy to 1/10 of a degree). Testing was not possible on loose sand for angles greater than about 30 degrees, because this exceeded the sand's internal angle of friction.

7.2.2 Results

Sinkage Results

As expected, the vehicle sunk less when outfitted with the wider 3" tracks. The vehicle with the 2" tracks had an average maximum sinkage 1.75 mm lower than with the 3" tracks. The plot below shows a comparison of the measured sinkage with the theoretical maximum sinkage of the vehicle outfitted with 4.75" sprockets at a distance of 400 mm and a track tension of 0 lbs:

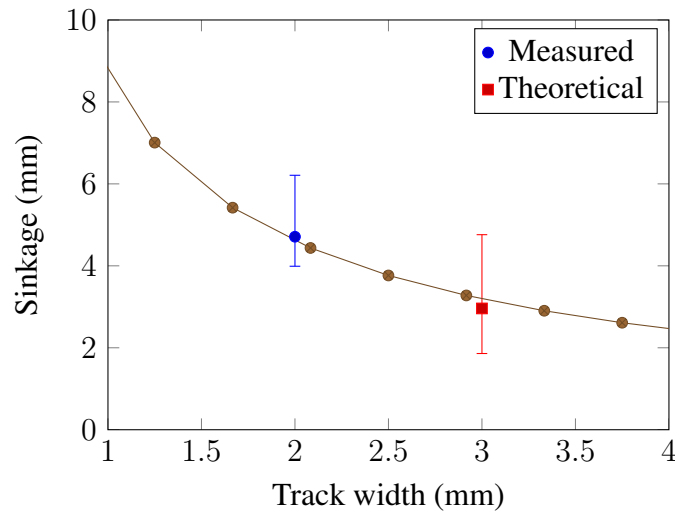


Figure 7.2: Plot of sinkage versus track width.

Track tension does not appear in typical equations for sinkage. However, field testing shows a slight decrease in sinkage as tension increases. We theorize that this is because the higher track tension is better able to spread out the weight of the vehicle across the entire length of the tracks. While the lower track tension leads to higher pressure at the points where the sprockets interact with the track.

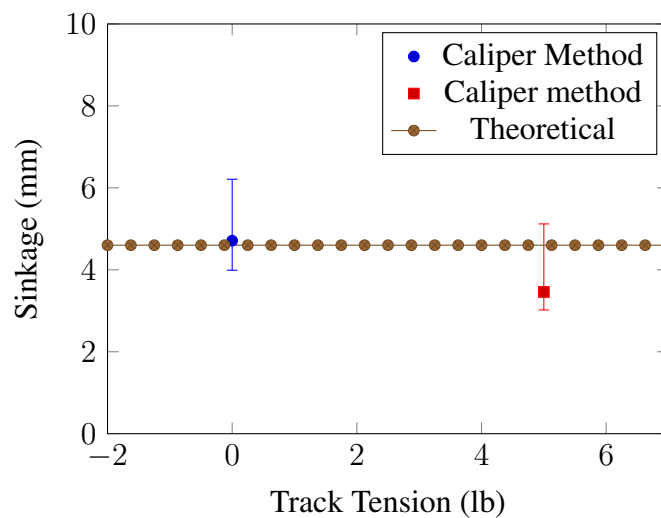


Figure 7.3: Plot of sinkage versus track tension.

Sprocket diameter is another variable that does not appear in the simple maximum pressure equation. Yet our results show a slight downward trend of sinkage with sprocket diameter. This is likely due to the fact that the larger diameter has a slightly larger surface that interacts with the track. Thus it is able to spread out its weight more efficiently. The plot below shows sinkage variation as a result of different ground sprocket diameters. The experimental sinkage was higher than that of the theoretical sinkage. However, it is important to point out the variation of this theory with the soil coefficients (k_c , k_{phi} , and n). For this work, these values were backed out from tables using the measured values from the soil.

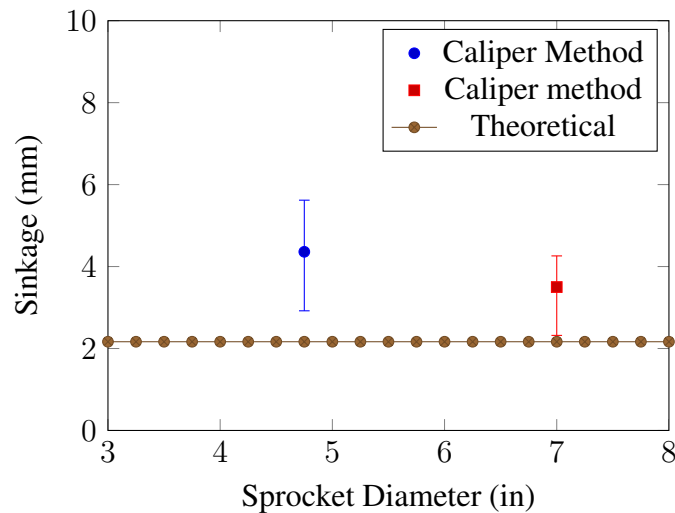


Figure 7.4: Plot of sinkage versus ground sprocket diameter.

Consistent with intuition and theory, the longer the track contact length, the smaller the sinkage. However, the difference between these values was not as significant as in Equation 3.2. This may be due to the fact that this vehicle is comparatively lightweight, and so this relationship may not be completely applicable at this weight. The plot below shows sinkage variation as a result of different contact lengths:

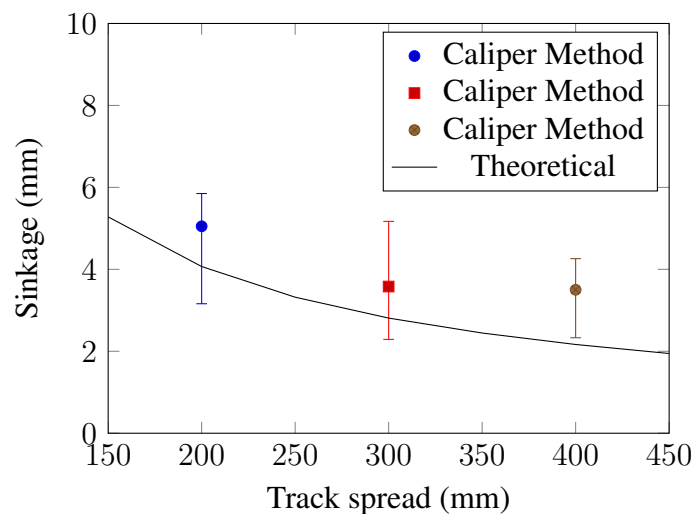


Figure 7.5: Plot of sinkage versus track contact length.

Maximum Slope Results

Table 7.1 documents the maximum traversible slope described in subsection 7.2.1 for each of the 36 tested conditions. For all tests, the motors were kept at their maximum spread and current draw was capped at 30 Amps.

From these tests it is evident that contact area had the greatest impact on maximum slope, particularly track length. The 400 mm track spread conditions had on average a 9.75° higher maximum slope compared to the 200 mm track spread conditions. The other variables did not show significant change across the conditions.

It is likely that these results would be dramatically affected by the type of terrain, so it is important to note that this was non-deformable and rough. Track width, sprocket diameter, and track tension may have had a larger effect on deformable terrain.

Table 7.1: Maximum slope results for 36 test conditions.

Track Width [cm]	Track Length [cm]	Sprocket Size [cm]	Track Slack [cm]	Max Slope [°]
5	40	12.7	2.5	47
5	40	12.7	0	47
5	40	12.7	-0.32	46
7.5	40	12.7	2.5	48
7.5	40	12.7	0	48
7.5	40	12.7	-0.32	47
7.5	40	17.8	2.5	47
7.5	40	17.8	0	47
7.5	40	17.8	-0.32	47
5	40	17.8	2.5	47
5	40	17.8	0	47
5	40	17.8	-0.32	47
5	35	17.8	2.5	45
5	35	17.8	0	43
5	35	17.8	-0.32	42
7.5	35	17.8	2.5	45
7.5	35	17.8	0	44
7.5	35	17.8	-0.32	43
7.5	35	12.7	2.5	45
7.5	35	12.7	0	44
7.5	35	12.7	-0.32	44
5	35	12.7	2.5	44
5	35	12.7	0	44
5	35	12.7	-0.32	43
7.5	30	17.8	2.5	38
7.5	30	17.8	0	38
7.5	30	17.8	-0.32	38
7.5	30	12.7	2.5	37
7.5	30	12.7	0	36
7.5	30	12.7	-0.32	36
5	30	17.8	2.5	38
5	30	17.8	0	38
5	30	17.8	-0.32	38
5	30	12.7	2.5	37
5	30	12.7	0	37
5	30	12.7	-0.32	37

7.3 Evaluation through Metrics

7.3.1 Reconfigurability Metric

The reconfigurability metric is the same for all configurations. Following the definitions set out in Chapter 2, the track tension aspect of this vehicle is manually reconfigurable and self contained. The track width, contact length, and sprocket diameter are also manually reconfigurable but not self contained since they require external intervention to swap components.

Based on the types of modularity outlined in [67], the sprocket attachment would be considered bus architecture. Each sprocket holder interface has the same hole pattern, allowing different sprocket holders for different diameter sprockets to attach at distinct locations along the chassis. Similarly, the track width is able to be changed by swapping out the tread.

This vehicle takes 480 seconds to reconfigure, which gives a scaled T_{rec} over 1. The vehicle has 3.9 kg of additional material to facilitate different configurations, which is less than the threshold and slightly greater than the objective. This value scales to $E_{rec}=0.037$. Using equation 2.2 with the same constants as section 2.4, $RC = 0.5 * 1 + 0.5 * .037 = 0.537$.

7.3.2 Mobility Metric

The mobility metric for this vehicle would ordinarily be a single value. But for the purpose of illustration, we will calculate it for each configuration to determine which configuration is most ideal.

Using the semi-empirical methods outlined in Chapter 3.3, a map of Go/No-Go terrain can be created as described in the proposed metric. Table 7.2 shows the Mobility metric value for the primary configurations of this vehicle. Since track tension is not included in the semi-empirical equations used in this system, those variants are omitted.

Table 7.2: Mobility metric for reconfigurable vehicle configurations.

Track Width [cm]	Track Length [cm]	Sprocket Size [cm]	M
5	40	12.7	0.791
7.5	40	12.7	0.791
7.5	40	17.8	0.852
5	40	17.8	0.852
5	35	17.8	0.852
7.5	35	17.8	0.852
7.5	35	12.7	0.793
5	35	12.7	0.791
7.5	30	17.8	0.852
7.5	30	12.7	0.793
5	30	17.8	0.852
5	30	12.7	0.791

The vehicles with the larger diameter had higher mobility metrics due to having a larger area component, which was the highest weighted element. The average drawbar pull values

for all configurations were greater than the objective function, so these values were largely washed out. Figure 7.6 below shows the distribution of drawbar pull for the Keweenaw Test site.

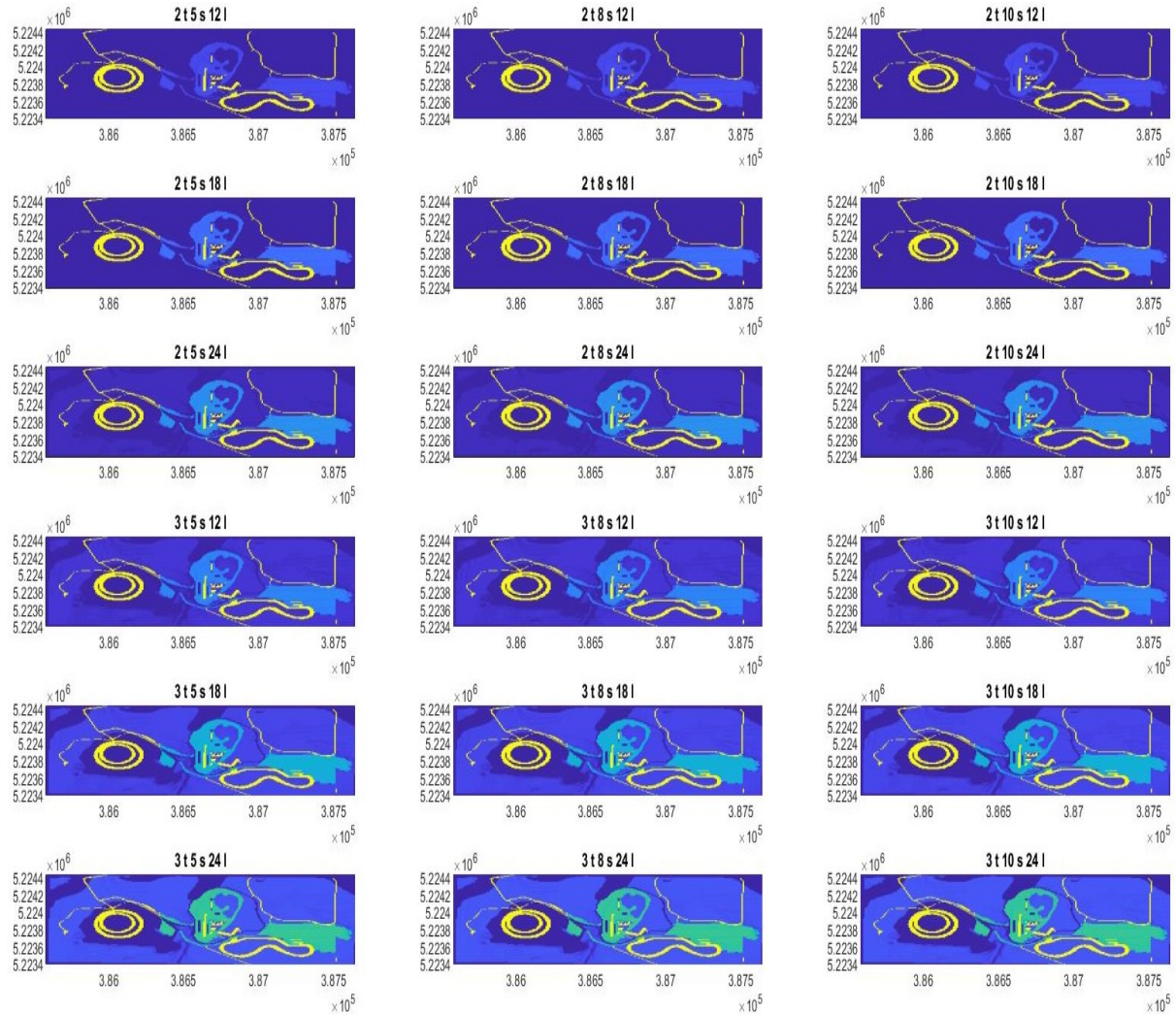


Figure 7.6: Aerial view of test sites showing drawbar pull where lighter colors are higher drawbar pull.

7.3.3 Complexity Metric

This vehicle has 2 actuators, and 2 links, each of length 1. Each track is one degree of freedom and each reconfigurability represents another degree of freedom, totalling 5. Using the metric from Chapter 4 with $n_{nl,t}=4$, $n_{nl,o}=2$, $n_{links,t}=4$, $n_{links,o}=2$, $n_{a,t}=8$, $n_{a,o}=4$, $n_{d,t}=6$, $n_{d,o}=4$, and coefficients set to 0.25 yields $C_{proposed} = 0.25 * 0 + 0.25 * 0 + 0.25 * 0 + 0.25 * 0.15 = 0.0375$. In contrast, the vehicle on its own without these reconfigurabilities would have a complexity of $C_{proposed} = 0.25 * 0 + 0.25 * 0 + 0.25 * 0 + 0.25 * 0 = 0$. In both cases, the low number of actuators and simple configuration drive this metric down significantly.

7.3.4 Optimization

To find the optimal set of parameters for this vehicle, we used the RMCVO system and constrained the physical parameters to the dimension extremes of the vehicle. We also limited the vehicle to only track configurations. 20 was selected as the population size through observation as a value that offered enough variation in a given generation but not so much that the solution converged too quickly. The optimization was terminated when the objective functions stopped changing within 1% of previous values, indicating that new parameter combinations were not significantly improving the ideal values. The table below documents the parameters used for this optimization:

For the [0.2, 0.6, 0.2] weights, averaging the two algorithms, the ideal track width was 0.07 m, the ideal length was 0.33 m, the ideal diameter was 0.18 m, and self-reconfigurability was preferred with an extent of reconfigurability of 1.63. For the [0.2, 0.2, 0.6] weights, there was high discrepancy between the two algorithms. Averaging these two, the best variables were 0.066 m for the width, 0.275 for the length, 0.18 for the diameter, and split decision on the reconfigurability dynamics. Finally, for the weighting scheme that highly favored low reconfigurability cost, width was preferred at 0.07 m, length at 0.275, diameter at 0.18, and no reconfigurability. Table 7.4 shows the metric values for these ideal parameters (last 3 rows) compared to the vehicle as is.

The PCPs below shows the optimal solutions for various weighting combinations.

Table 7.3: Mobility Metric Values.

Min Weight [kg]	18.7
Max Weight [kg]	18.7
Min Width [m]	0.05
Max Width [m]	0.075
Min Length [m]	0.3
Max Length [m]	0.6
Min Diameter [kg]	0.127
Max Diameter [kg]	0.178
Min Reconfigurability Extent [%]	0
Max Reconfigurability Extent [%]	0
Min Reconfigurability Dynamics	0
Max Reconfigurability Dynamics	2
Min Reconfigurability Style	6
Max Reconfigurability Style	13

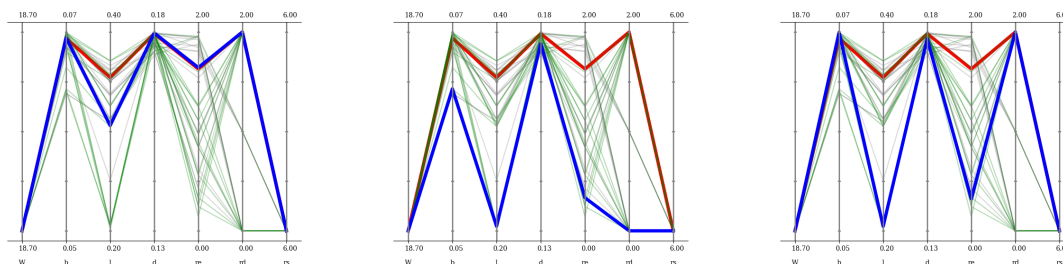


Figure 7.7: Parallel coordinate plots for the same set of variables with different weights. From left to right, the weights are: $[0.2, 0.6, 0.2]$, $[0.2, 0.2, 0.6]$, and $[0.6, 0.2, 0.2]$.

Table 7.4: Metric comparison for reconfigurable vehicle configurations.

Track Width [cm]	Track Length [cm]	Sprocket Size [cm]	Reconfigurability Dynamics	Reconfigurability Extent	R	M	C
5	40	12.7	1	1	0.537	0.79	0.0375
7.5	40	12.7	1	1	0.537	0.79	0.0375
7.5	40	17.8	1	1	0.537	0.852	0.0375
5	40	17.8	1	1	0.537	0.852	0.0375
5	35	17.8	1	1	0.537	0.852	0.0375
7.5	35	17.8	1	1	0.537	0.852	0.0375
7.5	35	12.7	1	1	0.537	0.793	0.0375
5	35	12.7	1	1	0.537	0.791	0.0375
7.5	30	17.8	1	1	0.537	0.852	0.0375
7.5	30	12.7	1	1	0.537	0.793	0.0375
5	30	17.8	1	1	0.537	0.852	0.0375
5	30	12.7	1	1	0.537	0.791	0.0375
7	33	17.8	2	1.63	0.072	0.891	0.0917
6.6	27.5	17.8	0	0	0	0.882	0
7	27.5	17.8	0	0	0	0.882	0

7.4 Mission-Level Validation

So far, we have shown that the optimization algorithm can select a preferred vehicle based on piecewise comparison of the candidate vehicle with existing configurations. In order to validate the utility of the full RMCVO system, we conceived three example missions to more fully capture performance in a real world scenario. These use cases all involve common autonomous vehicle tasks, but they are not exact replicas of any of the criteria for the metrics described in this work. In this way, we could determine the utility of the RMCVO process more honestly.

7.4.1 Rapid Mapping

The first mission is a mapping mission. The objective is to map 75% of a given terrain as quickly as possible. A potential application for this mission would be a lunar rover mission where the rover can only travel in shadow for a brief amount of time before returning to the sun to charge. The same environment that was used for the mobility metric calculations was used for this example as the intention of that metric is to use representative soil and grade data to the intended environment. It is assumed that the vehicle is able to adequately map at a range of 10 m away from the vehicle in all directions. Since our work focuses on large scale mobility and vehicle design, it is assumed that the vehicle has perfect localization and control such that it can precisely follow a given trajectory.

In order to calculate this time, we calculate slip empirically at each pixel. Since pixels measure 8.5 m, a robot traveling in the center of each pixel will fully map that pixel with the perception capabilities presented in this problem. We assume a boustrophedon pattern [301] for the required 75% of terrain. Using the relationships uncovered in [156], we can equate slope to slip. We multiply the nominal rotational speed of the motors operating at peak power by the radius of the drive sprocket and the complement of the slip percentage to get tangential velocity. Then we use a variation on Grenander's approach to the maximum subarray problem [302] to uncover the minimum sum of the time to move across enough traversible pixels to cover 75% of the environment.

Table 7.5 shows the results for this vehicle. The vehicles with the wider track width and longer track length had faster times to cover the terrain. These vehicles had a larger starting footprint, and thus higher thrust. Though their compaction was also larger, it was dwarfed by the thrust value.

7.4.2 Expedient Rescue

The second use case is designed to simulate a rescue mission where a robot needs to take supplies to a known location as quickly as possible. In the real world, the faster the vehicle could reach the site of the incident, the faster information could be gathered about the scene, medicine or protective equipment could be distributed, and the greater chance that the casualties would survive.

We combine the path planning described in Section 3.3 with the vehicle time described in the previous mission. Time to complete each segment of the shortest path is summed to create a single time to reach the target. These times are summarized in Table 7.5. These times largely followed the times from the previous mission except in the case where the paths could be shorter in a different configuration, which brought down the total time.

7.4.3 Maximum Sample Collection

Lastly, Mission 3 is a retrieval mission evaluated by the maximum amount of samples that can be collected in five hours. Such a mission approximates collection of soil samples in a vast or dangerous environment for geologic classification. Time constraints can be placed on such missions due to weather, fuel, and access limits on certain sites. The manipulation of the soil samples is not a focus of this work and is assumed to be uniform across the configurations. We also assume number of samples that the vehicle can carry at once is constrained by its drawbar pull, and not by a volumetric capacity. We also specify that the weight of the material can be

place in such a way that the weight can be directly transferred via drawbar pull. Thus, a vehicle with high drawbar pull would be able to carry more samples without needing to drop them off at the starting location.

To calculate the maximum collection in five hours, we calculate the time to get from a start point to collection site. We use the minimum drawbar pull along this path to determine how much material can be dragged during this traverse. We multiply that number by how many complete trips (there and back) can be completed in 5 hours. For example, the fastest vehicles were able to make 25 trips in 5 hours, while the slower vehicles were able to make 8 trips.

Table 7.5 shows the results from this mission as well as the previous two. For this comparison, the number of trips greatly diminished the impact of higher drawbar pull. For example, the vehicle with 5 cm by 40 cm tracks and 12.7 cm sprockets had a lower collection weight compared to the vehicle with the same track but larger sprockets even though its minimum drawbar pull was 3 times higher.

7.4.4 Mission-Level Comparison

A summary of the results from all three missions is presented in 7.5. Based on this table, the vehicles with wide and long tracks had the shortest time to cover the terrain. However, the vehicles with thin or short tracks had a faster time to reach an isolated person when path planning was optimized using A*. Finally, the Vehicles with the larger diameter sprockets had a higher capability of carrying samples and out performed the vehicles with smaller sprockets for all conditions in Mission 3.

If we consider the [0.2, 0.6, 0.2] weighting scheme discussed in section 7.3.4, the ideal track dimensions were 0.075 m by 0.33 m, the ideal diameter was 0.178 m, and self-reconfigurability was preferred with an extent of reconfigurability of 1.63. The performance of this vehicle within the three missions is also documented in 7.5. Since this theoretical vehicle configuration could reconfigure automatically, the number of transitions throughout the path was also incorporated into the total time. This reconfiguration lead to a much higher performance on Mission 3 because the vehicle could reconfigure in areas with small drawbar pull. The minimum drawbar pull was 5 times as great as the next highest conditions. This cost a bit of time, but resulted in more material being moved per trek.

Table 7.5: Sample mission performance.

Track Width [cm]	Track Length [cm]	Sprocket Size [cm]	Mapping time [hr]	Rescue Time [hr]	Collection Quantity [kg]
5	40	12.7	93.8	0.148	0.322
7.5	40	12.7	92.9	0.118	3.13
7.5	40	17.8	91.3	0.123	3.6
5	40	17.8	92.2	0.118	4.93
5	35	17.8	92.2	0.118	4.93
7.5	35	17.8	91.3	0.123	3.6
7.5	35	12.7	92.9	0.118	3.13
5	35	12.7	93.8	0.148	0.321
7.5	30	17.8	91.3	0.123	3.7
7.5	30	12.7	92.9	0.118	3.13
5	30	17.8	92.2	0.118	4.9
5	30	12.7	93.8	0.148	0.321
7.5	33	17.8	87.2	0.123	18

From this comparison, we can see that the optimized vehicle performed well in the mission scenarios, but was not the highest scoring in every single one of them. There are two levels where the user must place preference on the system (the inter- and intra-metric levels), and these may not exactly correspond to the missions we used as evaluation metrics. For example, this vehicle had the highest M value. However, these missions did not require traversal over the entire area, so the very high coverage that this vehicle boasts was not capitalized on. Additionally, the metrics performed well overall. Table 7.6 prevents a normalized sum of the three missions where the higher number, the closer to the best value (higher value for the quantity collected and lower value for the times). The idealized vehicle performed best compared to the other candidate vehicles.

Table 7.6: Scaled sample mission performance.

Track Width [cm]	Track Length [cm]	Sprocket Size [cm]	Norm Mapping time	Norm Rescue Time	Norm Collection Quantity	Sum
5	40	12.7	0	0	0	0
7.5	40	12.7	0.137	0.99	0.159	1.29
7.5	40	17.8	0.379	0.832	0.185	1.4
5	40	17.8	0.243	0.99	0.261	1.5
5	35	17.8	0.243	0.99	0.261	1.5
7.5	35	17.8	0.379	0.83	0.185	1.4
7.5	35	12.7	0.137	0.99	0.159	1.29
5	35	12.7	0	0	0	0
7.5	30	17.8	0.379	0.832	0.191	1.4
7.5	30	12.7	0.137	0.797	0.159	1.29
5	30	17.8	0.243	1	0.26	1.5
5	30	12.7	0	0	0	0
7.5	0.33	0.178	1	0.83	1	2.83

As for the other metrics, the reconfigurability cost payed off in decreasing the total time for the missions based on reconfiguration throughout the path. The optimal configuration selected for the missions featured self-reconfigurability and was capped at 1.63 times reconfiguration extent, indicating that this time was permissible given our time threshold and objectives. Complexity did not appear as much in these missions, but we were able to show directly how the complexity of the system could be minimized by increasing the weighting of those variables in Table 7.4.

7.5 Conclusions

Field testing with this vehicle showed trends consistent with theory for track width and track length. We also demonstrated the effect of uncommon variables like track tension. Experimental results for sinkage followed the calculations closely, with the additional variations based on track tension and drawbar pull, which are not in these semi-empirical equations. We also compared different methods of pressure prediction including a low fidelity pressure array and color change film. Finally, we evaluated maximum slope climbing ability with a rigid surface.

We utilized our proposed metrics to evaluate the testbed robot in 12 configurations. We also compared the metric values with these existing configurations to the ideal configuration developed through optimization using genetic algorithms. Through this testing, we were able to identify preferred configurations based on the prioritization of the three metrics.

To evaluate the real-world relevance of the three proposed metrics, we constructed three example missions that are common for unmanned vehicles. Using these missions, we were able to show good performance using the optimized parameters. However, it was out-performed by several of the other compared configurations for individual missions. This result underscores the challenge of mapping a mission to a series of weights and generalizing performance into

single metrics. Future research may increase the utility of the RMCVO system through smarter weighting methodologies or increased ability to tailor the process to a specific mission. Overall, the system had the best combined score when each mission score was normalized, indicating correlation between the metrics presented in this work and real world scenarios.

Chapter 8

Conclusion

8.1 Summary

In this thesis, we presented a cohesive examination of reconfigurability in small unmanned vehicles. We first looked at the state of the art in reconfigurability, mobility, and complexity metrics. Along the way, we clarified ambiguities in modular terminology. Next, we developed our own quantifiable metrics for our two costs: reconfigurability and complexity, and one benefit: mobility.

The reconfigurability metric represents a new value in the world of vehicle design. Typically, reconfigurability has been quantified in terms of the extent or features that it affords a system. In this work, we incorporate those benefits into our mobility objective function and focus on summarizing the latent downsides of reconfigurability including transition time, monetary cost, and additional required equipment.

Our metric for mobility is particularly relevant for unmanned vehicles and incorporates key robotic use cases including mapping, searching, and collecting. It is able to express far more information than empirical metrics like VCI and MMP and each of its three elements has a physical meaning. Additionally, compared to drawbar pull, it represents a vehicle's ability over a variety of different terrain.

Our complexity metric incorporates physical and control considerations for unmanned vehicles. In this way, it is more expressive than existing complexity or degrees of freedom metrics. Like the other metrics, it is adjustable based on the user's priorities and is scaled to the parameters of the mission.

These three objective functions are combined into a single optimization interface using multiple algorithms. This system is validated in multiple ways: first in comparison with other measures, then experimentally using a novel reconfigurable tracked vehicle, and finally through a combination of theoretical and experimental mission scenarios.

The vehicle used to evaluate the metrics was created with multiple adjustabilities which enable it to serve as a testbed for terramechanics testing and reconfigurable vehicle design. Its design also helped inform principles of reconfigurable design.

8.2 Contributions

The unique aspects of this work lie in both the optimization framework and its validation:

1. Primary: A quantifiable system for comparing the mobility benefits of reconfigurability along with the various costs for small, tracked unmanned ground vehicles that enables design optimization (Chapter 5). The RMCVO framework incorporates reconfigurability, mobility, and complexity into a single system and outputs ideal parameters given user's acceptable limits and comparative valuations.
2. Formalized definitions and novel quantitative metrics for reconfigurability (Chapter 2), mobility (Chapter 3), and complexity (Chapter 4). These definitions are specifically shaped for relevance to unmanned ground vehicles, including elements like coverage and degrees of freedom.
3. Design and implementation of an unmanned, manually reconfigurable tracked vehicle for terramechanics testing and best practices for implementing reconfigurability in small, tracked unmanned ground vehicles (Chapter 6). The testbed designed and constructed for this effort offers a wide variety of adjustments through the swapping of modular components. The mechanism integrates variability in track length, track width, sprocket size, and track tension.
4. Comparison of mobility performance with different characteristics using the custom manually reconfigurable tracked vehicle (Chapter 7). The custom vehicle provides an ideal way to test the theory presented in the first half of the thesis.

8.3 Future Research

This research focused on unmanned ground vehicles between 5 and 60 kg. A future avenue for research would be the effect of reconfigurability on lighter or heavier vehicles. Lighter vehicles are especially viable for space applications where transportation costs drive down vehicle weight. Exploration into heavier vehicles would be applicable for larger farming, construction, and military use.

Another extension of this work would be exploration into air- and water-based robotic platforms. The mobility criteria for these vehicles would be very different than the metric presented in this work; but the reconfigurability and complexity metrics may be applicable for such vehicles.

Furthermore, as DEM methodologies become more ubiquitous, they would be valuable to incorporate for more accurate mobility estimations. The mobility estimations used in the RMCVO system are all semi-empirical, which have been used for years, but lack the fidelity of DEM simulations. Project Chrono [286] offers an open source DEM simulation system that would be relevant for this purpose. The downsides to these methods are the heft of the programs necessary to create the simulation and the increased time and resource burden that they require to run.

Higher fidelity maps or a methodology for stochastic estimation of smaller obstacles would also improve the accuracy of the coverage estimations. Currently, the maps are taken to be ground truth and obstacles besides slopes are completely ignored. Wasfy and Jayakumar provide a concise exploration of using stochastic strategies for speed-made-good estimations that could be adapted here [165].

The reconfigurable vehicle described in Chapter 6 could also be improved in the future. Current limitations and ideas for improvement are provided in A.6 including methods for this vehicle to have self-contained reconfigurability or self-reconfigurability. Expanding the capabilities of this vehicle enhance its utility for further terramechanics testing and offer insight into hands on reconfigurable vehicle design.

Finally, additional experimental testing could be conducted including higher fidelity pressure testing, drawbar pull testing, and slip testing. Drawbar pull would provide further validation of the semi-empirical equations used to calculate average drawbar pull. Testing could also be conducted to examine the turning capabilities of such a robot. For this work, the vehicle was assumed to be able to achieve any turn required to adhere to the prescribed path, but this is not an accurate assumption. Steering considerations were not a focus of this work but are presented briefly in B.

8.4 Conclusions

In this thesis, we demonstrated how reconfigurability, mobility, and complexity could be quantified and optimized to drive vehicle design. Our definitions and metrics provide a framework for others to continue exploration in reconfigurable mobility metrics. Our RMCVO system affords an environment-based methodology for optimizing vehicle design with prioritization for mission specificity, adjustable priorities, and meaningful numerical comparisons. Using this system, we were able to find ideal parameters for a small tracked vehicle. These ideas were validated through terramechanics calculations, simulation, and experimental testing. It is our hope that the ideas and framework presented in this thesis will be a benefit to robotics researchers curious about reconfigurability quantification and engineers working to develop relevant and versatile ground vehicles.

Appendix A

Test Vehicle Design and Iteration

A.1 Introduction

This appendix documents additional details in the design and refinement of the manually reconfigurable tracked vehicle described in Chapter 6.

A.2 Design Process

This first design iteration (Figure A.1) featured a sheet metal chassis similar to Pantaleo’s suspension testing device. The chassis (shown in red) had multiple holes to allow multiple mounting positions for the motor subsystem (blue) and idle sprocket subsystem (yellow), which allowed for various track lengths. The track sprockets are supported on both sides, which is a feature that is continued throughout all design iterations. The outer sprocket supports are connected to the main body through standoffs in the center of each side (instead of the ends) so that the track is the first thing that would impact an obstacle if hit head on. A medium torque Polulu motor/gearbox with integrated encoder [303] was selected based on estimations of vehicle weight and easy of use. Lynxmotion Modular Track System [304] sprockets and tracks were chosen for their varied sizes and common interfaces. As development progressed, the desire for track tensioning, or at least fine adjustment of travel distance, became apparent. Track tension was added as an additional parameter for study.

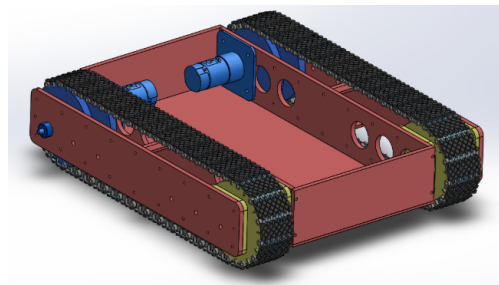


Figure A.1: Version 1 of the modular tracked vehicle design.

Portions of this chapter were presented in the ISTVS 20th International and 9th Americas Conference Proceedings[202] and the ISTVS Student Speaker Series on December 8th, 2021

The next major step in the evolution of the design (A.2) was a triangular track design with interchangeable sprocket mounts to allow multiple sprocket sizes and a constant ride height. The motor was also moved to the center of the vehicle so that the weight distribution would not be affected when the track contact length changed. Additionally, since the motor was decoupled from the changing sprocket diameters, the gear ratio of the vehicle could remain constant. To get a high wrap angle above 90° , the motors needed to be placed fairly high above the vehicle, which resulted in a lot of wasted track on the diagonals that would likely not engage with obstacles. In order to support the raised motor, 1 in square aluminum tubes and 0.25 in aluminum plates were chosen over the sheet metal. Tension could be adjusted by moving nuts that support the spring that support the motor mounts (shown in green below the blue motor subsystem). As the nuts below the motor supports are moved up, the spring is compressed and the track tension increases. Two nuts are used to prevent them from loosening as the track moves over the idle roller. The opposite occurs when the nuts are lowered. The nuts are moved up based on dividing the desired tension by the spring's spring rate. It was decided that this placement for the tension system would likely be extremely unstable as the motor's torque would be opposed by opposite displacements on the two spring supports. The general form of adjusting the tension through the spring compression was used in successive designs.

To decouple the motor from the ground sprocket diameter and achieve a wrap angle greater than 90° , a trapezoidal track shape was adopted in the fifth revision (A.3). This track shape, along with an h-shaped chassis also ensured that the track was the first thing to engage with obstacles, even if they were very tall. Additionally, as the vehicle became more robust and required more sprockets, it also became heavier. A VEX Mini CIM 12 V brushed DC motor with 10:1 VersaPlanetary gearbox was selected over the previous Pololu motors to provide higher torque [288]. This motor plus gearbox made the vehicle very wide. At the smallest track contact length, the vehicle was about two times wider than it was long. Though convenient to mount the motors in line with the sprocket and gearbox, this seemed unreasonable for small ground vehicles that are usually longer than they are wide or perhaps have a square footprint.

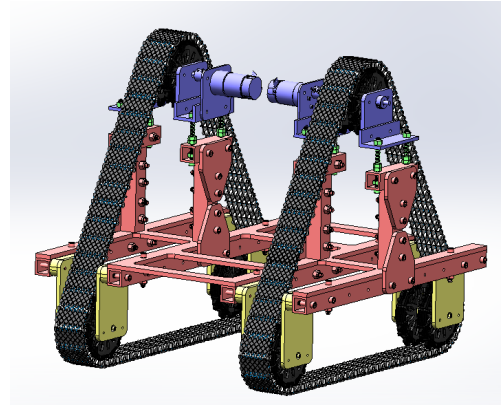


Figure A.2: Version 4 of the modular tracked vehicle design.

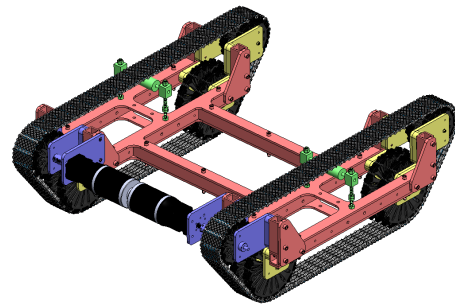


Figure A.3: Version 5 of the modular tracked vehicle design.

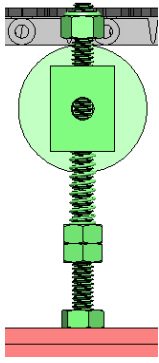


Figure A.4: Side view of track tensioning system.

In this design, the tension mechanism is also separate from the motor and idle sprockets and takes the form of an idle roller on the same spring system used in Design 4. The mechanism is shown in Figure A.4. The two nuts below the spring can be moved up and down in accordance with the required tension.

A.3 Fabrication

The planar Aluminum components were cut using a water jet at NREC. Though the vehicle was designed with mostly planar custom components, these parts were not rectangular and had many holes at precise distances, making the water jet the most reasonable tool.

The frame was cut from 0.19" and 0.125" Aluminum with 1" extruded Aluminum square tubing for the sprocket supports. The extruded Aluminum tubing was milled by hand at the CMU Robotics Institute's Field Robotics Center. Parts were first rough cut using a cold saw, then faced and drilled using the mill. Finally, holes were tapped by hand or reamed using the mill as needed. Both the water jet and milled parts were finished in the sand blaster.

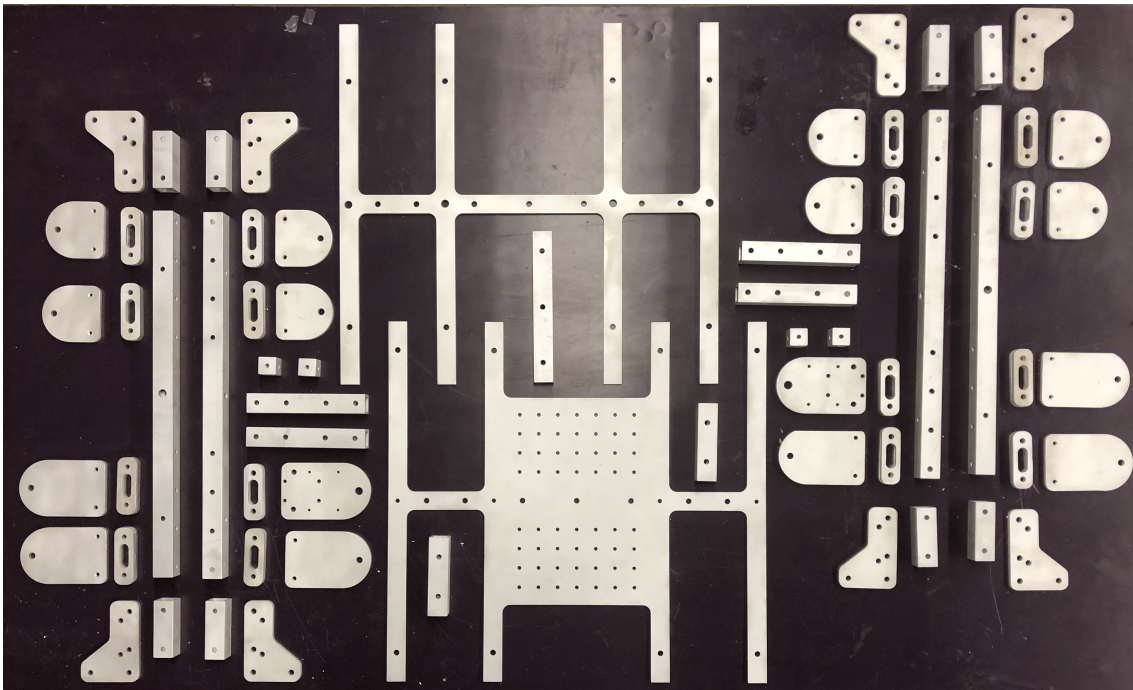


Figure A.5: Water jet and manually milled components.

The motor shrouds were made from PLA using a 3D printer from the CMU Robotics Club.

The sprocket and track components were assembled by hand. This involved bolting teeth on the sprockets and screwing them to a central hub, as well as putting together the links of the track using a plastic dowel and locking pins.

Finally, the hardware and electronics were attached to the vehicle via the array of holes in the bottom plate of the vehicle. Acrylic plates were used to cover unused holes to prevent

debris from coming up through the bottom of the chassis. The battery is held in place with angle stock and a Velcro strap.

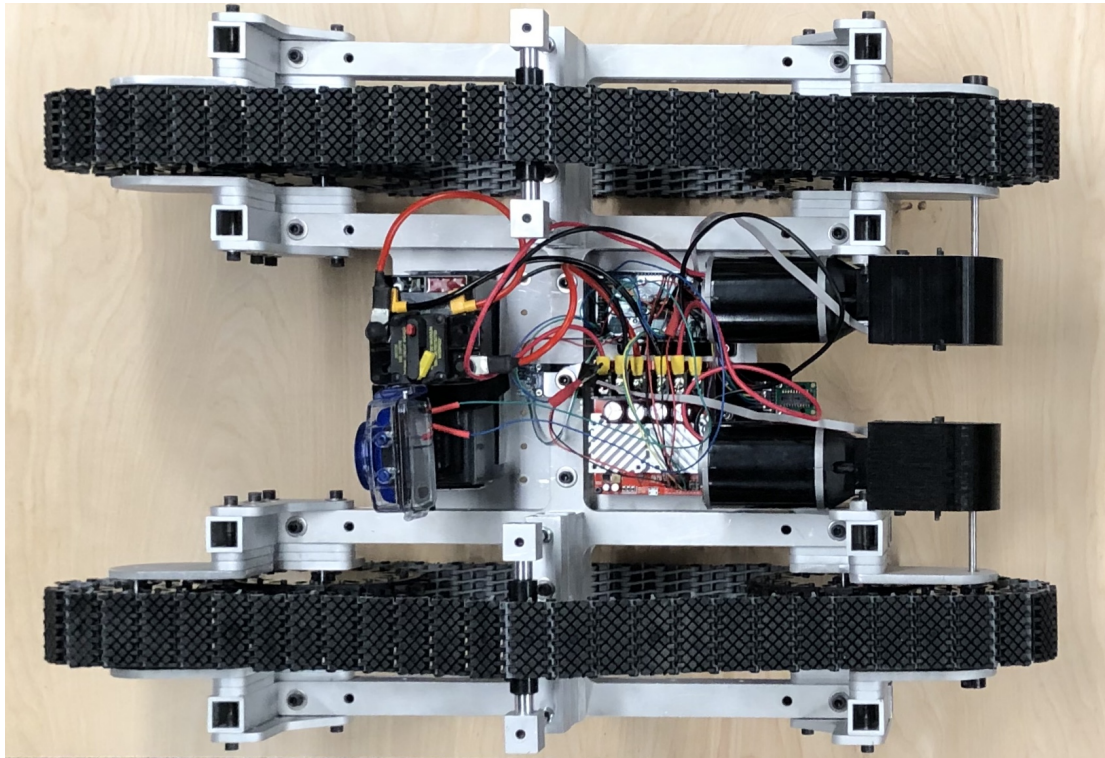


Figure A.6: Top view of the completed vehicle.

Most of the Aluminum components were attached using 1/4-20 bolts and the electronics were secured to the base plate using 8-32 bolts to reduce the amount of required tools. The socket cap bolts made assembly and reassembly convenient, however, the motor assembly contains some hard-to-read areas.

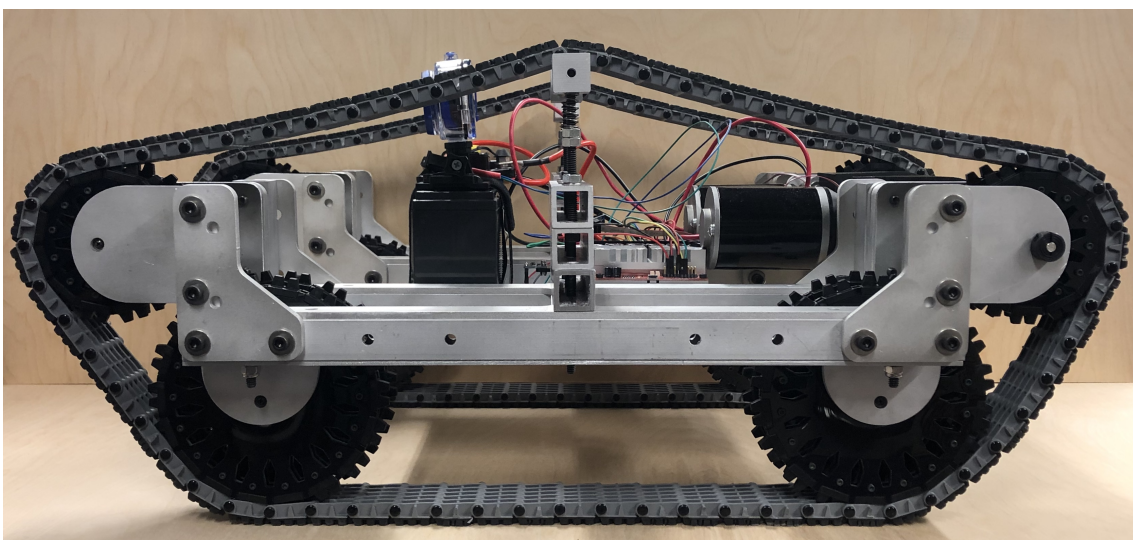


Figure A.7: Side view of the completed vehicle.

A.4 Vehicle Iteration

After the first tests varying the tension, we observed the block that the idle roller was secured to was binding on the vertical support bolt. This meant that the forces on the track were transferred at least partially through the bolt, instead of the spring. We replaced the bolt with a shaft and the nuts with shaft collars. This allowed the block to move smoothly even with high force from the spring.



Figure A.8: Close-up view of old tension system (left) with bolts and nuts and new tension system (right) with shafts and shaft collars.

With this change we also increased the length of adjustability since some configurations were maximizing our current constraints. Since each track link is 1 inch from joint to joint, the overall length of the track is somewhat limited. For example, in the smallest track configuration, adding 1 track link (i.e. 0.5 in to each side of the angled track segment), results in almost a 2 inch change in height. Therefore, our adjustability needed to be almost 2 inches to ensure that we could get to the proper height for the desired tension.

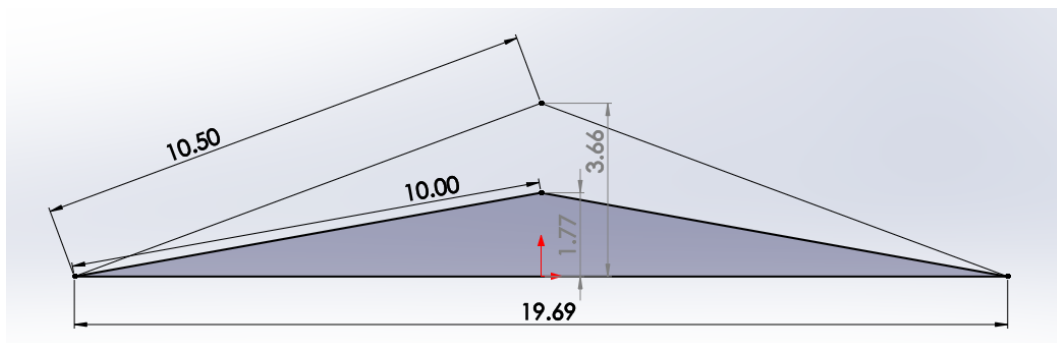


Figure A.9: Illustration of the change in vertical distance as a result of the addition of one track link (0.5 in on each diagonal leg)

Throughout these system tests, we also encountered various issues related to power transmission where the vehicle would slow or stop on one or both sides. For example, the following plot of current shows one motor as it gradually becomes disconnected from the output shaft.

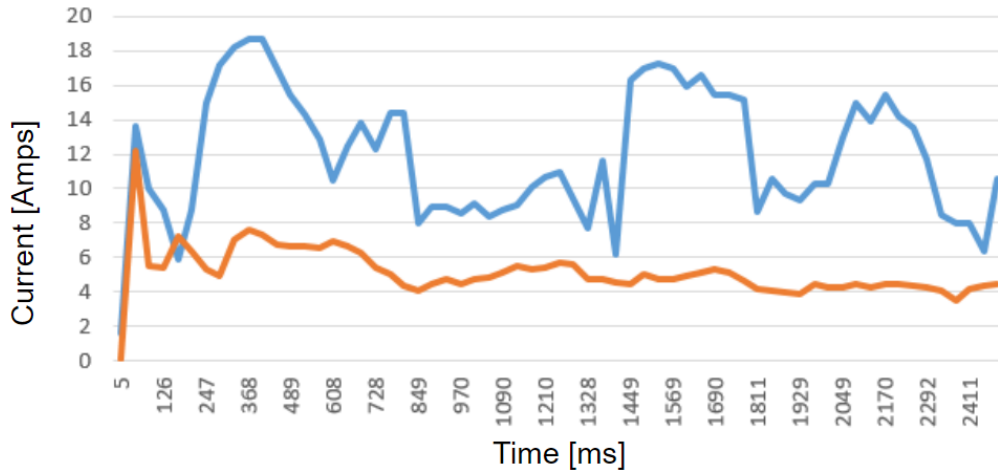


Figure A.10: Plot of left and right motor current draw over the course of one traverse of an obstacle course. The blue line shows an expected variation in current as the vehicle drives over different obstacles. The orange line shows the current for the motor that becomes completely unlinked from the track throughout the trial.

This issue was largely caused by different set screws in the driveline loosening up. A few different changes were made to address this issue. Initially, permanent thread locker kept the set screws in place. But after a while this issue came back. Where possible, the set screws were replaced with bolts with socket heads that could be tightened more easily. Other set screws were replaced with screws with barbs on the bottom to dig into the shaft. The following plot shows the left and right motor current draw after these changes.

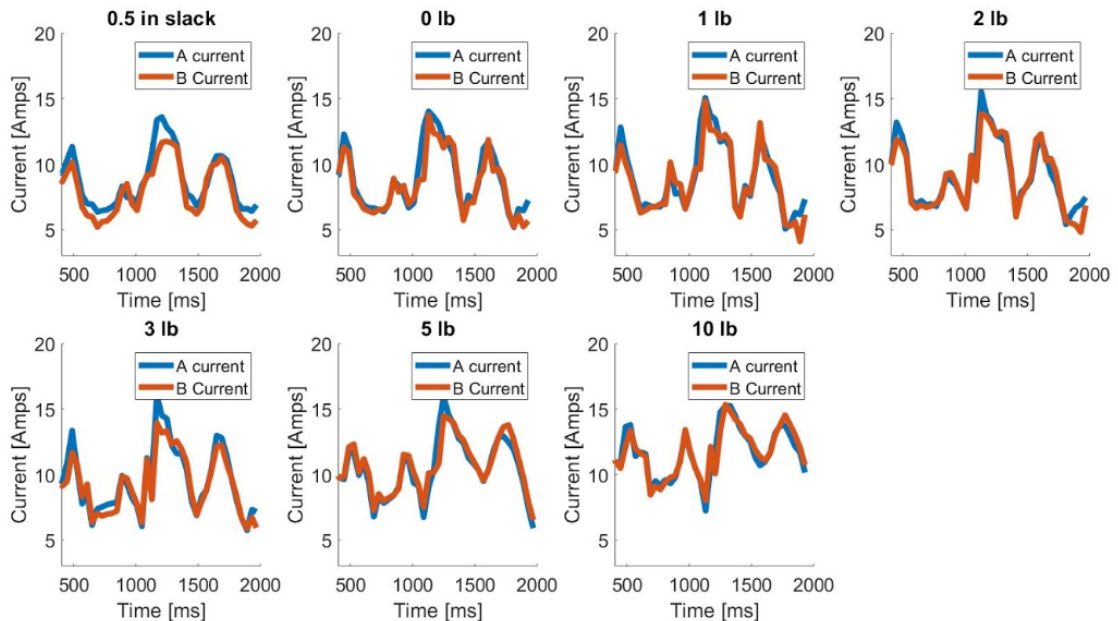


Figure A.11: Left and right motor alignment for 10 trials at 10 lbs.

Based on this alignment, the average of the left and right motor current was used as the primary value for current draw. The plot below shoes a promising result with no clear temporal effects over the course of 10 trials.

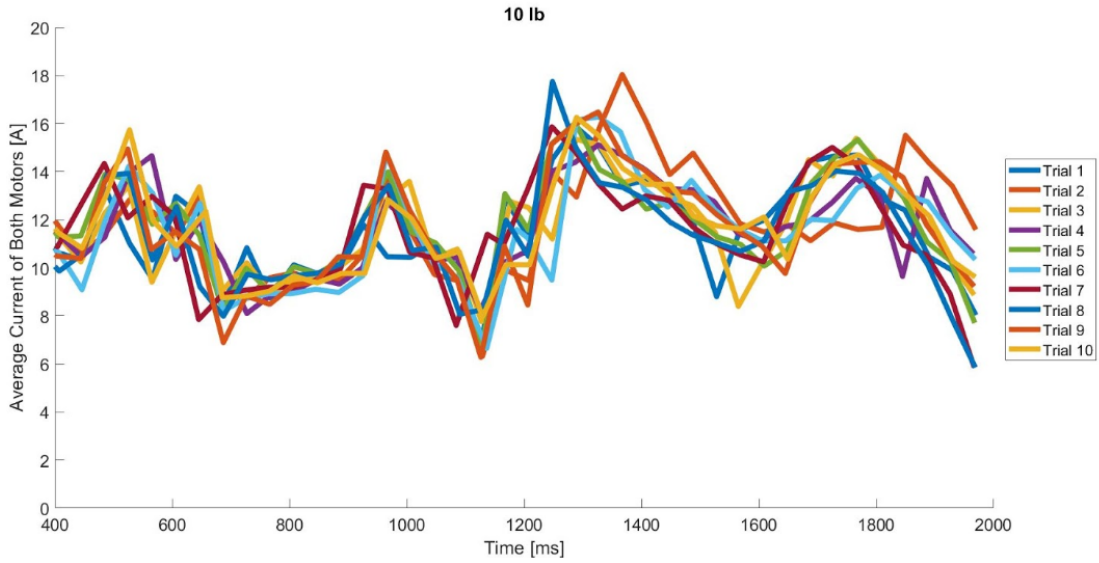


Figure A.12: Plot of 10 trials with the 10 lb track tension condition. There is no clear trend from trail 1 to trial 10, which indicates that the driveline is not loosening up over the course of the trials.

A fifth wheel subsystem was added to the vehicle to measure ground speed. The optical flow sensor needed an inordinate amount of light below the vehicle and needed to be only a few centimeters off the ground in order to get any measurements, even with lens adjustment. Design for the fifth wheel subsystem was loosely based on Wesson, et al.’s modification of an ATV for terramechanics testing [13]. A US Digital E2 optical encoder with 500 CPR was selected [305].

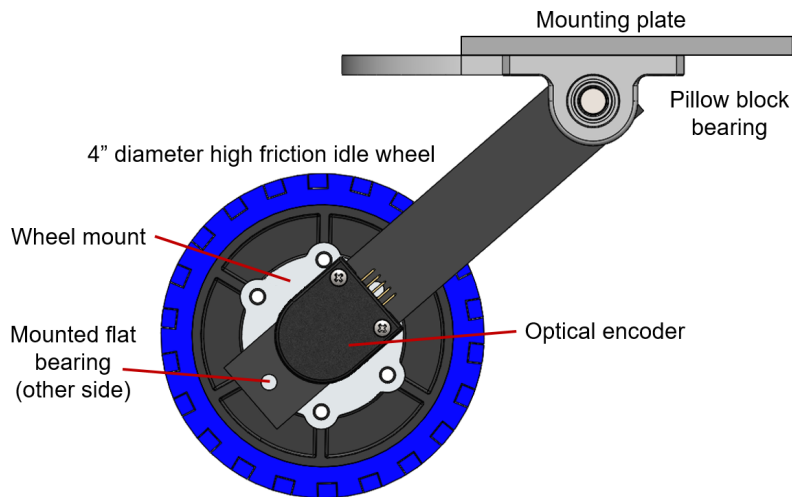


Figure A.13: Side view of fifth wheel assembly CAD with key components labeled.

A.5 Limitations

The square tube and plate design made fabrication simple. The chassis is extremely stable and most of it’s individual components have yield strengths more than ten times the maximum stress caused by expected forces based on FEA conducted with SolidWorks. This being said,

the chassis could likely be a great deal lighter, at the expense of some of this factor of safety and longer machining time.

One of the primary shortcomings of this vehicle is that it was designed for assembly, but not necessarily reassembly. For example, there are only two mounting plates that connect both the ground and rear idle sprockets. However, this means that they are essentially linked, so if the ground sprocket is moved, the rear sprocket will also shift. Additionally, the flat plate design made water jet cutting viable, but some 3-dimensional aligning features would have made it faster to change configurations. Lastly, the tapped components would have a longer life if they had helicoils or reinforcement of some kind.

The weakest portions of this vehicle are the off-the-shelf sprockets. Their faces are comprised of 1/8 in Lexan sheets [304], the idle rollers connect to their mounts through bearings with 4-mm thick walls, and the powered sprockets connect to their shaft with set screws as mentioned in Section A.4. The teeth are also constructed from Lexan [304] but are almost double the thickness of the sprocket faces. The vehicle was driven from a height of 4 feet onto concrete. The only things that were damaged were the bearings on the sprockets that impacted the ground first and the bolts that hold them in place.

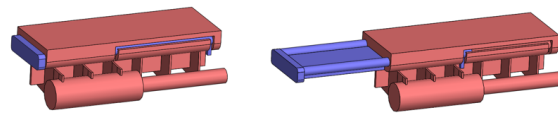
Finally, the vehicle is not at all sealed from the elements. The motor shrouds are designed to protect the motor gearboxes and encoders from debris, the electronics are protected from the bottom by the chassis and their mounting plates, and the idle bearings are partially protected by their axles and mounts. But the vehicle is in no way sealed from either debris or moisture. In order to make this device more useful in outdoor environments, the electronics section should definitely be enclosed, perhaps with a bent sheet metal cover.

A.6 Possible Extensions

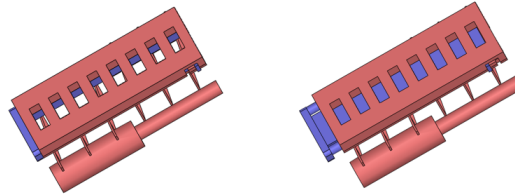
A.6.1 Towards Self-Contained Modularity

In a field setting, any detachable component is another item that must be remembered, carried, and maintained. For example, arm mechanisms can add functionality to the backpack-portable Dragon Runner 10, but at the expense of added soldier payload and maintenance [306]. However, creating a shifting component may increase complexity and reduce repairability compared to a module that can be completely removed and remedied on its own. Modules also create a degree of dynamic redundancy. For example, if one set of treads is damaged in the field, they could be replaced with the other set of treads, even if these replacements are designed for a slightly different terrain (one example of dynamic redundancy as defined by [48]).

Currently, changing sprocket diameter and track width of this vehicle both require additional components. Changing track tension and track contact length can both be done without additional parts, though they require hex keys, which would be an extra item to keep track of if repair tools were not already packed. In order to transform this vehicle into one without separate components that have to be carried, a few manually reconfigurable designs were explored. These designs were not implemented but present a step off point for further consideration into the trade-offs between of independent modules or transformable components.



(a) CAD model for reconfigurable track link that can expand in width.



(b) CAD model for a shutter design that can change surface area.

Figure A.14: Example designs for self-contained reconfigurable track links based on the hobby links used for this vehicle.

A.6.2 Towards Self-Reconfigurability

A completely autonomous system necessitates the ability to reconfigure automatically. To this end, several designs were drafted and evaluated to determine the possibility of self-reconfigurability for each current modularity.

Ground Contact Length

Design development for track contact length variation resulted in six different configurations for a vehicle that could double its contact length while maintaining relatively constant center of mass and ground clearance:

1. Separately Actuated Arms: The track shape transitions from a trapezoid with the long side down to a trapezoid with the short side down through three arms, one on each point. Each arm is actuated by its own motor.
2. Paired Arms: The track shape transitions from a trapezoid with the long side down to a trapezoid with the short side down through three arms, one on each point. Each point is actuated by its own motor and arms on the left and right are linked.
3. Dual Lead Screw Linkage: The track contact length changes as racks are moved in opposite directions from two center pinions. Each pinion is connected to a lead screw that raises or lowers the third point of the triangular-shaped track to maintain constant overall tread travel length.
4. Single Lead Screw Linkage: The track contact length changes as racks are moved in opposite directions from a center pinion. The pinion is connected to a lead screw that raises or lowers the third point of the triangular-shaped track to maintain constant overall tread travel length.
5. Expanding Track: The track is stretchable and is expanded through a rack and pinion system.

6. Movable Vehicle Weight: Track shape is changed through a single arm and a mobile weight is shifted to maintain near constant center of mass.

There were four main strategies for reconfigurability: revolute joints, linear mechanisms with constant track length, linear mechanisms with variable track length, and variable vehicle mass.

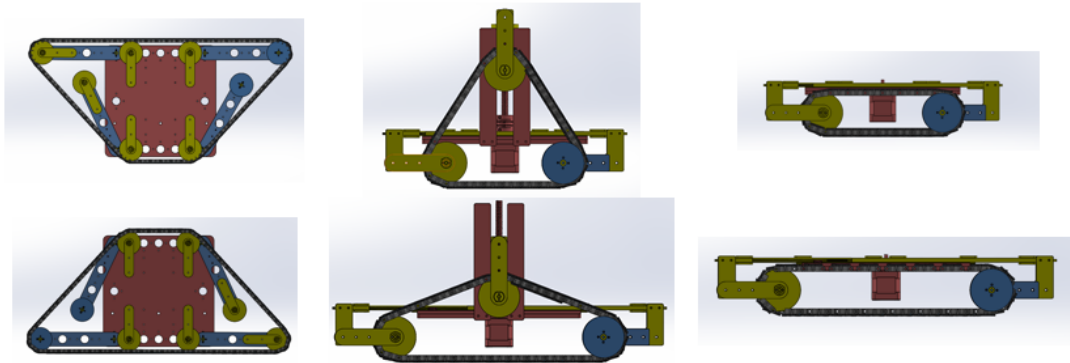


Figure A.15: Left: Separately Actuated Arms Design, Center: Lead Screw Linkage Design, Right: Expanding Track Design.

These designs were compared through a matrix that included ratings for number of motors, largest number of linked components, number of supporting sprockets, ease of achieving desired track tension, average drive sprocket wrap angle, number of sprocket transitions and ease of changing component dimensions. Each of these criteria was also rated by importance and the score for each vehicle was the sum of the products between the individual ratings and corresponding importance.

Ultimately, Design 3, the Dual Lead Screw Linkage, was deemed most promising for its comparatively low number of actuators and linked mechanisms. This offers a happy-medium between control complexity and mechanical complexity.

A.6.3 Control of a Self-Reconfigurable vehicle

A novel robotic system lacks real world utility if it is not controllable. As discussed in 7.5, simple PID control using encoders on the drive motors needed to be tuned for each individual condition to provide an equally smooth ride.

With an autonomous reconfigurable system, an important question to address is when to transform between configurations. Possible strategies include using an IMU to detect roughness, using a known map of terrain, or perceiving the terrain with vision, laser, light, or a combination[307].

$$F_{yaw} = 2l_1 C_{\alpha f} \delta_f(t) - \left(\frac{2l_1^2 C_{\alpha f} + 2l_2^2 C_{\alpha r}}{V_x} \right) \Omega_z - \left(\frac{2l_1 C_{\alpha f} - 2l_1 C_{\alpha r}}{V_x} \right) V_y \quad (\text{B.2})$$

When a vehicle is at steady state during the turn, the cornering force on the front and rear tires are as follows [132]:

$$F_{lateral,front} = \frac{W}{g} \frac{V^2}{R} \frac{l_2}{L} \quad (\text{B.3})$$

$$F_{lateral,rear} = \frac{W}{g} \frac{V^2}{R} \frac{l_1}{L} \quad (\text{B.4})$$

If the vehicle does not skid, its minimum turning radius is a function of the maximum steering angle and separation between the front and rear tires (called wheelbase, L).

$$r_{turning} = \frac{L}{\delta_{max}} \quad (\text{B.5})$$

A vehicle is directionally stable if it can stabilize its direction in a finite time after a disturbance. This criterion puts a limit on the vehicle's forward velocity (V_x) and is heavily dependent on wheelbase. This limit can be written as [132]:

$$V_x < \sqrt{\frac{gL}{-K_{us}}} \quad (\text{B.6})$$

Here, K_{us} is the understeer coefficient and can be calculated from the following equation:

$$K_{us} = \frac{W_f}{C_{\alpha f}} - \frac{W_r}{C_{\alpha r}} \quad (\text{B.7})$$

The variables $C_{\alpha f}$ and $C_{\alpha r}$ again refer to the cornering stiffness of each wheel and W_f and W_r represent the weight on each wheel.

B.3 MI Variable Definitions

Table B.1 shows the expressions for the elements in Equations 3.31 and 3.32 [106, 9]:

Table B.1: Mobility index elements.

Symbol	Name	Expression
CPF	Contact pressure factor	$\frac{W}{mbl}$
WF	Weight factor	$\begin{cases} 1.0 & W \leq 222.4 \text{ kN}(50,000 \text{ lbs}) \\ 1.2 & 222.4 \text{ kN}(50,000 \text{ lbs}) \geq W > 311.4 \text{ kN}(70,000 \text{ lbs}) \\ 1.4 & 311.4 \text{ kN}(70,000 \text{ lbs}) \geq W > 444.8 \text{ kN}(100,000 \text{ lbs}) \\ 1.8 & 444.8 \text{ kN}(100,000 \text{ lbs}) \leq W \end{cases}$
TEF	Traction element factor	$\frac{10+b}{100}$
GFW	Grouser factor - wheels	$1 + 0.05c_{GF}$ where $\begin{cases} c_{GF} = 1 & \text{if chains are used} \\ c_{GF} = 0 & \text{if chains are not used} \end{cases}$
GFT	Grouser factor - tracks	$\begin{cases} 1.0 & h_g \leq 3.8 \text{ cm}(1.5 \text{ in}) \\ 1.1 & h_g > 3.8 \text{ cm}(1.5 \text{ in}) \end{cases}$
WLF	Wheel load factor	$\frac{W}{2000}$
EF	Engine factor	$\begin{cases} 1.0 & P \geq 8.2 \text{ kW/tonne}(10 \text{ hp/ton}) \text{ of vehicle weight} \\ 1.05 & P < 8.2 \text{ kW/tonne}(10 \text{ hp/ton}) \text{ of vehicle weight} \end{cases}$
TF	Transmission factor	$\begin{cases} 1.0 & \text{Automatic Transmission} \\ 1.05 & \text{Manual Transmission} \end{cases}$
TRF	Track factor	$\frac{b}{100}$
CF	Clearance factor	$\frac{l_c}{10}$
BF	Bogie factor	$\frac{W}{n_b l_s b}$

In Table B.1, W is vehicle weight, m is number of wheels or tracks on the ground, b is the inflated, unloaded width of the wheel or track, l is the length of the wheel or track, P is engine power, h_g is the height of a grouser, n_b is the number of bogies supporting tracks in contact with the ground, l_s is the length of one shoe of the track and l_c is the clearance of the vehicle.

Appendix C

Terminology Listing

The table below shows the documents collected in order to dissect the term "reconfigurability" throughout literature. The column "Individual" notes whether the source indicated that individual robots were reconfiguring with respect to one another. The column "Self vs. Manual" indicates if the document made a distinction between self and manual reconfigurability or if they only referred to automatic (A) or manual (M) reconfigurability. In the "Publisher" column, ICRA is the IEEE International Conference on Robotics and Automation, the IEEE Transactions on Robotics, TORA is IEEE Transactions on Robotics and Automation, and TOM is IEEE/ASME Transactions on Mechatronics. The vast majority of these documents are not included in the bibliography unless they were relevant for further discussion.

Author	Title	Publisher	Year	Field	Individual	Self vs Manual
Y.-W. Ma ; R. Krishnamurti	REPLICA—A reconfigurable partitionable highly parallel computer architecture for active multi-sensory perception of 3-dimensional objects	ICRA 1984	1984	Computer Architecture	N	M
H. Asada ; A. By	Kinematics of workpart fixturing	ICRA 1985	1985	Manipulation	N	Y
L. Kelmar ; P.K. Khosla	Automatic generation of kinematics for a reconfigurable modular manipulator system	ICRA 1988	1988	Manipulation	N	M
T. Fukuda ; S. Nakagawa	Dynamically reconfigurable robotic system	ICRA 1988	1988	Mobile	Y	Y
T. Fukuda ; S. Nakagawa ; Y. Kawauchi ; M. Buss	Structure decision method for self organising robots based on cell structures-CEBOT	ICRA 1989	1989	Mobile	Y	Y
D. Schmitz ; P. Khosla ; R. Hoffman ; T. Kanade	CHIMERA: a real-time programming environment for manipulator control	ICRA 1989	1989	Computer Architecture	N	M
S. Lee ; S. Kim	A self-reconfigurable dual-arm system	ICRA 1991	1991	Manipulation	Y	Y
K. Tarabanis ; R.Y. Tsai ; D.S. Goodman	Modeling of a computer-controlled zoom lens	ICRA 1992	1992	Sensing	N	M

Appendix C. Terminology Listing

R. Hui ; N. Kircanski ; A. Goldenberg ; C. Zhou ; P. Kuzan ; J. Wiercinski ; D. Gershon ; P. Sinha	Design of the IRIS facility- a modular, reconfigurable and expandable robot test bed	ICRA 1993	1993	Manipulation	N	M
Y. Fujioka ; M. Kameyama	2400-MFLOPS reconfigurable parallel VLSI processor for robot control	ICRA 1993	1993	Processor	N	A
S.M. Bhandarkar H.R. Arabia	A novel reconfigurable multiprocessor for robot vision	ICRA 1994	1994	Processor	N	Y
Y. Kawauchi M. Inaba T. Fukuda	Dynamically reconfigurable intelligent system of cellular robotic system (CEBOT) with entropy min/max hybrid algorithm	ICRA 1994	1994	Control	Y	Y
J. Budenske ; M. Gini	Why is it so difficult for a robot to pass through a doorway using ultrasonic sensors?	ICRA 1994	1994	Control	N	A
M. Yim	New locomotion gaits	ICRA 1994	1994	Mobile	Y	Y
S. Murata ; H. Kurokawa ; S. Kokaji	Self-assembling machine	ICRA 1994	1994	Mobile	Y	A
G.S. Chirikjian	Kinematics of a metamorphic robotic system	ICRA 1994	1994	Mobile	Y	Y
S.R. Habibi ; A.A. Goldenberg	Design and control of a reconfigurable industrial hydraulic robot	ICRA 1995	1995	Manipulation	N	M
A. Pamecha ; I. Ebert-Uphoff ; G.S. Chirikjian	Useful metrics for modular robot motion planning	TORA	1997	Manipulation	Y	Y
S. Mascaro J. Spano H.H. Asada	A reconfigurable holonomic omnidirectional mobile bed with unified seating (RHOMBUS) for bedridden patients	ICRA 1997	1997	Service	N	A
G. Yang I.-M. Chen	A novel kinematic calibration algorithm for reconfigurable robotic systems	ICRA 1997	1997	Control	N	M
S.G. Kaufman ; B.L. Spletzer ; T.L. Guess	Freeform fabrication of polymer-matrix composite structures	ICRA 1997	1997	Fabrication	N	A
M.M. Moghadam ; A.A. Goldenberg	Robustness and performance trade-offs in torque control of robots with harmonic drive transmission	ICRA 1997	1997	Manipulation	N	M
M. Kircanski ; N. Kircanski	Resolved-rate and resolved-acceleration-based robot control in the presence of actuators' constraints	ICRA 1997	1997	Manipulation	N	M
C.J.J. Paredis ; P.K. Khosla	Agent-based design of fault tolerant manipulators for satellite docking	ICRA 1997	1997	Space	N	Y

Appendix C. Terminology Listing

R.M. Voyles ; A. Agah ; P.K. Khosla ; G.A. Bekey	Tropism-based cognition for the interpretation of context-dependent gestures	ICRA 1997	1997	Architecture	N	M
M. Wada ; H.H. Asada	Design and control of a variable footprint mechanism for holonomic omnidirectional vehicles and its application to wheelchairs	TORA	1999	Service	N	N
E. Park ; D.M. Tilbury ; P.P. Khargonekar	Modular logic controllers for machining systems: formal representation and performance analysis using Petri nets	TORA	1999	Manufacturing	S	M
Guilin Yang ; I-Ming Chen ; Wee Kiat Lim ; Song Huat Yeo	Design and kinematic analysis of modular reconfigurable parallel robots	ICRA 1999	1999	Manipulation	N	M
R.M. Crowder ; V.N. Dubey ; P.H. Chappell ; D.R. Whatley	A multi-fingered end effector for unstructured environments	ICRA 1999	1999	Manipulation	N	A
M. Yim D.G. Duff K.D. Roufas	PolyBot: a modular reconfigurable robot	ICRA 2000	2000	Mobile	Y	Y
R. Kolluru K.P. Valavanis S.A. Smith N. Tsourveloudis	Design and analysis of a reconfigurable robotic gripper for limp material handling	ICRA 2000	2000	Manipulation	N	A
H. Bojinov A. Casal T. Hogg	Emergent structures in modular self-reconfigurable robots	ICRA 2000	2000	Mobile	Y	Y
H. Lipson J.B. Pollack	Towards continuously reconfigurable self-designing robotics	ICRA 2000	2000	Mobile	N	Y
S.J. Blind ; C.C. McCullough ; S. Akella ; J. Ponce	A reconfigurable parts feeder with an array of pins	ICRA 2000	2000	Manipulation	N	A
C. Unsal ; P.K. Khosla	Mechatronic design of a modular self-reconfiguring robotic system	ICRA 2000	2000	Mobile	Y	Y
J.H. Yakey ; S.M. LaValle ; L.E. Kavraki	Randomized path planning for linkages with closed kinematic chains	TORA	2001	Manipulation	Y	A
Shige Wang K.G. Shin	Reconfigurable software for open architecture controllers	ICRA 2001	2001	Software	N	M
Y. Tang M.C. Zhou	Design of reconfigurable semiconductor manufacturing systems with maintenance and failure	ICRA 2001	2001	Manufacturing	Y	M
K. Ohashi K.G. Shin	Model-based control for reconfigurable manufacturing systems	ICRA 2001	2001	Control	N	M
I-Ming Chen Yan Gao	Closed-form inverse kinematics solver for reconfigurable robots	ICRA 2001	2001	Manipulation	N	M

Appendix C. Terminology Listing

J. Kubica A. Casal T. Hogg	Complex behaviors from local rules in modular self-reconfigurable robots	ICRA 2001	2001	Control	Y	Y
Hye-Kyung Cho ; Young-Jo Cho ; Bum-Jae You	Integration of schema-based behaviors and variable-resolution cognitive maps for stable indoor navigation	ICRA 2001	2001	Planning	N	A
J. Butterfass ; M. Grebenstein ; H. Liu ; G. Hirzinger	DLR-Hand II: next generation of a dextrous robot hand	ICRA 2001	2001	Manipulation	N	A
C. Eldershaw ; M. Yim	Motion planning of legged vehicles in an unstructured environment	ICRA 2001	2001	Planning	Y	A
A. Castano ; P. Will	Representing and discovering the configuration of Conro robots	ICRA 2001	2001	Mobile	Y	Y
D. Kalita ; P.P. Khar-gonekar	Formal verification for analysis and design of logic controllers for reconfigurable machining systems	TORA	2002	Manufacturing	S	M
Shige Wang ; K.G. Shin	Constructing reconfigurable software for machine control systems	TORA	2002	Control	N	M
Wei-Min Shen ; B. Salemi ; P. Will	Hormone-inspired adaptive communication and distributed control for CONRO self-reconfigurable robots	TORA	2002	Mobile	Y	Y
J.E. Walter ; J.L. Welch ; N.M. Amato	Concurrent metamorphosis of hexagonal robot chains into simple connected configurations	TORA	2002	Mobile	Y	Y
R.W. Brennan ; M. Fletcher ; D.H. Norrie	An agent-based approach to reconfiguration of real-time distributed control systems	TORA	2002	Control	-	M
S. Murata ; E. Yoshida ; A. Kamimura ; H. Kurokawa ; K. Tomita ; S. Kokaji	M-TRAN: self-reconfigurable modular robotic system	TOM	2002	Mobile	Y	Y
K. Stoy ; Wei-Min Shen ; P.M. Will	Using role-based control to produce locomotion in chain-type self-reconfigurable robots	TOM	2002	Mobile	y	Y
A. Castano ; A. Behar ; P.M. Will	The Conro modules for reconfigurable robots	TOM	2002	Mobile	Y	M
M. Yim ; Ying Zhang ; K. Roufas ; D. Duff ; C. Eldershaw	Connecting and disconnecting for chain self-reconfiguration with PolyBot	TOM	2002	Mobile	Y	Y

Appendix C. Terminology Listing

M.W. Pryor ; R.C. Taylor ; C. Kapoor ; D. Tesar	Generalized software components for reconfiguring hyper-redundant manipulators	TOM	2002	Mobile	Y	Y
O. Mori T. Omata	Coupling of two 2-link robots with a passive joint for reconfigurable planar parallel robot	ICRA 2002	2002	Manipulation	Y	A
J.W. Suh S.B. Homans M. Yim	Telecubes: mechanical design of a module for self-reconfigurable robotics	ICRA 2002	2002	Mobile	Y	Y
Z. Butler K. Kotay D. Rus K. Tomita	Generic decentralized control for a class of self-reconfigurable robots	ICRA 2002	2002	Control	Y	Y
A. Dumitrescu I. Suzuki M. Yamashita	High speed formations of reconfigurable modular robotic systems	ICRA 2002	2002	Planning	Y	A
B.H.B. Yeung J.K. Mills	Development of a six degree-of-freedom reconfigurable gripper for flexible fixtureless assembly	ICRA 2002	2002	Manipulation	N	Y
K.C. Prevas ; C. Unsal ; M.O. Efe ; P.K. Khosla	A hierarchical motion planning strategy for a uniform self-reconfigurable modular robotic system	ICRA 2002	2002	Mobile	Y	Y
D. Popa ; Byoung Hun Kang ; Jeongsik Sin ; Jie Zou	Reconfigurable micro-assembly system for photonics applications	ICRA 2002	2002	Manufacturing	Y	M
J. Kubica ; E. Rieffel	Creating a smarter membrane: automatic code generation for modular self-reconfigurable robots	ICRA 2002	2002	Manipulation	N	Y
P. Pirjanian ; C. Leger ; E. Mumm ; B. Kennedy ; M. Garrett ; H. Aghazarian ; S. Farritor ; P. Schenker	Distributed control for a modular, reconfigurable cliff robot	ICRA 2002	2002	Mobile	Y	Y
M. Hafez ; M.D. Lichter ; S. Dubowsky	Optimized binary modular reconfigurable robotic devices	ICRA 2002	2002	Sensing	N	A
Tsai-Yen Li ; Yang-Chuan Shie	An incremental learning approach to motion planning with roadmap management	ICRA 2002	2002	Planning	N	A
Z. Butler ; R. Fitch ; D. Rus ; Yuhang Wang	Distributed goal recognition algorithms for modular robots	ICRA 2002	2002	Planning	Y	Y
S. Chitta ; J.R. Ostrowski	Motion planning for heterogeneous modular mobile systems	ICRA 2002	2002	Planning	N	Y
M. Badescu ; J. Morman ; C. Mavroidis	Workspace optimization of 3-UPU parallel platforms with joint constraints	ICRA 2002	2002	Manipulation	N	Y

Appendix C. Terminology Listing

S. Vassilvitskii ; M. Yim ; J. Suh	A complete, local and parallel reconfiguration algorithm for cube style modular robots	ICRA 2002	2002	Planning	Y	Y
S. Matsumoto ; Y. Ohkami ; Y. Wakabayashi ; M. Oda ; H. Ueno	Satellite capturing strategy using agile Orbital Servicing Vehicle, Hyper-OSV	ICRA 2002	2002	Space	N	A
M.D. Lichter ; V.A. Sujan ; S. Dubowsky	Computational issues in the planning and kinematics of binary robots	ICRA 2002	2002	Planning	N	M
H. Darabi ; M.A. Jafari ; A.L. Buczak	A control switching theory for supervisory control of discrete event systems	TORA	2003	Control	-	A
M. Sugi ; Y. Maeda ; Y. Aiyama ; T. Harada ; T. Arai	A holonic architecture for easy reconfiguration of robotic assembly systems	TORA	2003	Manufacturing	-	M
W.W. Melek ; A.A. Goldenberg	Neurofuzzy control of modular and reconfigurable robots	TOM	2003	Manipulation	N	M
M. Hafez ; M.D. Lichter ; S. Dubowsky	Optimized binary modular reconfigurable robotic devices	TOM	2003	Manipulation	N	A
Wei-Min Shen P. Will B. Khoshnevis	Self-assembly in space via self-reconfigurable robots	ICRA 2003	2003	Space	Y	Y
Y. Maeda H. Kikuchi H. Izawa H. Ogawa M. Sugi T. Arai	An easily reconfigurable robotic assembly system	ICRA 2003	2003	Manufacturing	Y	M
K. Stoy W.-M. Shen P. Will	Implementing configuration dependent gaits in a self-reconfigurable robot	ICRA 2003	2003	Mobile	Y	Y
Z.M. Bi W.A. Gruver W.J. Zhang	Adaptability of reconfigurable robotic systems	ICRA 2003	2003	Other	N	Y
E. Inohira A. Konno M. Uchiyama	Layered multi-agent architecture with dynamic reconfigurability	ICRA 2003	2003	Computer Architecture	N	Y
T. Yamawaki O. Mori T. Omata	Nonholonomic dynamic rolling control of reconfigurable 5R closed kinematic chain robot with passive joints	ICRA 2003	2003	Mobile	N	Y
B. Khoshnevis P. Will Wei-Min Shen	Highly compliant and self-tightening docking modules for precise and fast connection of self-reconfigurable robots	ICRA 2003	2003	Mobile	Y	Y
S.Y. Chen ; Y.F. Li	Dynamically reconfigurable visual sensing for 3D perception	ICRA 2003	2003	Sensing	N	Y
A. Kamimura ; H. Kurokawa ; E. Toshida ; K. Tomita ; S. Murata ; S. Kokaji	Automatic locomotion pattern generation for modular robots	ICRA 2003	2003	Mobile	Y	Y

Appendix C. Terminology Listing

S.G. Roh K.H. Park K.W. Yang J.H. Park H.S. Kim H.G. Lee H.R. Choi	Development of Dynamically Reconfigurable Personal robot	ICRA 2004	2004	Service	N	M
S. Saidani	Self-reconfigurable robots topodynamic	ICRA 2004	2004	Control	Y	Y
Y. Yamada N. Torii M. Gotoh Y. Komura	Reconfigurable parts feeding system using arrayed vibratory units made by stereolithography	ICRA 2004	2004	Manufacturing	N	M
Yang Zhiyong Huang Tian	A new method for tuning PID parameters of a 3 DoF reconfigurable parallel kinematic machine	ICRA 2004	2004	Control	N	M
J.-P. Clerc G.J. Wiens	Reconfigurable multi-agent robots with mixed modes of mobility	ICRA 2004	2004	Mobile	Y	A
M. Rubenstein K. Payne P. Will Wei-Min Shen	Docking among independent and autonomous CONRO self-reconfigurable robots	ICRA 2004	2004	Mobile	Y	Y
P.J. White K. Kopanski H. Lipson	Stochastic self-reconfigurable cellular robotics	ICRA 2004	2004	Mobile	Y	Y
B. Salemi Wei-Min Shen	Distributed behavior collaboration for self-reconfigurable robots	ICRA 2004	2004	Planning	Y	Y
N. Brener F. Benamar P. Bidaud	Analysis of self-reconfigurable modular systems: a design proposal for multi-modes locomotion	ICRA 2004	2004	Mobile	Y	Y
S.A. Patterson ; K.A. Knowles ; B.E. Bishop	Toward magnetically-coupled reconfigurable modular robots	ICRA 2004	2004	Mobile	Y	Y
J. Vogan ; A. Wingert ; J.-S. Plante ; S. Dubowsky ; M. Hafez ; D. Kacher ; F. Jolesz	Manipulation in MRI devices using electrostrictive polymer actuators: with an application to reconfigurable imaging coils	ICRA 2004	2004	Manipulation	N	A
A.I. Mourikis ; S.I. Roumeliotis	Analysis of positioning uncertainty in reconfigurable networks of heterogeneous mobile robots	ICRA 2004	2004	Uncertainty	Y	A
P. He ; M.H. Jin ; L. Yang ; R. Wei ; Y.W. Liu ; H.G. Cai ; H. Liu ; N. Seitz ; J. Butterfass ; G. Hirzinger	High performance DSP/FPGA controller for implementation of HIT/DLR dexterous robot hand	ICRA 2004	2004	Hardware	N	M
T. Yamawaki ; T. Omata ; O. Mori	4R and 5R parallel mechanism mobile robots	ICRA 2004	2004	Mobile	N	Y

Appendix C. Terminology Listing

Dawen Xie ; N.M. Amato	A kinematics-based probabilistic roadmap method for high DOF closed chain systems	ICRA 2004	2004	Planning	N	A
A. Ko ; T.L. Lau ; H.Y.K. Lau	Topological representation and analysis method for multi-port and multi-orientation docking modular robots	ICRA 2004	2004	Mobile	Y	Y
A. Golovinsky ; M. Yim ; Ying Zhang ; C. Eldershaw ; D. Duff	PolyBot and PolyKinetic/spl trade/ System: a modular robotic platform for education	ICRA 2004	2004	Education	N	Y
Li Chen ; Yuechao Wang ; Shugen Ma ; Bin Li	Studies on lateral rolling locomotion of a snake robot	ICRA 2004	2004	Mobile	Y	M
T. Huang ; M. Li ; X.M. Zhao ; J.P. Mei ; D.G. Chetwynd ; S.J. Hu	Conceptual design and dimensional synthesis for a 3-DOF module of the TriVariant-a novel 5-DOF reconfigurable hybrid robot	TOR	2005	Manipulation	N	M
B. Roy ; H.H. Asada	Design of a Reconfigurable Robot Arm for Assembly Operations inside an Aircraft Wing-Box	ICRA 2005	2005	Manipulation	N	A
Lining Sun ; Hui Xie ; Weibin Rong ; Liguo Chen	Task-Reconfigurable System for MEMS Assembly	ICRA 2005	2005	Manipulation	N	M
J. Carlson ; R.R. Murphy ; S. Christopher ; J. Casper	Conflict Metric as a Measure of Sensing Quality	ICRA 2005	2005	Testing	N	A
Liping Zhang ; Shugen Ma ; Bin Li ; Guowei Zhang ; Xinyuan He ; Minghui Wang ; Zheng Zhang ; Binggang Cao	Locomotion Analysis and Experiment for Climbing Motion of RPRS	ICRA 2005	2005	Mobile	N	A
Jungwon Yoon ; Jeha Ryu	A Novel Reconfigurable Ankle/Foot Rehabilitation Robot	ICRA 2005	2005	Service	N	M
Roderich Gross ; Michael Bonani ; Francesco Mondada ; Marco Dorigo	Autonomous Self-Assembly in Swarm-Bots	TOR	2006	Mobile	Y	Y
E.R. Wade ; H.H. Asada	Design of a Broadcasting Modem for a DC PLC Scheme	TOM	2006	Mobile	Y	A
Y. Yamada	Dynamic reconfiguration of reconfigurable manufacturing systems using particle swarm optimization	ICRA 2006	2006	Manufacturing	Y	Y

Appendix C. Terminology Listing

Feili Hou Wei-Min Shen	Mathematical foundation for hormone-inspired control for self-reconfigurable robotic systems	ICRA 2006	2006	Mobile	Y	Y
D.J. Christensen K. Stoy	Selecting a meta-module to shape-change the ATRON self-reconfigurable robot	ICRA 2006	2006	Planning	Y	Y
D.J. Christensen	Evolution of shape-changing and self-repairing control for the ATRON self-reconfigurable robot	ICRA 2006	2006	Mobile	Y	Y
N. Atay ; B. Bayazit	A motion planning processor on reconfigurable hardware	ICRA 2006	2006	Processor	N	M
Wei-Min Shen ; M. Krivokon ; Harris Chiu ; J. Everist ; M. Rubenstein ; J. Venkatesh	Multimode locomotion via SuperBot robots	ICRA 2006	2006	Mobile	Y	A
K. Edwards ; R. Alqasemi ; R. Dubey	Design, construction and testing of a wheelchair-mounted robotic arm	ICRA 2006	2006	Service	N	M
R. Gross ; E. Tuci ; M. Dorigo ; M. Bonani ; F. Mondada	Object transport by modular robots that self-assemble	ICRA 2006	2006	Mobile	Y	Y
Yan Meng	An agent-based mobile robot system using configurable SOC technique	ICRA 2006	2006	Mobile	Y	Y
Nicola Ng Pak Robert J. Webster Arianna Menciassi Paolo Dario	Electrolytic Silicone Bourdon Tube Microactuator for Reconfigurable Surgical Robots	ICRA 2007	2007	Surgery	Y	A
Farhad Aghili Kourosh Parsa	Configuration Control and Recalibration of a New Reconfigurable Robot	ICRA 2007	2007	Space	Y	A
Rakesh Murthy Aditya N. Das Dan Popa Harry Stephanou	M3: Multiscale, Deterministic and Reconfigurable Macro-Micro Assembly System for Packaging of MEMS	ICRA 2007	2007	Manufacturing	Y	M
Isolde Dressler ; Mathias Haage ; Klas Nilsson ; Rolf Johansson ; Anders Robertsson ; Torgny Brogardh	Configuration Support and Kinematics for a Reconfigurable Gantry-Tau Manipulator	ICRA 2007	2007	Manipulation	N	M
Colin D'Souza ; Byung Hwa Kim ; Richard Voyles	Morphing Bus: A rapid deployment computing architecture for high performance, resource-constrained robots	ICRA 2007	2007	Hardware	N	M

Appendix C. Terminology Listing

David Johan Christensen ; Jason Campbell	Locomotion of Miniature Catom Chains: Scale Effects on Gait and Velocity	ICRA 2007	2007	Mobile	Y	Y
Michael P. Kummer ; Jake J. Abbott ; Karl Vollmers ; Bradley J. Nelson	Measuring the Magnetic and Hydrodynamic Properties of Assembled-MEMS Microrobots	ICRA 2007	2007	Sensing	N	M
Wen-Hong Zhu ; Tom Lamarche	Modular Robot Manipulators Based on Virtual Decomposition Control	ICRA 2007	2007	Manipulation	N	M
Oscar Ljungkrantz ; Knut Akesson ; Johan Richardsson ; Kristin Andersson	Implementing a Control System Framework for Automatic Generation of Manufacturing Cell Controllers	ICRA 2007	2007	Manufacturing	N	M
Feili Hou Wei-Min Shen	Distributed, dynamic, and autonomous reconfiguration planning for chain-type self-reconfigurable robots	ICRA 2008	2008	Planning	Y	Y
Byoung Kwon An	Em-cube: cube-shaped, self-reconfigurable robots sliding on structure surfaces	ICRA 2008	2008	Mobile	Y	Y
Guangjun Liu ; Xiaojia He ; Jing Yuan ; Sajan Abdul ; Andrew A. Goldenberg	Development of modular and reconfigurable robot with multiple working modes	ICRA 2008	2008	Manipulation	N	M
Sajan Abdul ; Guangjun Liu	Decentralised fault tolerance and fault detection of modular and reconfigurable robots with joint torque sensing	ICRA 2008	2008	Manipulation	N	M
A. Sprowitz ; M. Asadpour ; Y. Bourquin ; A. J. Ijspeert	An active connection mechanism for modular self-reconfigurable robotic systems based on physical latching	ICRA 2008	2008	Mobile	Y	Y
Masahiro Shimizu ; Takuma Kato ; Max Lungarella ; Akio Ishiguro	Adaptive reconfiguration of a modular robot through heterogeneous inter-module connections	ICRA 2008	2008	Mobile	Y	Y
Young-Sik Kwon ; Hoon Lim ; Eui-Jung Jung ; Byung-Ju Yi	Design and motion planning of a two-moduled indoor pipeline inspection robot	ICRA 2008	2008	Mobile	-	A
Sam D. Herbert ; Andrew Drenner ; Nikolaos Papanikolopoulos	Loper: A quadruped-hybrid stair climbing robot	ICRA 2008	2008	Mobile	N	M
Farhad Aghili ; Kourosh Parsa	A Reconfigurable Robot With Lockable Cylindrical Joints	TOR	2009	Space	N	A

Appendix C. Terminology Listing

Se-gon Roh ; Kwang Woong Yang ; Jae Hoon Park ; Hyung-pil Moon ; Hong-Seok Kim ; Hogil Lee ; Hyouk Ryeol Choi	A Modularized Personal Robot DRP I: Design and Implementation	TOR	2009	Service	N	M
Jian S. Dai ; Delun Wang ; Lei Cui	Orientation and Workspace Analysis of the Multifingered Metamorphic Hand—Metahand	TOR	2009	Manipulation	N	A
Denny Oetomo ; David Daney ; Jean-Pierre Merlet	Design Strategy of Serial Manipulators With Certified Constraint Satisfaction	TOR	2009	Manipulation	N	A
Denny Oetomo David Daney Kanako Harada Jean-Pierre Merlet Arianna Menciassi Paolo Dario	Topology design of surgical reconfigurable robots by interval analysis	ICRA 2009	2009	Surgery	Y	A
Yu-chen ho Ching-hu lu I-han chen Shih-shinh huang Ching-yao wang Li-chen fu	Active-learning assisted self-reconfigurable activity recognition in a dynamic environment	ICRA 2009	2009	Service	N	Y
Kanako Harada ; Ekawahyu Susilo ; Arianna Menciassi ; Paolo Dario	Wireless reconfigurable modules for robotic endoluminal surgery	ICRA 2009	2009	Surgery	N	Y
Stephen Matsysik ; Jennifer Walter	Using a pocket-filling strategy for distributed reconfiguration of a system of hexagonal metamorphic robots in an obstacle-cluttered environment	ICRA 2009	2009	Mobile	Y	A
Mirko Bordinon ; Kasper Stoy ; Ulrik Pagh Schultz	A virtual machine-based approach for fast and flexible reprogramming of modular robots	ICRA 2009	2009	Control	Y	Y
Masahiro Shimizu ; Kenji Suzuki	A self-repairing structure for modules and its control by vibrating actuation mechanisms	ICRA 2009	2009	Mobile	N	Y
Yugang Liu ; Guangjun Liu	Track–Stair Interaction Analysis and Online Tipover Prediction for a Self-Reconfigurable Tracked Mobile Robot Climbing Stairs	TOM	2009	Mobile	N	Y
Yugang Liu ; Guangjun Liu	Interaction Analysis and Online Tip-Over Avoidance for a Reconfigurable Tracked Mobile Modular Manipulator Negotiating Slopes	TOM	2010	Mobile	N	Y

Appendix C. Terminology Listing

Graham G. Ryland Harry H. Cheng	Novel locomotion of iMobot, an intelligent reconfigurable mobile robot	ICRA 2010	2010	Mobile	Y	A
Graham G. Ryland Harry H. Cheng	Design of iMobot, an intelligent reconfigurable mobile robot with novel locomotion	ICRA 2010	2010	Mobile	Y	A
Kevin C. Galloway Rekha Jois Mark Yim	Factory floor: A robotically reconfigurable construction platform	ICRA 2010	2010	Manufacturing	Y	Y
Patrick Grosch Raffaele Di Gregorio Javier López Federico Thomas	Motion planning for a novel reconfigurable parallel manipulator with lockable revolute joints	ICRA 2010	2010	Manipulation	N	A
Michael D.M. Kutzer Matthew S. Moses Christopher Y. Brown Mehran Armand David H. Scheidt Gregory S. Chirikjian	Design of a new independently-mobile reconfigurable modular robot	ICRA 2010	2010	Mobile	Y	Y
Yugang Liu Guangjun Liu	Interaction analysis and posture optimization for a reconfigurable tracked mobile modular manipulator negotiating slopes	ICRA 2010	2010	Mobile	N	Y
Guangjun Liu Yugang Liu	Spring assisted modular and reconfigurable robot: Design, analysis and control	ICRA 2010	2010	Manipulation	N	Y
Michael Hofbauer ; Mathias Brandstötter ; Christoph Schörghuber ; Gerald Steinbauer	On-line kinematics reasoning for reconfigurable robot drives	ICRA 2010	2010	Control	Y	Y
Feili Hou ; Wei-Min Shen	On the complexity of optimal reconfiguration planning for modular reconfigurable robots	ICRA 2010	2010	Control	Y	A
Chris E. Thorne ; Nikita Skorodinski ; Hughes Tipton ; Travis Van Schoyck ; Mark Yim	Brake design for dynamic modular robots	ICRA 2010	2010	Mobile	Y	A
Kevin C. Wolfe ; Michael D.M. Kutzer ; Mehran Armand ; Gregory S. Chirikjian	Trajectory generation and steering optimization for self-assembly of a modular robotic system	ICRA 2010	2010	Mobile	Y	Y
Hongxing Wei ; Yingpeng Cai ; Haiyuan Li ; Dezhong Li ; Tianmiao Wang	Sambot: A self-assembly modular robot for swarm robot	ICRA 2010	2010	Mobile	Y	Y

Appendix C. Terminology Listing

Saleh Ahmad ; Guangjun Liu	A door opening method by modular re-configurable robot with joints working on passive and active modes	ICRA 2010	2010	Manipulation	N	A
Wen-Hong Zhu	FPGA-based adaptive friction compensation for precision control of harmonic drivers	ICRA 2010	2010	FPGA	-	M
Isolde Dressler ; Torgny Brogårdh ; Anders Robertsson	A kinematic error model for a parallel Gantry-Tau manipulator	ICRA 2010	2010	Manufacturing	N	M
Jens Windau ; Wei-Min Shen	An Inertia-Based Surface Identification System	ICRA 2010	2010	Sensing	Y	Y
Kenneth C. Cheung ; Erik D. Demaine ; Jonathan R. Bachrach ; Saul Griffith	Programmable Assembly With Universally Foldable Strings (Moteins)	TOR	2011	Microbots	Y	S
"Guangjun Liu Department of Aerospace Engineering , Ryerson University, Toronto, Canada						
; Yugang Liu ; Andrew A. Goldenberg"	Design, Analysis, and Control of a Spring-Assisted Modular and Reconfigurable Robot	TOM	2011	Manipulation	N	Y
Mohamed Khalgui ; Olfa Mosbahi ; Zhiwu Li ; Hans-Michael Hanisch	Reconfiguration of Distributed Embedded-Control Systems	TOM	2011	Control	Y	Y
Noppadol Chadil Marong Phadoongsidhi Kawee Suwannasit Poramate Manoonpong Pudit Laksanacharoen	A reconfigurable spherical robot	ICRA 2011	2011	Mobile	N	A
Jie Zhao Xindan Cui Yanhe Zhu Shufeng Tang	A new self-reconfigurable modular robotic system UBot: Multi-mode locomotion and self-reconfiguration	ICRA 2011	2011	Mobile	Y	Y
Chytra Pawashe Eric Diller Steven Floyd Metin Sitti	Assembly and disassembly of magnetic mobile micro-robots towards deterministic 2-D reconfigurable micro-systems	ICRA 2011	2011	Microbots	Y	A
Yi Sun Shugen Ma	Decoupled kinematic control of terrestrial locomotion for an ePaddle-based reconfigurable amphibious robot	ICRA 2011	2011	Mobile	N	A

Appendix C. Terminology Listing

Yan Meng Yuyang Zhang Abhay Sampath Yaochu Jin Bernhard Sendhoff	Cross-Ball: A new morphogenetic self-reconfigurable modular robot	ICRA 2011	2011	Mobile	Y	Y
E. Martinson ; B. Fransen	Dynamically reconfigurable microphone arrays	ICRA 2011	2011	Sensing	N	Y
Stephen S. Nestinger ; Harry. H. Cheng	Mobile-R: A reconfigurable cooperative control platform for rapid deployment of multi-robot systems	ICRA 2011	2011	Control	Y	A
Rodrigo Moreno ; Jonatan Gomez	Central pattern generators and hormone inspired messages: A hybrid control strategy to implement motor primitives on chain type modular reconfigurable robots	ICRA 2011	2011	Control	Y	A
Young-Sik Kwon ; Byung-Ju Yi	Design and Motion Planning of a Two-Module Collaborative Indoor Pipeline Inspection Robot	TOR	2012	Mobile	-	A
Ryan Montague ; Chris Bingham ; Kais Atallah	Servo Control of Magnetic Gears	TOM	2012	Control	N	A
Kevin C. Wolfe Matthew S. Moses Michael D.M. Kutzer Gregory S. Chirikjian	M3Express: A low-cost independently-mobile reconfigurable modular robot	ICRA 2012	2012	Mobile	Y	A
Stefano Mintchev ; Cesare Stefanini ; Alexis Girin ; Stefano Marrazza ; Stefano Orofino ; Vincent Lebastard ; Luigi Manfredi ; Paolo Dario ; Frederic Boyer	An underwater reconfigurable robot with bio-inspired electric sense	ICRA 2012	2012	Marine	N	M
Scott Koziol ; Paul Hasler ; Mike Stilman	Robot path planning using Field Programmable Analog Arrays	ICRA 2012	2012	Hardware	N	A
Marcel Bergerman ; Sanjiv Singh ; Bradley Hamner	Results with autonomous vehicles operating in specialty crops	ICRA 2012	2012	Agriculture	N	M
Luzius Brodbeck ; Liyu Wang ; Fumiya Iida	Robotic body extension based on Hot Melt Adhesives	ICRA 2012	2012	General	N	Y
Sagar Chowdhury ; Petr Svec ; Chenlu Wang ; Wolfgang Losert ; Satyandra K. Gupta	Gripper synthesis for indirect manipulation of cells using Holographic Optical Tweezers	ICRA 2012	2012	Microbots	N	M

Appendix C. Terminology Listing

Wen-Hong Zhu ; Tom Lamarche ; Erick Dupuis ; David Jameux ; Patrick Barnard ; Guangjun Liu	Precision Control of Modular Robot Manipulators: The VDC Approach With Embedded FPGA	TOR	2013	Manipulation	N	M
Sheila Russo ; Kanako Harada ; Tommaso Ranzani ; Luigi Manfredi ; Cesare Stefanini ; Arianna Menciassi ; Paolo Dario	Design of a Robotic Module for Autonomous Exploration and Multimode Locomotion	TOM	2013	Mobile	Y	Y
Saleh Ahmad ; Hongwei Zhang ; Guangjun Liu	Multiple Working Mode Control of Door-Opening With a Mobile Modular and Reconfigurable Robot	TOM	2013	Manipulation	N	A
Nicholas Morozovsky ; Robert Moroto ; Thomas Bewley	RAPID: An Inexpensive Open Source Dynamometer for Robotics Applications	TOM	2013	Testing	N	M
Mohammad Norouzi ; Jaime Valls Miro ; Gamini Dissanayake	A statistical approach for uncertain stability analysis of mobile robots	ICRA 2013	2013	Mobile	N	A
Aditya N. Das ; Stephen Savoie	Quasi-static evaluation of a modular and Reconfigurable Manufacturing Cell	ICRA 2013	2013	Manipulation	N	M
M. Pacheco ; M. Moghadam ; A. Magnússon ; B. Silverman ; H. H. Lund ; D. J. Christensen	Fable: Design of a modular robotic playware platform	ICRA 2013	2013	Mobile	N	Y
Michael Brunner ; Bernd Brüggemann ; Dirk Schulz	Hierarchical rough terrain motion planning using an optimal sampling-based method	ICRA 2013	2013	Mobile	N	A
Luca Carbonari ; Massimo Callegari ; Giacomo Palmieri ; Matteo-Claudio Palpacelli	Analysis of Kinematics and Reconfigurability of a Spherical Parallel Manipulator	TOR	2014	Manipulation	N	A
Jonas Neubert ; Arne Rost ; Hod Lipson	Self-Soldering Connectors for Modular Robots	TOR	2014	Mobile	Y	Y
Dinh Quan Nguyen Marc Gouttefarde Olivier Company François Pierrot	On the analysis of large-dimension reconfigurable suspended cable-driven parallel robots	ICRA 2014	2014	Manipulation	N	M
Jan-Philipp Kobler ; Jens Kotalarski ; G. Jakob Lexow ; Omid Majdani ; Tobias Ortmaier	Design optimization of a bone-attached, redundant and reconfigurable parallel kinematic device for skull surgery	ICRA 2014	2014	Surgery	N	M

Appendix C. Terminology Listing

Ye Ding ; Ignacio Galiana ; Alan Asbeck ; Brendan Quinlivan ; Stefano Marco Maria De Rossi ; Conor Walsh	Multi-joint actuation platform for lower extremity soft exosuits	ICRA 2014	2014	Service	N	M
Zhiguo Shi ; Guangjun Liu	Torque estimation of robot joint with harmonic drive transmission using a redundant adaptive robust extended Kalman filter	ICRA 2014	2014	Sensing	N	M
Aaron Becker ; Erik D. Demaine ; Sándor P. Fekete ; James McLurkin	Particle computation: Designing worlds to control robot swarms with only global signals	ICRA 2014	2014	Microbots	N	M
J. Casalilla ; M. Valles ; M. Diaz-Rodriguez ; V. Mata ; A. Soriano ; A. Valera	Implementation of dynamic controllers using real-time middleware for a low-cost parallel robot	ICRA 2014	2014	Control	N	A
Olivier Chocron ; Urbain Prieur ; Laurent Pino	A Validated Feasibility Prototype for AUV Reconfigurable Magnetic Coupling Thruster	TOM	2014	UAVs	N	A
Matteo-Claudio Palpacelli ; Luca Carbonari ; Giacomo Palmieri ; Massimo Callegari	Analysis and Design of a Reconfigurable 3-DoF Parallel Manipulator for Multimodal Tasks	TOM	2015	Manipulation	N	A
Andrew J. Petruska Joseph B. Brink Jake J. Abbott	First demonstration of a modular and reconfigurable magnetic-manipulation system	ICRA 2015	2015	Manipulation	N	M
Lorenzo Gagliardini Stéphane Caro Marc Gouttefarde Alexis Girin	A reconfiguration strategy for Reconfigurable Cable-Driven Parallel Robots	ICRA 2015	2015	Manipulation	N	M
José Baca ; Bradley Woosley ; Prithviraj Dasgupta ; Carl Nelson	Real-time distributed configuration discovery of modular self-reconfigurable robots	ICRA 2015	2015	Planning	Y	Y
John W. Romanishin ; Kyle Gilpin ; Sebastian Claici ; Daniela Rus	3D M-Blocks: Self-reconfiguring robots capable of locomotion via pivoting in three dimensions	ICRA 2015	2015	Mobile	Y	Y
Miu-Ling Lam ; Bin Chen ; Yaozhong Huang	A novel volumetric display using fog emitter matrix	ICRA 2015	2015	Display	N	A
Nicholas D'Amore ; Constance Ciarleglio ; David L. Akin	IMU-based manipulator kinematic identification	ICRA 2015	2015	Manipulation	N	M

Appendix C. Terminology Listing

Chi-An Chen ; Thomas Collins ; Wei-Min Shen	A near-optimal dynamic power sharing scheme for self-reconfigurable modular robots	ICRA 2016	2016	Mobile	Y	Y
Emanuel Pablo Vega ; Olivier Chocron ; Mohamed Benbouzid	A Flat Design and a Validated Model for an AUV Reconfigurable Magnetic Coupling Thruster	TOM	2016	Marine	N	A
Seonghun Hong ; Dongeun Choi ; Sungchul Kang ; Hyeongcheol Lee ; Woosub Lee	Design of manually reconfigurable modular manipulator with three revolute joints and links	ICRA 2016	2016	Manipulation	N	Y
Amir Firouzeh ; Marco Salerno ; Jamie Paik	Stiffness Control With Shape Memory Polymer in Underactuated Robotic Origamis	TOR	2017	Manipulation	N	A
Christoph H. Belke ; Jamie Paik	Mori: A Modular Origami Robot	TOM	2017	Mobile	Y	Y
Changsheng Li ; Xiaoyi Gu ; Hongliang Ren	A Cable-Driven Flexible Robotic Grasper With Lego-Like Modular and Reconfigurable Joints	TOM	2017	Manipulation	N	M
Amir Firouzeh ; Jamie Paik	Grasp Mode and Compliance Control of an Underactuated Origami Gripper Using Adjustable Stiffness Joints	TOM	2017	Manipulation	N	A
S. Baraldo ; A. Valente	Smooth joint motion planning for high precision reconfigurable robot manipulators	ICRA 2017	2017	Manipulation	N	M
Constantinos Vrohidis ; Charalampos P. Bechlioulis ; Kostas J. Kyriakopoulos	Safe decentralized and reconfigurable multi-agent control with guaranteed convergence	ICRA 2017	2017	Control	-	A
Rainier F. Natividad ; Manuel R. Del Rosario ; Peter C.Y. Chen ; Chen-Hua Yeow	A hybrid plastic-fabric soft bending actuator with reconfigurable bending profiles	ICRA 2017	2017	Soft	N	A
Yaohui Chen ; Sing Le ; Qiao Chu Tan ; Oscar Lau ; Fang Wan ; Chaoyang Song	A reconfigurable hybrid actuator with rigid and soft components	ICRA 2017	2017	Manipulation	N	M
Yosuke Suzuki ; Yuhei Tsutsui ; Masato Yaegashi ; Satoshi Kobayashi	Modular robot using helical magnet for bonding and transformation	ICRA 2017	2017	Mobile	Y	Y
Andrea Giusti ; Jörn Malzahn ; Nikolaos G. Tsagarakis ; Matthias Althoff	Combined inverse-dynamics/passivity-based control for robots with elastic joints	ICRA 2017	2017	Manipulation	N	M

Appendix C. Terminology Listing

Mehmet Mutlu ; Simon Hauser ; Alexandre Bernardino ; Auke Ijspeert	Playdough to Roombots: Towards a Novel Tangible User Interface for Self-reconfigurable Modular Robots	ICRA 2018	2018	Mobile	Y	Y
Mansour Ataei ; Amir Khajepour ; Soo Jeon	Reconfigurable Integrated Stability Control for Four- and Three-wheeled Urban Vehicles With Flexible Combinations of Actuation Systems	TOM	2018	Control	N	M
W. Ding ; T. Dertert ; J. De La Cruz ; B. Corves	Reconfiguration Analysis and Motion Planning of a Novel Reconfigurable Mobile Manipulator Torso	ICRA 2018	2018	Manipulation	N	A
Matthew A. Robertson ; Masato Murakami ; Wyatt Felt ; Jamie Paik	A Compact Modular Soft Surface With Reconfigurable Shape and Stiffness	TOM	2019	Haptics	N	A
Gaofeng Li ; Dezhen Song ; Shan Xu ; Lei Sun ; Jingtai Liu	A Hybrid Model and Model-Free Position Control for a Reconfigurable Manipulator	TOM	2019	Manipulation	N	M
Shihong Fang ; Anna Choromanska	Reconfigurable Network for Efficient Inferencing in Autonomous Vehicles	ICRA 2019	2019	Control	-	A
Shinkyu Park ; Erkan Kayacan ; Carlo Ratti ; Daniela Rus	Coordinated Control of a Reconfigurable Multi-Vessel Platform: Robust Control Approach	ICRA 2019	2019	Marine	Y	M
Abdullah A. Hayat ; Rizuwana Parween ; Mohan R. Elara ; K. Paruraman ; Prathap S. Kandasamy	Panthera: Design of a Reconfigurable Pavement Sweeping Robot	ICRA 2019	2019	Mobile	N	Y
Christos K. Verginis ; Constantinos Vrohidis ; Charalampos P. Bechlioulis ; Kostas J. Kyriakopoulos ; Dimos V. Dimarogonas	Reconfigurable Motion Planning and Control in Obstacle Cluttered Environments under Timed Temporal Tasks	ICRA 2019	2019	Planning	-	A
Paul Motzki ; Frank Khelfa ; Lukas Zimmer ; Marvin Schmidt ; Stefan Seelecke	Design and Validation of a Reconfigurable Robotic End-Effector Based on Shape Memory Alloys	TOM	2019	Manipulation	N	A
Chuanqi Zheng ; Kiju Lee	WheeLeR: Wheel-Leg Reconfigurable Mechanism with Passive Gears for Mobile Robot Applications	ICRA 2019	2019	Mobile	N	A
Dickson Chun Fung Li ; Zerui Wang ; Bo Ouyang ; Yun-Hui Liu	A Reconfigurable Variable Stiffness Manipulator by a Sliding Layer Mechanism	ICRA 2019	2019	Manipulation	N	A

Appendix C. Terminology Listing

Zhongyi Li ; Weihai Chen ; Shaoping Bai	A Novel Reconfigurable Revolute Joint with Adjustable Stiffness	ICRA 2019	2019	Service	N	M
Nir Meiri ; David Zarrouk	Flying STAR, a Hybrid Crawling and Flying Sprawl Tuned Robot	ICRA 2019	2019	UAVs	N	A
Hiroshi Kawano	Linear Heterogeneous Reconfiguration of Cubic Modular Robots via Simultaneous Tunneling and Permutation	ICRA 2019	2019	Mobile	Y	Y
Tønnes F. Nygaard ; Charles P. Martin ; Jim Torrensen ; Kyrr Glette	Self-Modifying Morphology Experiments with DyRET: Dynamic Robot for Embodied Testing	ICRA 2019	2019	Mobile	N	Y
Gustavo Freitas ; Fernando Lizarralde ; Liu Hsu ; Ney R. Salvi dos Reis	Kinematic reconfigurability of mobile robots on irregular terrains	ICRA 2019	2019	Mobile	N	Y
Christoph H. Belke ; Jamie Paik	Automatic Couplings With Mechanical Overload Protection for Modular Robots	TOM	2019	Mobile	Y	Y
Tomohiro Hayakawa ; Tomoya Kamimura ; Shizuo Kaji ; Fumitoshi Matsuno	Autonomous Distributed System for Gait Generation for Single-Legged Modular Robots Connected in Various Configurations	TOR	2020	Mobile	N	M
Bingguo Mu ; Pakpong Chirattananon	Universal Flying Objects: Modular Multirotor System for Flight of Rigid Objects	TOR	2020	UAVs	N	M
Claudio Pose ; Juan Ignacio Giribet ; Ignacio Mas	Fault tolerance analysis for a class of reconfigurable aerial hexarotor vehicles	TOM	2020	UAVs	N	M
Tarcisio Marinelli Pereira Silva;Marcel Araujo Clementino;Vagner Candido de Sousa;Carlos De Marqui	An Experimental Study of a Piezoelectric Metastructure With Adaptive Resonant Shunt Circuits	TOM	2020	Sensing	N	A
Jiahao Wu;Zerui Wang;Wei Chen;Yaqing Wang;Yun-hui Liu	Design and Validation of a Novel Leaf Spring-Based Variable Stiffness Joint With Reconfigurability	TOM	2020	Mobile	N	M
Gaofeng Li;Dezhen Song;Shan Xu;Lei Sun;Jingtai Liu	On Perpendicular Curve-Based Model-Less Control Considering Incomplete Orientation Constraint	TOM	2021	Manipulation	N	M
Sa-Reum Kim;Dae-Young Lee;Sang-Joon Ahn;Je-Sung Koh;Kyu-Jin Cho	Morphing Origami Block for Lightweight Reconfigurable System	TOR	2021	Mobile	Y	A

Appendix C. Terminology Listing

Xinyang Tian;Qiang Zhan	A Hermaphrodite Electromechanical Connector for Self-Reconfigurable Robot Modules	TOM	2021	Mobile	Y	Y
Alberto Dalla Libera;Nicola Castaman;Stefano Ghidoni;Ruggero Carli	Autonomous Learning of the Robot Kinematic Model	TOR	2021	Manipulation	Y	Y
Matthew J. Doyle;João V. Amorim Marques;Isaac Vandermeulen;Christopher Parrott;Yue Gu;Xinyu Xu;Andreas Kolling;Roderich Groß	Modular Fluidic Propulsion Robots	TOR	2021	Mobile	Y	Y
Madan Mohan Rayguru;Rajesh Elara Mohan;Rizuwana Parween;Lim Yi;Anh Vu Le;Spandan Roy	An Output Feedback Based Robust Saturated Controller Design for Pavement Sweeping Self-Reconfigurable Robot	TOM	2021	Mobile	Y	Y
Gaofeng Li;Jingtai Liu;Ioannis Sarakoglou;Nikos SE G Tsagarakis	An Angle-Axis Space-based Orientability Index Characterizing Complete Orientations	TOM	2021	Manipulation	N	Y
Binbin Li;Lei Ma;Deqing Huang;Yongkui Sun	A Flexibly Assembled and Maneuverable Reconfigurable Modular Multi-rotor Aerial Vehicle	TOM	2021	UAVs	N	A
Qianqian Wang;Dongdong Jin;Ben Wang;Neng Xia;Ho Ko;Bonaventure Yiu Ming Ip;Thomas Wai Hong Leung;Simon Chun Ho Yu;Li Zhang	Reconfigurable Magnetic Microswarm for Accelerating tPA-Mediated Thrombolysis under Ultrasound Imaging	TOM	2021	Medicine	Y	A
Tao Jin;Long Li;Tianhong Wang;Guopeng Wang;Jianguo Cai;Yingzhong Tian;Quan Zhang	Origami-Inspired Soft Actuators for Stimulus Perception and Crawling Robot Applications	TOR	2021	Mobile	Y	A
Florian Richter;Peter V. Gavrilov;Hoi Man Lam;Amir Degani;Michael C. Yip	ARCSnake: Reconfigurable Snakelike Robot With Archimedean Screw Propulsion for Multidomain Mobility	TOR	2021	Mobile	N	A
Mohammad Amin Karimi;Vahid Alizadehyazdi;Heinrich M. Jaeger;Matthew Spenko	A Self-Reconfigurable Variable-Stiffness Soft Robot Based on Boundary-Constrained Modular Units	TOR	2021	Mobile	Y	Y

Appendix C. Terminology Listing

Jin Huat Low;Phone May Khin;Qian Qian Han;Haicheng Yao;Yee Seng Teoh;Yadan Zeng;Si Li;Jun Liu;Zhuangjian Liu;Pablo Valdivia y Alvarado;I-Ming Chen;Benjamin Chee Keong Tee;Raye Chen Hua Yeow	Sensorized Reconfigurable Soft Robotic Gripper System for Automated Food Handling	TOM	2021	Manipulation	N	A
Edoardo Romiti;Jörn Malzahn;Navvab Kashiri;Francesco Iacobelli;Marco Ruzzon;Arturo Laurenzi;Enrico Mingo Hoffman;Luca Muratore;Alessio Margan;Lorenzo Baccelliere;Stefano Cordasco;Nikos Tsagarakis	Toward a Plug-and-Work Reconfigurable Cobot	TOM	2021	Manipulation	N	Y
Anuruddha Bhat-tacharjee;Yitong Lu;Aaron T. Becker;MinJun Kim	Magnetically Controlled Modular Cubes With Reconfigurable Self-Assembly and Disassembly	TOR	2021	Mobile	Y	Y
Deborah Wang;Brandon Lutz;Peter J. Cobb;Philip Dames	RASCAL: Robotic Arm for Sherds and Ceramics Automated Locomotion	ICRA 2021	2021	Manipulation	N	M
Edoardo Romiti;Navvab Kashiri;Jörn Malzahn;Nikos Tsagarakis	Minimum-Effort Task-based Design Optimization of Modular Reconfigurable Robots	ICRA 2021	2021	Manipulation	N	Y
Yuxiao Tu;Guanqi Liang;Tin Lun Lam	Graph Convolutional Network based Configuration Detection for Freeform Modular Robot Using Magnetic Sensor Array	ICRA 2021	2021	Mobile	Y	Y
Wei Cheah;Tomas B. Garcia-Nathan;Keir Groves;Simon Watson;Barry Lennox	Path Planning for a Reconfigurable Robot in Extreme Environments	ICRA 2021	2021	Mobile	N	A
Shihao Feng;Yuping Gu;Weijie Guo;Yuqin Guo;Fang Wan;Jia Pan;Chaoyang Song	An Overconstrained Robotic Leg with Coaxial Quasi-direct Drives for Omni-directional Ground Mobility*	ICRA 2021	2021	Mobile	N	M
Yaohui Chen;Hoam Chung;Bernard Chen;Ho Yi Ping;Yonghang Sun	Pneumatic actuation-based bidirectional modules with variable stiffness and closed-loop position control	ICRA 2021	2021	Manipulation	N	M

Appendix C. Terminology Listing

Shen Li;Daehyung Park;Yoonchang Sung;Julie A. Shah;Nicholas Roy	Reactive Task and Motion Planning under Temporal Logic Specifications	ICRA 2021	2021	Manipulation	N	Y
Xiao Xiao;Shilei Xu;Changsheng Li;Xiaoyi Gu;Huxin Gao;Max Q.-H. Meng;Hongliang Ren	Magnetically-Connected Modular Reconfigurable Mini-robotic System with Bilateral Isokinematic Mapping and Fast On-site Assembly towards Minimally Invasive Procedures	ICRA 2021	2021	Surgery	N	M
Jiangfan Yu;Lidong Yang;Xingzhou Du;Hui Chen;Tiantian Xu;Li Zhang	Adaptive Pattern and Motion Control of Magnetic Microrobotic Swarms	TOR	2021	Microbots	Y	A
Yanghui Zhu;Qingcong Wu;Bai Chen;Dawen Xu;Ziyan Shao	Design and Evaluation of a Novel Torque-Controllable Variable Stiffness Actuator With Reconfigurability	TOM	2022	Service	N	M
Chang Liu;Samuel J. Wohlever;Maria B. Ou;Taskin Padir;Samuel M. Felton	Shake and Take: Fast Transformation of an Origami Gripper	TOR	2022	Manipulation	N	A
Thomas M. Roehr	Active Exploitation of Redundancies in Reconfigurable Multirobot Systems	TOR	2022	Space	Y	Y
Phone Thiha Kyaw;Anh Vu Le;Prabakaran Veerajagadheswar;Mohan Rajesh Elara;Theint Theint Thu;Nguyen Huu Khanh Nhan;Phan Van Duc;Minh Bui Vu	Energy-Efficient Path Planning of Reconfigurable Robots in Complex Environments	TOR	2022	Mobile	Y	Y
Qianqian Wang;Shihao Yang;Li Zhang	Magnetic Actuation of a Dynamically Reconfigurable Microswarm for Enhanced Ultrasound Imaging Contrast	TOM	2022	Microbots	Y	A
Brian H. Do;Valory Banashek;Allison M. Okamura	Dynamically Reconfigurable Discrete Distributed Stiffness for Inflated Beam Robots	ICRA 2020	2020	Mobile	N	A
Meibao Yao;Xueming Xiao;Yang Tian;Hutao Cui;Jamie Paik	An Actuation Fault Tolerance Approach to Reconfiguration Planning of Modular Self-folding Robots	ICRA 2020	2020	Mobile	N	A
Vignesh Sushrutha Raghavan;Dimitrios Kanoulas;Darwin G. Caldwell;Nikos G. Tsagarakis	Agile Legged-Wheeled Reconfigurable Navigation Planner Applied on the CEN-TAURO Robot	ICRA 2020	2020	Mobile	N	A

Appendix C. Terminology Listing

Jaimie Carlson;Jason Friedman;Christopher Kim;Cynthia Sung	REBOund: Untethered Origami Jumping Robot with Controllable Jump Height	ICRA 2020	2020	Mobile	N	A
S. Jain;T. Stalin;V. Subramaniam;J. Agarwal;P. Valdivia y Alvarado	A Soft Gripper with Retractable Nails for Advanced Grasping and Manipulation	ICRA 2020	2020	Manipulation	N	A
Austin Nicolai;Gina Olson;Yiğit Mengüç;Geoffrey A. Hollinger	Learning to Control Reconfigurable Staged Soft Arms	ICRA 2020	2020	Manipulation	N	M
Chao Liu;Sencheng Yu;Mark Yim	A Fast Configuration Space Algorithm for Variable Topology Truss Modular Robots	ICRA 2020	2020	Mobile	N	Y
Huan Nguyen;Tung Dang;Kostas Alexis	The Reconfigurable Aerial Robotic Chain: Modeling and Control	ICRA 2020	2020	UAVs	Y	M
Dimitri A. Schreiber;Florian Richter;Andrew Bilan;Peter V. Gavrilov;Hoi Man Lam;Casey H. Price;Kalind C. Carpenter;Michael C. Yip	ARCSnake: An Archimedes' Screw-Propelled, Reconfigurable Serpentine Robot for Complex Environments	ICRA 2020	2020	Mobile	N	A
Claudio Pose;Juan Giribet;Ignacio Mas	Fault tolerance analysis of a hexarotor with reconfigurable tilted rotors	ICRA 2020	2020	UAVs	N	A
Wansoo Kim;Pietro Balatti;Edoardo Lamon;Arash Ajoudani	MOCA-MAN: A MOBILE and reconfigurable Collaborative Robot Assistant for conjoined huMAN-robot actions	ICRA 2020	2020	Service	N	M
Senthur Raj;R P Manu Aatitya;S Jack Samuel;J Veejay Karthik;D. Ezhilarasi	Ibex: A reconfigurable ground vehicle with adaptive terrain navigation capability	ICRA 2020	2020	Mobile	N	A
Qianqian Wang;Ben Wang;Jiangfan Yu;Kathrin Schweizer;Bradley J. Nelson;Li Zhang	Reconfigurable Magnetic Microswarm for Thrombolysis under Ultrasound Imaging	ICRA 2020	2020	Microbots	Y	A

Annotated Bibliography

- [1] *DARPA Subterranean Challenge*. 2020. URL: <https://www.subtchallenge.com/index.html> (visited on 06/16/2020).
- [2] *DARPA Subterranean Challenge Gallery*. 2020. URL: <https://www.subtchallenge.com/gallery.html> (visited on 06/17/2020).
- [3] *OzBot Titan: the lifesaving police robot*. BIA5 Pty Ltd. 2020. URL: <https://bia5.com/ozbot-titan-the-lifesaving-police-robot/> (visited on 06/17/2020).
- [4] *DARPA SubT Challenge*. 2020. URL: <https://research.csiro.au/robotics/category/darpa-subt-challenge/> (visited on 06/17/2020).
- [5] *Explorer*. 2020. URL: <https://www.subt-explorer.com/> (visited on 06/17/2020).
- [6] François Michaud et al. “Multi-Modal Locomotion Robotic Platform Using Leg-Track-Wheel Articulations”. In: *Autonomous Robots* 18 (2005), pp. 137–156.
- [7] SNU BioRobotics Lab. *origami wheel robot base on magic-ball origami structure*. Online video clip. YouTube, Dec. 26, 2013. URL: <https://www.youtube.com/watch?v=EiInnP8RzFI> (visited on 07/19/2020).
- [8] J. Y. Wong. *A mentor, friend and colleague - recollections of Dr. Mieczyslaw Gregory Bekker*. Aug. 5, 2015. URL: <https://www.istvs.org/newswire/bekker> (visited on 08/22/2018).
- [9] Jody D. Priddy and William E. Willoughby. “Clarification of vehicle cone index with reference to mean maximum pressure”. In: *Journal of Terramechanics* 43.2 (Apr. 2006), pp. 85–96. URL: <http://www.sciencedirect.com/science/article/pii/S0022489804001120> (visited on 06/06/2016).
- [10] *Mars Exploration Rover-Spirit*. URL: <https://www.jpl.nasa.gov/missions/mars-exploration-rover-spirit-mer-spirit/> (visited on 07/10/2019).
- [11] *NASA’s Mars Rover has Uncertain Future as Sixth Anniversary Nears*. Dec. 31, 2009. URL: <https://mars.nasa.gov/mer/gallery/press/spirit/20091231a.html> (visited on 06/06/2018).
- [12] William Smith et al. “Comparison of discrete element method and traditional modeling methods for steady-state wheel-terrain interaction of small vehicles”. In: *Journal of Terramechanics* 56 (2014), pp. 61–75. ISSN: 0022-4898. DOI: <https://doi.org/10.1016/j.jterra.2014.08.004>. URL: <http://www.sciencedirect.com/science/article/pii/S0022489814000676>.
- [13] Kyle D. Wesson et al. “Instrumenting an All-Terrain Vehicle for Off-Road Mobility Analysis”. In: (Jan. 2007), p. 56.

- [14] Luis Rocha. *Complex Systems Modeling: Using Metaphors from Nature in Simulation and Scientific Models*. Los Alamos National Laboratory, 2003. URL: <https://informatics.indiana.edu/rocha/publications/complex/csm.html> (visited on 09/25/2019).
- [15] Herbert A. Simon. *The Sciences of the Artificial*. 3rd ed. MIT Press, 1969. URL: <https://mitpress.mit.edu/books/sciences-artificial>.
- [16] Thomas A. Hemphill. *Autonomous Vehicles, Complexity and the 'Big Picture'*. InsideSources. May 30, 2019. URL: <https://www.insidesources.com/autonomous-vehicles-complexity-and-the-big-picture/> (visited on 09/30/2019).
- [17] Jennifer P. Wisdom et al. "Innovation adoption: a review of theories and constructs". In: *Adm Policy Ment Health* 41 (4 2014), pp. 480–502. URL: <https://doi.org/10.1007/s10488-013-0486-4> (visited on 07/10/2019).
- [18] Jr. Lucien A. Schmit. "Structural Design by Systematic Synthesis". In: 1960.
- [19] Friedrich Pfeiffer, Jürgen Eltze, and Hans-Jürgen Weidemann. "Six-legged technical walking considering biological principles". In: *Robotics Auton. Syst.* 14 (1995), pp. 223–232.
- [20] Bo Li et al. "Optimization method of vehicle handling stability based on response surface model with D-optimal test design". In: *Journal of Mechanical Science and Technology* 34 (June 2020). DOI: 10.1007/s12206-020-0502-z.
- [21] Dimitrios Apostolopoulos. *Analytical Configuration of Wheeled Robotic Locomotion*. PhD thesis. Apr. 2001. URL: <http://ri.cmu.edu/publications/analytical-configuration-of-wheeled-robotic-locomotion/> (visited on 06/13/2017).
- [22] M. MahmoodiKaleibar et al. "Optimization of suspension system of offroad vehicle for vehicle performance improvement". In: *Journal of Central South University of Technology* 20 (Apr. 2013). DOI: 10.1007/s11771-013-1564-1.
- [23] *IRIS: Your Eyes and Ears on the Ground - and Under it*. 2019. URL: <http://robot-team.com/products/iris/> (visited on 06/16/2020).
- [24] Qinetiq. *Robots for Defense and Commercial Use*. URL: <https://qinetiq-na.com/products/unmanned-systems/> (visited on 06/28/2019).
- [25] *Soviet Union Lunar Rovers*. Mar. 18, 2010. URL: https://www.nasa.gov/mission_pages/LRO/multimedia/lroimages/lroc-20100318.html (visited on 09/06/2018).
- [26] Byron Spice. *CMU's Iris Lunar Rover Meets Milestone for Flight*. 2020. URL: <https://www.scs.cmu.edu/news/2020/cmus-iris-lunar-rover-meets-milestone-flight> (visited on 04/08/2023).
- [27] Afreen Siddiqi. *Reconfigurability in space systems : architecting framework and case studies*. PhD thesis. 2006.
- [28] Kasper Stoy, David Brandt, and David Christensen. *Self-Reconfigurable Robots: An Introduction*. Cambridge, Massachusetts: The MIT Press, 2010. ISBN: 978-0-262-01371-0.

- [29] Paul Moubarak and Pinhas Ben-Tzvi. “Modular and reconfigurable mobile robotics”. In: *Robotics and Autonomous Systems* 60.12 (2012), pp. 1648–1663. ISSN: 0921-8890. DOI: <https://doi.org/10.1016/j.robot.2012.09.002>. URL: <http://www.sciencedirect.com/science/article/pii/S0921889012001480>.
- [30] Xilun Ding, Xianwen Kong, and Jian Dai, eds. *Advances in Reconfigurable Mechanisms and Robotics II*. Switzerland: Springer, 2016. ISBN: 978-3-319-23327-7.
- [31] S. Sankhar Reddy Chennareddy, Anita Agrawal, and Anupama Karuppiah. *Modular Self-Reconfigurable Robotic Systems: A Survey on Hardware Architectures*. 2017. URL: <https://www.hindawi.com/journals/jr/2017/5013532/> (visited on 06/14/2020).
- [32] Jian Dai, Matteo Zoppi, and Xianwen Kong, eds. *Advances in Reconfigurable Mechanisms and Robotics I*. London: Springer-Verlag, 2012. ISBN: ISBN 978-1-4471-4141-9.
- [33] Mark Yim et al. “Modular Reconfigurable Robots in Space Applications”. In: *Autonomous Robots* 14.2 (Mar. 2003), pp. 225–237. ISSN: 1573-7527. DOI: 10.1023/A:1022287820808. URL: <https://doi.org/10.1023/A:1022287820808>.
- [34] V. Zykov et al. “Evolved and Designed Self-Reproducing Modular Robotics”. In: *IEEE Transactions on Robotics* 23.2 (Apr. 2007), pp. 308–319. DOI: 10.1109/TRO.2007.894685.
- [35] Robert A. Freitas and William B Zachary. “A Self-Replicating, Growing Lunar Factory”. In: 1981. URL: <http://www.rfreitas.com/Astro/GrowingLunarFactory1981.htm> (visited on 09/25/2019).
- [36] K. Zacny et al. “Mars2020 sample acquisition and caching technologies and architectures”. In: *2014 IEEE Aerospace Conference*. 2014, pp. 1–12.
- [37] Nourredine Boubekri. “Robots in flexible manufacturing systems”. In: *Robotics* 3.3 (1987), pp. 421–426. ISSN: 0167-8493. DOI: [https://doi.org/10.1016/0167-8493\(87\)90058-1](https://doi.org/10.1016/0167-8493(87)90058-1). URL: <http://www.sciencedirect.com/science/article/pii/0167849387900581>.
- [38] R. Murthy et al. “M3: Multiscale, Deterministic and Reconfigurable Macro-Micro Assembly System for Packaging of MEMS”. In: *Proceedings 2007 IEEE International Conference on Robotics and Automation*. 2007, pp. 668–673.
- [39] Lining Sun et al. “Task-Reconfigurable System for MEMS Assembly”. In: *Proceedings of the 2005 IEEE International Conference on Robotics and Automation*. 2005, pp. 832–837.
- [40] B. Roy and H. H. Asada. “Design of a Reconfigurable Robot Arm for Assembly Operations inside an Aircraft Wing-Box”. In: *Proceedings of the 2005 IEEE International Conference on Robotics and Automation*. 2005, pp. 590–595.
- [41] T. Fukuda and S. Nakagawa. “Dynamically reconfigurable robotic system”. In: *Proceedings. 1988 IEEE International Conference on Robotics and Automation*. 1988, 1581–1586 vol.3.
- [42] K. H. Wurst. “The Conception and Construction of a Modular Robot System”. In: *Proceedings. 16th Annual Symposium on Industrial Robotics*. 1986.

- [43] Donald Schmitz, Pradeep Khosla, and Takeo Kanade. *The CMU Reconfigurable Modular Manipulator System*. Technical Report. Carnegie Mellon University, May 1988. URL: <http://citeseerx.ist.psu.edu/viewdoc/download?doi=10.1.1.900.7964&rep=rep1&type=pdf> (visited on 07/26/2020).
- [44] Toshio Fukuda et al. “Cell Structured robotic system CEBOT: Control, planning and communication methods”. In: *Robotics and Autonomous Systems 7.2* (1991). Special Issue Intelligent Autonomous Systems, pp. 239–248. ISSN: 0921-8890. DOI: [https://doi.org/10.1016/0921-8890\(91\)90045-M](https://doi.org/10.1016/0921-8890(91)90045-M). URL: <http://www.sciencedirect.com/science/article/pii/092188909190045M>.
- [45] Mark Yim. *Locomotion with a Unit-Modular Reconfigurable Robot*. PhD thesis. Dec. 1994. URL: <http://i.stanford.edu/pub/cstr/reports/cs/tr/95/1536/CS-TR-95-1536.pdf> (visited on 09/25/2019).
- [46] Gregory S. Chirikjian. “Metamorphic hyper-redundant manipulators”. In: 1993.
- [47] Jungwon Seo, Jamie Paik, and Mark Yim. “Modular Reconfigurable Robotics”. In: *Annual Review of Control, Robotics, and Autonomous Systems 2.1* (2019), pp. 63–88. DOI: 10.1146/annurev-control-053018-023834. eprint: <https://doi.org/10.1146/annurev-control-053018-023834>. URL: <https://doi.org/10.1146/annurev-control-053018-023834>.
- [48] Johannes Specht, Markus Jochim, and Wilfried Steiner. *Terminology Proposal: Redundancy for Fault Tolerance*. Jan. 16, 2013. URL: <http://www.ieee802.org/1/files/public/docs2013/new-tsn-specht-redundancy-terminology-20130115-v01.pdf> (visited on 06/09/2020).
- [49] Amin Moosavian and Fengfeng (Jeff) Xi. “Modular design of parallel robots with static redundancy”. In: *Mechanism and Machine Theory 96* (2016), pp. 26–37. ISSN: 0094-114X. DOI: <https://doi.org/10.1016/j.mechmachtheory.2015.08.012>. URL: <http://www.sciencedirect.com/science/article/pii/S0094114X15001974>.
- [50] Kirby Witte. *Design, characterization, and implementation of lower-limb exoskeletons for performance augmentation during walking and running*. PhD thesis. Dec. 2018.
- [51] D. Kalita and P. P. Khargonekar. “Formal verification for analysis and design of logic controllers for reconfigurable machining systems”. In: *IEEE Transactions on Robotics and Automation 18.4* (2002), pp. 463–474.
- [52] Satoshi Murata and Haruhisa Kurokawa. “Prototypes of Self-Organizing Robots”. In: *Self-Organizing Robots*. Tokyo: Springer Tokyo, 2012, pp. 105–130. ISBN: 978-4-431-54055-7. DOI: 10.1007/978-4-431-54055-7_7. URL: https://doi.org/10.1007/978-4-431-54055-7_7.
- [53] M. Yim, D. G. Duff, and K. D. Roufas. “PolyBot: a modular reconfigurable robot”. In: *Proceedings 2000 ICRA. Millennium Conference. IEEE International Conference on Robotics and Automation. Symposia Proceedings (Cat. No.00CH37065)*. Vol. 1. 2000, 514–520 vol.1.
- [54] Wei-Min Shen, B. Salemi, and P. Will. “Hormone-inspired adaptive communication and distributed control for CONRO self-reconfigurable robots”. In: *IEEE Transactions on Robotics and Automation 18.5* (2002), pp. 700–712.
- [55] J. Neubert, A. Rost, and H. Lipson. “Self-Soldering Connectors for Modular Robots”. In: *IEEE Transactions on Robotics 30.6* (2014), pp. 1344–1357.

- [56] National Research Council. *Visionary Manufacturing Challenges for 2020*. Washington, DC: The National Academies Press, 1998. ISBN: 978-0-309-06182-7. DOI: 10.17226/6314. URL: <https://www.nap.edu/catalog/6314/visionary-manufacturing-challenges-for-2020>.
- [57] Michel-Alexandre Cardin. “Enabling Flexibility in Engineering Systems: A Taxonomy of Procedures and a Design Framework”. In: *Journal of Mechanical Design* 136 (Jan. 2014). DOI: 10.1115/1.4025704.
- [58] E. Fricke and A. P. Schulz. *Design for Changeability (DfC): Principles to Enable Changes in Systems Throughout Their Entire Lifecycle*. 2005, pp. 342–359.
- [59] R. de Neufville and S. Scholtes. *Flexibility In Engineering Design*. Cambridge, MA: MIT Press, 2011.
- [60] A. N. Das and S. Savoie. “Quasi-static evaluation of a modular and Reconfigurable Manufacturing Cell”. In: *2013 IEEE International Conference on Robotics and Automation*. 2013, pp. 258–263.
- [61] Karl Ulrich and Karen Tung. “Fundamentals of Product Modularity”. In: *Management of Design* 39 (Jan. 1991), pp. 219–231. DOI: 10.1007/978-94-011-1390-8_12.
- [62] Olivier L. de Weck, William David Nadir, and Jaime Gustav Wong. “Modular Structures for Manned Space Exploration: The Truncated Octahedron as Building Block”. In: 2005.
- [63] M. Yim et al. “Modular Self-Reconfigurable Robot Systems [Grand Challenges of Robotics]”. In: *IEEE Robotics Automation Magazine* 14.1 (Mar. 2007), pp. 43–52. DOI: 10.1109/MRA.2007.339623.
- [64] A. Pamecha, I. Ebert-Uphoff, and G. S. Chirikjian. “Useful metrics for modular robot motion planning”. In: *IEEE Transactions on Robotics and Automation* 13.4 (1997), pp. 531–545.
- [65] A. Castano, A. Behar, and P. M. Will. “The Conro modules for reconfigurable robots”. In: *IEEE/ASME Transactions on Mechatronics* 7.4 (2002), pp. 403–409.
- [66] I. -. Chen and J. W. Burdick. “Enumerating the nonisomorphic assembly configurations of modular robotic systems”. In: *Proceedings of 1993 IEEE/RSJ International Conference on Intelligent Robots and Systems (IROS '93)*. Vol. 3. 1993, 1985–1992 vol.3.
- [67] Karl Ulrich and Steven Eppiner. *Product Design Development*. 6th ed. McGraw-Hill Education, 2015. ISBN: 978-0078029066.
- [68] Jian Dai and J. Jones. “Mobility in Metamorphic Mechanisms of Foldable/Erectable Kinds”. In: *Journal of Mechanical Design - J MECH DESIGN* 121 (Sept. 1999). DOI: 10.1115/1.2829470.
- [69] Continental. *Continental presents two new tyre technology concepts for greater safety and comfort*. Sept. 4, 2018. URL: <https://www.continental-oman.com/car/media-services/newsroom/20180329-two-new-tire-technology-concepts> (visited on 05/23/2019).
- [70] Hankook Tire Global. *[Promotional Video] 2014 Design Innovation "Boostrac" "Alpik" "Hyblade"*. Nov. 27, 2014. URL: <https://www.youtube.com/watch?v=mMBbDgh-icE> (visited on 05/24/2019).

- [71] Defense Acquisition University. *Key Performance Parameters (KPPs)*. ACQuipedia. 2022. URL: <https://www.dau.edu/acquipedia/pages/articledetails.aspx#!346>.
- [72] Joseph M. Juran. “Pareto, Lorenz, Cournot Bernoulli, Juran and Others”. In: *Industrial Quality Control* (1950), p. 25.
- [73] Dan Sullivan. *The 80% Approach*. The Strategic Coach Inc., 2013.
- [74] Ehud Kroll, E. Lenz, and J.R. Wolberg. “KNOWLEDGE-BASED SOLUTION TO THE DESIGN-FOR-ASSEMBLY PROBLEM.” In: 1 (June 1988), pp. 104–108.
- [75] Brian H. Wilcox et al. “Athlete: A cargo handling and manipulation robot for the moon”. In: *Journal of Field Robotics* 24.5 (2007), pp. 421–434. DOI: <https://doi.org/10.1002/rob.20193>. eprint: <https://onlinelibrary.wiley.com/doi/pdf/10.1002/rob.20193>. URL: <https://onlinelibrary.wiley.com/doi/abs/10.1002/rob.20193>.
- [76] Gustavo Freitas et al. “Kinematic reconfigurability control for an environmental mobile robot operating in the Amazon rain forest”. In: *Journal of Field Robotics* 27.2 (2010), pp. 197–216. DOI: <https://doi.org/10.1002/rob.20334>. eprint: <https://onlinelibrary.wiley.com/doi/pdf/10.1002/rob.20334>. URL: <https://onlinelibrary.wiley.com/doi/abs/10.1002/rob.20334>.
- [77] Hiroaki Inotsume et al. “Modeling, Analysis, and Control of an Actively Reconfigurable Planetary Rover for Traversing Slopes Covered with Loose Soil”. In: *Journal of Field Robotics* 30.6 (2013), pp. 875–896. DOI: <https://doi.org/10.1002/rob.21479>. eprint: <https://onlinelibrary.wiley.com/doi/pdf/10.1002/rob.21479>. URL: <https://onlinelibrary.wiley.com/doi/abs/10.1002/rob.21479>.
- [78] William Reid et al. “Sampling-based hierarchical motion planning for a reconfigurable wheel-on-leg planetary analogue exploration rover”. In: *Journal of Field Robotics* 37.5 (2020), pp. 786–811. DOI: <https://doi.org/10.1002/rob.21894>. eprint: <https://onlinelibrary.wiley.com/doi/pdf/10.1002/rob.21894>. URL: <https://onlinelibrary.wiley.com/doi/abs/10.1002/rob.21894>.
- [79] Rui Xu and Changying Li. “A modular agricultural robotic system (MARS) for precision farming: Concept and implementation”. In: *Journal of Field Robotics* 39.4 (2022), pp. 387–409. DOI: <https://doi.org/10.1002/rob.22056>. eprint: <https://onlinelibrary.wiley.com/doi/pdf/10.1002/rob.22056>. URL: <https://onlinelibrary.wiley.com/doi/abs/10.1002/rob.22056>.
- [80] Troy P. Cordie et al. “Modular field robot deployment for inspection of dilapidated buildings”. In: *Journal of Field Robotics* 36.4 (2019), pp. 641–655. DOI: <https://doi.org/10.1002/rob.21872>. eprint: <https://onlinelibrary.wiley.com/doi/pdf/10.1002/rob.21872>. URL: <https://onlinelibrary.wiley.com/doi/abs/10.1002/rob.21872>.
- [81] P. Schenker et al. “New planetary rovers for long range Mars science and sample return”. In: 1998. URL: <https://citeseerx.ist.psu.edu/viewdoc/download;jsessionid=0D6CAC940709CC42CE69750F79141C89?doi=10.1.1.98.4254&rep=rep1&type=pdf>.

- [82] *Unmanned Ground Vehicles*. FLIR Systems, Inc. 2020. URL: <https://www.flir.com/browse/government-defense/unmanned-ground-systems/> (visited on 08/07/2020).
- [83] Christopher Johnson. *Comparative Analysis of Lightweight Robotic Wheeled and Tracked Vehicle*. MS thesis. Apr. 26, 2012. URL: https://vtechworks.lib.vt.edu/bitstream/handle/10919/76994/etd-05082012-183556_Johnson_CP_T_2012.pdf?sequence=1 (visited on 05/11/2020).
- [84] Xueshan Gao et al. “Dynamics and stability analysis on stairs climbing of wheel-track mobile robot”. In: *International Journal of Advanced Robotic Systems* 14.4 (2017), p. 1729881417720783. DOI: 10.1177/1729881417720783. eprint: <https://doi.org/10.1177/1729881417720783>. URL: <https://doi.org/10.1177/1729881417720783>.
- [85] D. Cui et al. “The structure design and analysis of a wheel-track robot”. In: *2016 IEEE International Conference on Mechatronics and Automation*. 2016, pp. 2530–2535.
- [86] Yoram Koren and Moshe Shpitalni. “Design of reconfigurable manufacturing systems”. In: *Journal of Manufacturing Systems* 29.4 (2010), pp. 130–141. ISSN: 0278-6125. DOI: <https://doi.org/10.1016/j.jmsy.2011.01.001>. URL: <https://www.sciencedirect.com/science/article/pii/S0278612511000021>.
- [87] Nur Ozge Ozaltin et al. “An Investigation on the Implications of Design Process Phases on Artifact Novelty”. In: *Journal of Mechanical Design* 137.5 (May 2015). 051001. ISSN: 1050-0472. DOI: 10.1115/1.4028530. eprint: https://asmedigitalcollection.asme.org/mechanicaldesign/article-pdf/137/5/051001/6226128/md_137_05_051001.pdf. URL: <https://doi.org/10.1115/1.4028530>.
- [88] George Dieter and Linda Schmidt. *Engineering Design*. 5th ed. McGraw-Hill, 2013. ISBN: 978-0-07-339814-3.
- [89] Troy Peter Cordie. “Modular Reconfigurable Field Robotics”. In: *Queensland University of Technology* (2022). URL: https://eprints.qut.edu.au/230503/1/Troy_Cordie_Thesis.pdf.
- [90] *Vehicle Dynamics Terminology*. Warrendale, PA, Jan. 24, 2008. DOI: https://doi.org/10.4271/J670_200801. URL: https://saemobilus.sae.org/content/j670_200801.
- [91] L Bruzzone and Giuseppe Quaglia. “Locomotion systems for ground mobile robots in unstructured environments”. In: *Mechanical sciences* 3.2 (2012), pp. 49–62.
- [92] U.S. Army. “High Mobility Robotic Platform Study, Vol. 1, Contract DAAE07-98-C-L024, CDRL A002”. In: ().
- [93] David Wettergreen. *My Gallery*. Carnegie Mellon University. URL: http://www.fr.cri.cmu.edu/projects/lri/scarab/images/WA_testing/gallery.y.html (visited on 08/29/2018).
- [94] Алексей Краснер. *P.3 racecar wheel spin*. Dec. 25, 2016. URL: <https://www.youtube.com/watch?v=Fyj4Q5khK9A> (visited on 08/29/2018).
- [95] *How to get your car unstuck from mud or sand*. URL: <https://www.budgetdirect.com.au/blog/how-to-get-your-car-unstuck-from-mud-or-sand.html> (visited on 08/29/2018).

- [96] J.Y. Wong. “An introduction to terramechanics”. In: *Journal of Terramechanics* 21.1 (1984), pp. 5–17. ISSN: 0022-4898. DOI: [https://doi.org/10.1016/0022-4898\(84\)90004-1](https://doi.org/10.1016/0022-4898(84)90004-1). URL: <http://www.sciencedirect.com/science/article/pii/0022489884900041>.
- [97] M. G. Bekker. *Theory of Land Locomotion*. Ann Arbor: The University of Michigan Press, 1956. ISBN: 9780472750207.
- [98] Lutz Richter, Marco Bernasconi, and P Coste. “Analysis, Design and Test of Wheels for a 4 kg-class Mobile Device for the Surface of Mars”. In: Jan. 2002.
- [99] G. Meirion-Griffith and M. Spenko. “An empirical study of the terramechanics of small unmanned ground vehicles”. In: *2010 IEEE Aerospace Conference*. Mar. 2010, pp. 1–6. DOI: 10.1109/AERO.2010.5446993.
- [100] Carmine Senatore and Karl David Iagnemma. “Analysis of stress distributions under lightweight wheeled vehicles”. In: 2014.
- [101] G. Meirion-Griffith and M. Spenko. “Comprehensive pressure-sinkage model for small-wheeled unmanned ground vehicles on dilative, deformable terrain”. In: *2012 IEEE International Conference on Robotics and Automation*. May 2012, pp. 4052–4057. DOI: 10.1109/ICRA.2012.6224601.
- [102] Brook Haueisen et al. *Case Study of the Evaluation and Verification of a PackBot Model in NRMM*. 2005. URL: <http://citeseerx.ist.psu.edu/viewdoc/download?doi=10.1.1.1030.2370&rep=rep1&type=pdf>.
- [103] D. Rowland. *Tracked vehicle ground pressure and its effect on soft ground performance*. 4th International Conference for Terrain Vehicle Systems, Stockholm, 1972. URL: <http://www.slideshare.net/wolfhag/tracked-vehicle-ground-pressure> (visited on 06/11/2016).
- [104] S.A. Shoop. “Thawing soil strength measurements for predicting vehicle performance”. In: *Journal of Terramechanics* 30.6 (1993), pp. 405–418. ISSN: 0022-4898. DOI: [https://doi.org/10.1016/0022-4898\(93\)90034-U](https://doi.org/10.1016/0022-4898(93)90034-U). URL: <http://www.sciencedirect.com/science/article/pii/002248989390034U>.
- [105] H.B. Brown Jr. et al. “Millibot trains for enhanced mobility”. English. In: *IEEE/ASME Transactions on Mechatronics* 7.4 (2002). cited By 102, pp. 452–461. ISSN: 10834435. DOI: 10.1109/TMECH.2002.806226. URL: <https://www2.scopus.com/inward/record.uri?eid=2-s2.0-0036966760&doi=10.1109%5C%2FTMECH.2002.806226&partnerID=40&md5=079c7c9b9bfd43faa82ff86ee6d4d835>.
- [106] J.Y. Wong. *Terramechanics and Off-Road Vehicle Engineering: Terrain Behaviour, Off-Road Vehicle Performance and Design*. Elsevier Science, 2009. ISBN: 9780080942537.
- [107] Kent Massey. *Mobility Design for Tracked Robots*. PDF file. May 27, 2010.
- [108] Grant Gerhart. “The Bekker Model Analysis for Small Robotic Vehicles”. In: (Oct. 2004), p. 10. DOI: 10.4271/2004-01-2642.
- [109] Shane Barnett. *Development of a Tow Capacity Test Device for Small Unmanned Vehicles*. MS thesis. Dec. 15, 2005. URL: <http://citeseerx.ist.psu.edu/viewdoc/download?doi=10.1.1.499.6567&rep=rep1&type=pdf> (visited on 08/07/2019).

- [110] M. G. Bekker. *Off-the-road Locomotion*. Ann Arbor: The University of Michigan Press, 1972. ISBN: 9780472041428.
- [111] R. Gross et al. “Autonomous Self-Assembly in Swarm-Bots”. In: *IEEE Transactions on Robotics* 22.6 (Dec. 2006), pp. 1115–1130. DOI: 10.1109/TRO.2006.882919.
- [112] Kenneth L. Boyd. *Wheeled Versus Tracked Vehicle Study*. Mar. 1, 1985. URL: <http://www.dtic.mil/dtic/tr/fulltext/u2/a166390.pdf> (visited on 05/27/2016).
- [113] Unterseher Lutz. *Wheels or Tracks? On the ‘Lightness’ of Military Expeditions*. Memorandum. Project on Defense Alternatives, URL: <http://www.comw.org/pda/0007wheels.html> (visited on 06/06/2016).
- [114] Paul Hornback. *The Wheels Versus Track Dilemma*. PDF file. Armor, Mar. 1998. URL: <https://fas.org/man/dod-101/sys/land/docs/2wheels98.pdf> (visited on).
- [115] R.F. Unger et al. *Mobility Analysis for the TRADOC Wheeled Versus Tracked Vehicle Study*. Technical report (U.S. Army Engineer Waterways Experiment Station). U.S. Army Engineer Waterways Experiment Station, 1988. URL: <https://books.google.com/books?id=9sidtgAACAAJ>.
- [116] National Robotics Engineering Center. *Crusher*. URL: <https://www.nrec.ric.mu.edu/solutions/defense/other-projects/crusher.html> (visited on 05/22/2019).
- [117] Lauren C. Williams. *Army aims for robot vehicles on the battlefield by 2028*. June 6, 2018. URL: <https://defensesystems.com/articles/2018/06/06/sky-net-future-army.aspx> (visited on 06/28/2019).
- [118] National Research Council. *Technology Development for Army Unmanned Ground Vehicles*. 2002. URL: <https://www.nap.edu/read/10592/> (visited on 06/28/2019).
- [119] Army Technology. *Titan Unmanned Ground Vehicle*. URL: <https://www.army-technology.com/projects/titan-unmanned-ground-vehicle-ugv/> (visited on 06/28/2019).
- [120] *Products*. URL: <http://endeavorrobotics.com/products> (visited on 08/22/2018).
- [121] J. G. Hetherington and P. D. Smith. “The Survivability and Mobility of Armoured Fighting Vehicles - Tuition Using a Simple Computer Program”. In: *Journal of Terramechanics* (1986), pp. 131–140. URL: <https://www.sciencedirect.com/science/article/pii/0022489886900029> (visited on 08/19/2017).
- [122] Gareth Meirion-Griffith. *Advances in vehicle-terrain interaction modeling for small, rigid-wheeled vehicles operating on deformable terrain*. PhD thesis. May 2012.
- [123] Rui He et al. “Review of terramechanics models and their applicability to real-time applications”. In: *Journal of Terramechanics* 81 (2019). Terramechanics: Real-Time Applications, pp. 3–22. ISSN: 0022-4898. DOI: <https://doi.org/10.1016/j.jterra.2018.04.003>. URL: <http://www.sciencedirect.com/science/article/pii/S0022489817302665>.
- [124] R. Burnstein. *Probleme zur experimentellen Motorpflugmechanik*. Der Motorwagen, 1913.

- [125] B. P. Goriatchkin. *Theory and Development of Agricultural Machinery*. Moscow, 1936.
- [126] A. Reece. “The fundamental equation of earth-moving mechanics.” In: (1964).
- [127] J. Wong and A. Reece. “Prediction of rigid wheel performance based on the analysis of soil-wheel stresses”. In: (1967).
- [128] Jacques Heyman, Charles Augustin de Coulomb, and Charles Augustin Coulomb. *Coulomb’s memoir on statics: an essay in the history of civil engineering*. CUP Archive, 1972.
- [129] W. Söhne. “Fundamentals of pressure distribution and soil compaction under tractor tires”. In: (1958), pp. 9–28.
- [130] Colin Creager et al. *Drawbar Pull (DP) Procedures for Off-Road Vehicle Testing*. PDF file. NASA, Aug. 1, 2017.
- [131] Zoltan J. Janosi, Ben. Hanamoto, and Istituto elettrotecnico nazionale Galileo Ferraris. “The analytical determination of drawbar pull as a function of slip for tracked vehicles in deformable soils”. In: 1961.
- [132] J.Y. Wong. *Theory of Ground Vehicles*. John Wiley and Sons, Inc, 2008. ISBN: 9780470170380.
- [133] M. G. Bekker and E. V. Semonin. “Motion Resistance of Pneumatic Tyres”. In: (Apr. 1975). URL: https://www.researchgate.net/publication/282581028_MOTION_RESISTANCE_OF_PNEUMATIC_TYRES (visited on 09/26/2018).
- [134] Robert Bosch. *Automotive Handbook*. 4th ed. 1996.
- [135] M.G. Bekker. *Mechanics of Off-The-Road Locomotion*. Institution of Mechanical Engineers James Clayton Lecture, July 10, 1962. URL: <http://www.dtic.mil/dtic/tr/fulltext/u2/a457955.pdf> (visited on 06/06/2016).
- [136] A. H. Rajabi et al. “Prediction of obstacle climbing capability for tracked vehicles”. In: *2011 IEEE International Symposium on Safety, Security, and Rescue Robotics*. Nov. 2011, pp. 128–133. DOI: 10.1109/SSRR.2011.6106766.
- [137] J. C. Larminie. “Standards for the Mobility Requirements of Military Vehicles”. In: *Journal of Terramechanics* 25.3 (1988), pp. 171–189. URL: <http://anothersample.net/modifications-to-the-mean-maximum-pressure-system> (visited on 08/19/2017).
- [138] B. McLaurin. *Proposed revisions to MMP based on the results of tractive performance trials with single pneumatic tyres and a modular track system*. Version DERA/LS4/TR970122/1.0. Defense Evaluation and Research Agency. Aug. 1997. (Visited on 08/19/2016). Farnborough, Hampshire.
- [139] D. Rowland. *A Review of Vehicle Design for Soft Ground Operation*. 5th International Conference for Terrain Vehicle Systems, 1975. URL: <http://www.slideshare.net/wolfhag/tracked-vehicle-ground-pressure> (visited on 06/11/2016).
- [140] J. C. Larminie. “Modifications to the Mean Maximum Pressure System”. In: *Journal of Terramechanics* 29.2 (1992), pp. 239–255. URL: [https://doi.org/10.1016/0022-4898\(92\)90029-J](https://doi.org/10.1016/0022-4898(92)90029-J) (visited on 08/11/2016).
- [141] J.G. Kennedy and E. S. Rush. *Trafficability of Soils*. PDF file. Mar. 1968. URL: https://digital.library.unt.edu/ark:/67531/metadc303870/m2/1/high_res_d/metadc303870.pdf (visited on 09/07/2018).

- [142] J. Y. Wong. “On The Role of Mean Maximum Pressure as an Indicator of Cross-country Mobility for Tracked Vehicles”. In: *Journal of Terramechanics* 31.3 (1994), pp. 197–213. URL: <https://www.sciencedirect.com/science/article/pii/S0022489894900167> (visited on 08/19/2017).
- [143] J. Y. Wong. “Application of the Computer Simulation Model NTVPM-89 to the Development of a New Version of the Infantry Fighting Vehicle ASCOD”. In: *Journal of Terramechanics* 32.1 (1995), pp. 53–61. URL: <https://www.sciencedirect.com/science/article/pii/S002248989500004K> (visited on 08/19/2017).
- [144] Timothy Vong, Gary Haas, and Caledonia Henry. *NATO Reference Mobility model (NRMM) Modeling of the DEMO III Experimental Unmanned, Ground Vehicle (XUV)*. Apr. 1, 1999. URL: <http://www.dtic.mil/docs/citations/ADA362133> (visited on 08/09/2017).
- [145] Ulysses Contreras et al. *Soil Models and Vehicle System Dynamics*. Technical Report. U.S. Army TARDEC, May 7, 2013. URL: <http://www.dtic.mil/dtic/tr/fulltext/u2/a578850.pdf> (visited on 08/21/2018).
- [146] Michael McCullough et al. “Simple Terramechanics Models and their Demonstration in the Next Generation NATO Reference Mobility Model”. In: 2017.
- [147] Xingguo Song et al. “Locally supervised neural networks for approximating terramechanics models”. In: *Mechanical Systems and Signal Processing* 75 (2016), pp. 57–74. ISSN: 0888-3270. DOI: <https://doi.org/10.1016/j.ymssp.2015.12.028>. URL: <http://www.sciencedirect.com/science/article/pii/S088327015005932>.
- [148] Ian Dettwiller et al. “Improving accuracy of vehicle-terrain interface algorithms for wheeled vehicles on fine-grained soils through Bayesian calibration”. In: *Journal of Terramechanics* 77 (2018), pp. 59–68. ISSN: 0022-4898. DOI: <https://doi.org/10.1016/j.jterra.2018.03.001>. URL: <http://www.sciencedirect.com/science/article/pii/S0022489817300976>.
- [149] Alonzo Kelly et al. “Toward Reliable Off Road Autonomous Vehicles Operating in Challenging Environments”. In: *The International Journal of Robotics Research* 25.5-6 (2006), pp. 449–483. DOI: [10.1177/0278364906065543](https://doi.org/10.1177/0278364906065543). eprint: <https://doi.org/10.1177/0278364906065543>. URL: <https://doi.org/10.1177/0278364906065543>.
- [150] David Silver. “Learning Preference Models for Autonomous Mobile Robots in Complex Domains”. PhD thesis. Pittsburgh, PA: Carnegie Mellon University, Dec. 2010.
- [151] Sunglok Choi, Taemin Kim, and Wonpil Yu. “Robust Video Stabilization to Outlier Motion Using Adaptive RANSAC”. In: *Proceedings of the 2009 IEEE/RSJ International Conference on Intelligent Robots and Systems. IROS’09*. St. Louis, MO, USA: IEEE Press, 2009, pp. 1897–1902. ISBN: 978-1-4244-3803-7. URL: <http://dl.acm.org/citation.cfm?id=1733023.1733056>.
- [152] Graeme N. Wilson et al. “Velocity Selection for High-Speed UGVs in Rough Unknown Terrains Using Force Prediction”. In: *Intelligent Robotics and Applications*. Ed. by Chun-Yi Su, Subhash Rakheja, and Honghai Liu. Berlin, Heidelberg: Springer Berlin Heidelberg, 2012, pp. 387–396. ISBN: 978-3-642-33515-0.

- [153] David Stavens, Gabriel Hoffmann, and Sebastian Thrun. “Online Speed Adaptation Using Supervised Learning for High-Speed, Off-Road Autonomous Driving”. In: *IJCAI*. 2007.
- [154] National Robotics Engineering Center. *Cargo Unmanned Ground Vehicle*. URL: <https://www.nrec.ri.cmu.edu/nrec/solutions/defense/cargo-ugv.html> (visited on 05/22/2019).
- [155] Anthony Bouchard. *NASA’s Mars 2020 Rover Will Sport 20/20 Vision*. Nov. 1, 2017. URL: <https://www.labroots.com/trending/space/7216/nasa-s-mars-2020-rover-sport-20-20-vision> (visited on 05/22/2019).
- [156] *NG-NRMM-CDT*. Michigan Technological University. Aug. 7, 2019. URL: <https://www.mtu.edu/cdt/> (visited on 09/17/2019).
- [157] *Keweenaw Research Center*. Google Maps. URL: <https://goo.gl/maps/rGKZU7Udki4ejWp4A> (visited on 09/18/2019).
- [158] *Standard Practice for Classification of Soils for Engineering Purposes (Unified Soil Classification System)*. ASTM International. 2011. URL: https://compass.astm.org/EDIT/html_annot.cgi?D2487+17 (visited on 09/18/2019).
- [159] Scott Bradley Dr. Richard Gerth, Michael Letherwood, and Dr. David Gorsich. “The Data Used in the Next Generation NATO Reference Mobility Model Cooperative Demonstration of Technology”. In: Novi, MI, 2019.
- [160] *Cohesion Coefficient*. URL: <https://www.geotechdata.info/parameter/cohesion.html> (visited on 10/17/2019).
- [161] *Angle of Friction*. URL: <https://www.geotechdata.info/parameter/angle-of-friction.html> (visited on 10/17/2019).
- [162] M. A. Rahgozar and M. Saberian. “Geotechnical properties of peat soil stabilised with shredded waste tyre chips”. In: *Mires and Peat* 16 (2016), pp. 1–12. URL: mires-and-peat.net/media/map18/map_18_03.pdf (visited on 10/17/2019).
- [163] Satoshi Suzuki and Keiichi Abe. “Topological structural analysis of digitized binary images by border following”. In: *Computer Vision, Graphics, and Image Processing* 30.1 (1985), pp. 32–46. ISSN: 0734-189X. DOI: [https://doi.org/10.1016/0734-189X\(85\)90016-7](https://doi.org/10.1016/0734-189X(85)90016-7). URL: <https://www.sciencedirect.com/science/article/pii/0734189X85900167>.
- [164] Alvy Ray Smith. “Tint Fill”. In: *SIGGRAPH Comput. Graph.* 13.2 (Aug. 1979), pp. 276–283. ISSN: 0097-8930. DOI: 10.1145/965103.807456. URL: <https://doi.org/10.1145/965103.807456>.
- [165] Tamer Wasfy and Paramsothy Jayakumar. “Next-Generation NATO Reference Mobility Model Complex Terramechanics - Part 2: Requirements and Prototype”. In: (2019). URL: <https://apps.dtic.mil/sti/pdfs/AD1092819.pdf>.
- [166] Peter Hart, Nils Nilsson, and Bertram Raphael. “A Formal Basis for the Heuristic Determination of Minimum Cost Paths”. In: *IEEE Transactions on Systems Science and Cybernetics* 4.2 (1968), pp. 100–107. DOI: 10.1109/tssc.1968.300136. URL: <https://doi.org/10.1109/tssc.1968.300136>.

- [167] Steven N. Bacon et al. “Desert terrain characterization of landforms and surface materials within vehicle test courses at U.S. Army Yuma Proving Ground, USA”. In: *Journal of Terramechanics* 45.5 (2008), pp. 167–183. ISSN: 0022-4898. DOI: <https://doi.org/10.1016/j.jterra.2008.09.005>. URL: <http://www.sciencedirect.com/science/article/pii/S0022489808000542>.
- [168] Boris Delaunay. “Sur la sphère vide. A la mémoire de Georges Voronoï”. In: *Bulletin de l'Académie des Sciences de l'URSS. Classe des sciences mathématiques et na* (6 1934), pp. 793–600. URL: <https://zbmath.org/?q=an:0010.41101%7C60.0946.06> (visited on 03/27/2022).
- [169] *About*. 2019. URL: <https://opentopography.org/about> (visited on 03/27/2022).
- [170] Anthony Stentz. “The D* Algorithm for Real-Time Planning of Optimal Traverses”. In: *Carnegie Mellon University* (1994).
- [171] S.M. Shafaei and H. Mousazadeh. “Experimental comparison of locomotion system performance of ground mobile robots in agricultural drawbar works”. In: *Smart Agricultural Technology* 3 (2023), p. 100131. ISSN: 2772-3755. DOI: <https://doi.org/10.1016/j.atech.2022.100131>. URL: <https://www.sciencedirect.com/science/article/pii/S277237552200096X>.
- [172] Kyung Choi et al. “Framework of Reliability-Based Stochastic Mobility Map for Next Generation NATO Reference Mobility Model”. In: *Journal of Computational and Nonlinear Dynamics* 14 (Aug. 2018). DOI: 10.1115/1.4041350.
- [173] Joshua Summers and Jami J. Shah. “Mechanical Engineering Design Complexity Metrics: Size, Coupling, and Solvability”. In: *Journal of Mechanical Design* 132 (Feb. 2010). DOI: 10.1115/1.4000759.
- [174] The Editors of Encyclopaedia Britannica. *Computational Complexity*. Nov. 23, 2011. URL: <https://www.britannica.com/topic/computational-complexity> (visited on 07/20/2020).
- [175] G. Pahl et al. *Engineering Design: A Systematic Approach*. London: Springer-Verlag London Limited, 2007.
- [176] H Schleich et al. “State of the art of complexity management”. In: *ILIPT Project Report, Lueneburg* (2005).
- [177] Davide Falanga et al. “The Foldable Drone: A Morphing Quadrotor That Can Squeeze and Fly”. In: *IEEE Robotics and Automation Letters* PP (Dec. 2018), pp. 1–1. DOI: 10.1109/LRA.2018.2885575.
- [178] Richard Langevin. *Contradictions*. URL: <https://www.triz.org/triz/contradictions> (visited on 07/20/2020).
- [179] S. Tamaskar, K. Neema, and D. DeLaurentis. “Framework for Measuring Complexity of Aerospace Systems”. In: *Research in Engineering Design* 25.2 (2014), pp. 125–137. URL: <https://doi.org/10.1007/s00163-014-0169-5>.
- [180] Benjamin Shamah et al. “Steering and Control of a Passively Articulated Robot”. In: *SPIE, Sensor Fusion and Decentralized Control in Robotic Systems IV*. Vol. 4571. Oct. 2001.
- [181] Mason M.T., Srinivasa S.S., and Vazquez A.S. “Generality and Simple Hands”. In: *Robotics Research*. Ed. by Siegwart R. and Hirzinger G. Vol. 70. Berlin, Heidelberg: Springer Tracts in Advanced Robotics, Springer, 2011.

- [182] F. L. Hammond et al. “Towards a design optimization method for reducing the mechanical complexity of underactuated robotic hands”. In: *2012 IEEE International Conference on Robotics and Automation*. May 2012, pp. 2843–2850. DOI: 10.1109/ICRA.2012.6225010.
- [183] Lucia Seminara et al. “Active Haptic Perception in Robots: A Review”. In: *Frontiers in Neurorobotics* 13 (2019), p. 53. ISSN: 1662-5218. DOI: 10.3389/fnbot.2019.00053. URL: <https://www.frontiersin.org/article/10.3389/fnbot.2019.00053>.
- [184] J. Sitte and P. Winzer. “Mastering complexity in robot design”. In: *2004 IEEE/RSJ International Conference on Intelligent Robots and Systems (IROS) (IEEE Cat. No.04CH37566)*. Vol. 2. Sept. 2004, 1815–1819 vol.2. DOI: 10.1109/IROS.2004.1389660.
- [185] Joshua E Auerbach and Josh C. Bongard. “On the Relationship Between Environmental and Mechanical Complexity in Evolved Robots”. In: *The 2019 Conference on Artificial Life* 24 (2012), pp. 309–316. DOI: 10.1162/978-0-262-31050-5-ch041. eprint: <https://www.mitpressjournals.org/doi/pdf/10.1162/978-0-262-31050-5-ch041>. URL: <https://www.mitpressjournals.org/doi/abs/10.1162/978-0-262-31050-5-ch041>.
- [186] H.A. Bashir and V. Thomson. “Estimating design complexity”. In: *Journal of Engineering Design* (1999), pp. 247–257.
- [187] Jorge Angeles. *Rational Kinematics*. New York: Springer-Verlag, 1988.
- [188] Peter R. N. Childs. *Mechanical Design Engineering Handbook*. Oxford: Butterworth-Heinemann, 2014. ISBN: 978-0-08-097759-1.
- [189] Geoffrey Boothroyd. “Product design for manufacture and assembly”. In: *Computer-Aided Design* 26.7 (1994), pp. 505–520. ISSN: 0010-4485. DOI: [https://doi.org/10.1016/0010-4485\(94\)90082-5](https://doi.org/10.1016/0010-4485(94)90082-5). URL: <https://www.sciencedirect.com/science/article/pii/0010448594900825>.
- [190] Maria C. Yang. “A study of prototypes, design activity, and design outcome”. In: *Design Studies* 26.6 (2005), pp. 649–669. ISSN: 0142-694X. DOI: <https://doi.org/10.1016/j.destud.2005.04.005>. URL: <https://www.sciencedirect.com/science/article/pii/S0142694X0500030X>.
- [191] Daniel Glover. “Design considerations for space flight hardware”. In: 1990.
- [192] Hamdi Bashir and Vincent Thomson. “Estimating effort and time for design projects”. In: (Jan. 2001).
- [193] Francis Ysidro Edgeworth. *Mathematical Psychics*. McMaster University Archive for the History of Economic Thought, 1881. URL: <https://EconPapers.repec.org/RePEc:hay:hetboo:edgeworth1881>.
- [194] Vilfredo Pareto. *Manuale di Economia Politica*. Societa Editrice Libreria, 1906.
- [195] A. Charnes, W. W. Cooper, and R. O. Ferguson. “Optimal Estimation of Executive Compensation by Linear Programming”. In: *Management Science* 1.2 (1955), pp. 138–151. ISSN: 00251909, 15265501. URL: <http://www.jstor.org/stable/2627315>.

- [196] J. S. H. Kornbluth. “Engineering design: applications of goal programming and multiple objective linear and geometric programming”. In: *International Journal of Production Research* 24.4 (1986), pp. 945–953. DOI: 10.1080/00207548608919779. eprint: <https://doi.org/10.1080/00207548608919779>. URL: <https://doi.org/10.1080/00207548608919779>.
- [197] Alexandre Carvalho Leite. “On multi-objective optimization of planetary exploration rovers applied to ExoMars-type rovers”. In: *11th Symposium on Advanced Space Technologies in Robotics and Automation*. 2011. URL: <https://elib.dlr.de/70411/>.
- [198] Christophe Grand, Faiz Amar, and Philippe Bidaud. “Kinematic analysis and stability optimization of a reconfigurable legged-wheeled mini-rover”. In: (July 2002). DOI: 10.1117/12.474461.
- [199] Hans-Georg Beyer and Hans-Paul Schwefel. “Evolution strategies - A comprehensive introduction”. In: *Natural Computing* 1 (Mar. 2002), pp. 3–52. DOI: 10.1023/A:1015059928466.
- [200] K. Deb et al. “A fast and elitist multiobjective genetic algorithm: NSGA-II”. In: *IEEE Transactions on Evolutionary Computation* 6.2 (2002), pp. 182–197. DOI: 10.1109/4235.996017.
- [201] J. Blank and K. Deb. “pymoo: Multi-Objective Optimization in Python”. In: *IEEE Access* 8 (2020), pp. 89497–89509.
- [202] Hannah Lyness and Dimitrios Apostolopoulos. “A Modular Tracked Vehicle For Terramechanics Testing”. In: 2021.
- [203] Richard Brown. *Our new Unmanned Ground Vehicle takes on dangerous jobs*. Sept. 12, 2017. URL: <https://www.baesystems.com/en/article/our-new-unmanned-ground-vehicle-takes-on-dangerous-jobs> (visited on 06/28/2019).
- [204] Richard Brown. *Check Out the First Fully Modular Unmanned Ground Vehicle*. Feb. 17, 2016. URL: <https://www.inverse.com/article/11660-check-out-the-first-fully-modular-unmanned-ground-vehicle> (visited on 06/28/2019).
- [205] NIC Instruments. *ZEUS: The Ultimate Modular Robot*. URL: <http://www.nicltd.co.uk/zeus-ultimate-modular-unmanned-ground-vehicle/#ZEUS%20CONTENTS> (visited on 06/28/2019).
- [206] Adolphe Kegresse. “Motor-sledge”. US 1096815. May 12, 1914.
- [207] J. G. Hetherington and I. Littleton. “The Role of Mean Maximum Pressure in Specifying Cross-Country Mobility for Armoured Fighting Vehicle Design”. In: *Journal of Terramechanics* 24.4 (1987), pp. 263–280. URL: <https://www.sciencedirect.com/science/article/pii/0022489887900103> (visited on 08/19/2017).
- [208] *iRobot Announces Closing of Defense & Security Business Sale to Arlington Capital Partners*. Apr. 4, 2016. URL: <http://media.irobot.com/2016-04-04-iRobot-Announces-Closing-of-Defense-Security-Business-Sale-to-Arlington-Capital-Partners> (visited on 08/22/2018).

- [209] Frank Bottrill. “Improvements relating to Ped-rail Shoes for Heavy Road Vehicles”. GB 8844. Apr. 15, 1912. URL: https://worldwide.espacenet.com/publicationDetails/originalDocument?CC=GB&NR=191208844A&KC=A&FT=D&date=19121017&DB=EPODOC&locale=en_EP.
- [210] “Freak Vehicles for Air, Land, and Water”. In: *Popular Science Monthly* 123.3 (1933). Ed. by Raymond J. Brown, p. 96. URL: https://books.google.com/books?id=_CcDAAAAMBAJ&pg=PA96#v=onepage&q&f=false.
- [211] Roy A. Crop. “Wheeled vehicle convertible to crawler type”. US 2698667. Jan. 4, 1955.
- [212] Ross D. Farnsworth. “Convertible wheeled and tracked vehicle”. US 3500944. Mar. 17, 1970.
- [213] *Track N Go*. AD Boivin Inc. 2017. URL: <http://trucktracks.com/en/> (visited on 05/25/2017).
- [214] *Photos/Videos*. URL: <http://www.j-wheelz.com/gallery.html> (visited on 09/10/2018).
- [215] Dae-Young Lee et al. “Origami Wheel Transformer: A Variable-Diameter Wheel Drive Robot Using an Origami Struction”. In: *Soft Robotics* 4 (2 2017). URL: <https://www.liebertpub.com/doi/10.1089/soro.2016.0038>.
- [216] Brian Dodson. *Roadless wheel concept adjusts to all terrains*. Nov. 6, 2013. URL: <https://newatlas.com/roadless-adjustable-wheels-all-terrain/29607/> (visited on 05/24/2019).
- [217] Mohamad Alsalman et al. “Modeling of a variable diameter wheeled robot for traversing rough terrain”. In: *2016 IEEE International Conference on Advanced Intelligent Mechatronics (AIM)* (2016), pp. 745–750.
- [218] B. Eugene Daugherty. “Variable diameter pulley for a transmission”. US6152844A. May 10, 1999. URL: <https://patents.google.com/patent/US6152844A/en>.
- [219] B. Eugene Daugherty. “Gear-Cam Mechanism Of A Variable-Diameter Pulley”. US6152844A. Dec. 19, 2016. URL: <https://www.youtube.com/watch?v=qtZJ-skC2QQ>.
- [220] Noah R. Martin and Clayton E. Roby. “Spring-wheel”. US 1024091 A. Apr. 23, 1912.
- [221] Francois Hottebart. “Nonpneumatic deformable wheel”. US 6170544. Jan. 9, 2001.
- [222] Brian A. Russell. “Energy return wheel systems and methods”. US 6701985 B2. Mar. 9, 2004.
- [223] Avishay Novoplanski. “Deformable wheel assembly”. WO 2011092709 A2. Aug. 4, 2011.
- [224] *Mitas PneuTrac Ride and Drive*. Oct. 6, 2015. URL: <https://www.luminpdf.com/viewer/95ALm5W6MpojjspbSK> (visited on 05/27/2016).
- [225] Seok Ju Choi et al. “Airless Tire”. US 20140000777 A1. Jan. 2, 2014.
- [226] *Superelastic Tire*. NASA Glenn Research Center. URL: <https://nsts-prod.s3.amazonaws.com/t2p/prod/t2media/tops/pdf/LEW-TOPS-99.pdf> (visited on 09/03/2019).
- [227] Wayne Cunningham. *Goodyear debuts radical tire concept in Geneva*. Mar. 4, 2014. URL: <https://www.cnet.com/roadshow/news/goodyear-debuts-radical-tire-concept-in-geneva/> (visited on 05/28/2019).

- [228] *CTIS System*. Spicer Drivetrain Products, Dana Limited. URL: <http://spicerparts.com/products/ctis> (visited on 05/27/2016).
- [229] Phillip David Rodenbeck. “Magneto-rheological elastomer wheel assemblies with dynamic tire pressure control”. US 8176958 B2. May 15, 2012.
- [230] Mary A. Helmich. *State Styles - Not All Were Coaches*. 2008. URL: https://www.parks.ca.gov/?page_id=25449 (visited on 06/14/2020).
- [231] Jeff Barber. *Fox Live Valve is an Electronically Controlled Suspension System for Mountain Bikes*. Aug. 28, 2018. URL: <https://www.singletracks.com/mtb-gear/fox-live-valve-is-an-electronically-controlled-suspension-system-for-mountain-bikes/> (visited on 06/12/2020).
- [232] *FOX Live Valve technology meets the 2019 Ford F-150 Raptor*. 2020. URL: <https://www.ridefox.com/content.php?c=livevalve-raptor> (visited on 06/12/2020).
- [233] Guoying Xu et al. “Development and main research status of tracked vehicle suspension system”. In: 2017.
- [234] Eshcol S. Gross. “Stair climbing dolly”. US2515401A. Nov. 6, 1968. URL: <https://patents.google.com/patent/US3515401A/en>.
- [235] Ken Cox. *Development of a Wheelchair with Access for Most Users and Places*. 2014. URL: <https://www.resna.org/sites/default/files/conference/2014/Wheeled%5C%20Mobility/Cox.html> (visited on 07/23/2020).
- [236] Hankook Tire & Technology Group. *2016 Hankook Tire Design Innovation 'Connect to the Connector world'*. 2016. URL: <https://www.hankooktire.com/global/innovation.html> (visited on 05/24/2019).
- [237] Toshihiro Irie. *Unrolling the wheel*. Mar. 24, 2012. URL: <https://youtu.be/bC3B9xVtYRA> (visited on 09/10/2018).
- [238] C. Zheng and K. Lee. “WheeLeR: Wheel-Leg Reconfigurable Mechanism with Passive Gears for Mobile Robot Applications”. In: *2019 International Conference on Robotics and Automation (ICRA)*. 2019, pp. 9292–9298.
- [239] A. Kawakami et al. “SMC rover: planetary rover with transformable wheels”. In: *Proceedings of the 41st SICE Annual Conference. SICE 2002*. Vol. 1. Aug. 2002, 157–162 vol.1. DOI: 10.1109/SICE.2002.1195203.
- [240] Ken Nakagaki et al. “HERMITS: Dynamically Reconfiguring the Interactivity of Self-Propelled TUIs with Mechanical Shell Add-Ons”. In: *Proceedings of the 33rd Annual ACM Symposium on User Interface Software and Technology*. UIST '20. Virtual Event, USA: Association for Computing Machinery, 2020, pp. 882–896. ISBN: 9781450375146. DOI: 10.1145/3379337.3415831. URL: <https://doi.org/10.1145/3379337.3415831>.
- [241] Arthyr E. Benson. “Pneumatic Track”. US 32746811. May 22, 1956.
- [242] Walton W. Cushman. “Endless track and track assembly”. US 2867480. Jan. 6, 1959.
- [243] Giovanni Bonmartini. “Pneumatic tubular track, driving and carrying device”. US 3155436. Nov. 3, 1964.
- [244] *TTM-6901 GR*. NPO "Transport" Ltd. URL: <http://transport-ttm.com/en/production/ttm6901/?ItemID=1538> (visited on 06/13/2016).

- [245] Kubota Global. *U15-3 Kubota Mini-Excavator*. URL: https://www.kubota.com/products/machinery/in/en/pdf/U15_brochure.pdf (visited on 05/23/2019).
- [246] M. Wada and H. H. Asada. “Design and control of a variable footprint mechanism for holonomic omnidirectional vehicles and its application to wheelchairs”. In: *IEEE Transactions on Robotics and Automation* 15.6 (1999), pp. 978–989.
- [247] Mark Yim et al. “Modular Reconfigurable Robots in Space Applications”. In: *Auton. Robots* 14 (2003), pp. 225–237.
- [248] *IdealTrax Automatic Track Tensioning System*. 2018. URL: <https://www.gehl.com/idealtrax> (visited on 06/09/2020).
- [249] Chikyung Won. “Robotic platform”. US6431296B1. Mar. 27, 1998. URL: <https://patents.google.com/patent/US6431296B1/en>.
- [250] Pavlo E. Rudakevych. “Mobile robot vehicle”. US8074752B2. Dec. 9, 2008. URL: <https://patents.google.com/patent/US8074752>.
- [251] *Testudo UGV at AAD 2014*. Sept. 18, 2014. URL: https://www.armyrecognition.com/aad_2014_show_daily_news_coverage_report/new_testudo_ugv_unmanned_ground_vehicle_designed_for_reconnaissance_missions_at_aad_2014_1809145.html (visited on 08/22/2018).
- [252] Jinguo Liu et al. “Configuration representation of a link-type self-reconfigurable mobile robot”. In: *APCCAS 2008 - 2008 IEEE Asia Pacific Conference on Circuits and Systems*. Nov. 2008, pp. 737–740. DOI: 10.1109/APCCAS.2008.4746129.
- [253] B. Li et al. “AMOEBIA-I: A Shape-Shifting Modular Robot for Urban Search and Rescue”. In: *Advanced Robotics* 23.9 (2009), pp. 1057–1083. DOI: 10.1163/156855309X452485. eprint: <https://doi.org/10.1163/156855309X452485>. URL: <https://doi.org/10.1163/156855309X452485>.
- [254] Z. Guanghua, D. Zhicheng, and W. Wei. “Realization of a Modular Reconfigurable Robot for Rough Terrain”. In: *2006 International Conference on Mechatronics and Automation*. June 2006, pp. 289–294. DOI: 10.1109/ICMA.2006.257529.
- [255] Northrop Grumman Corporation. *Northrop Grumman Remotec - Robotic Platforms and Sub-Systems*. URL: <http://www.northropgrumman.com/Capabilities/Remotec/Pages/default.aspx> (visited on 05/24/2019).
- [256] *Our Story*. URL: <https://scewo.ch/en/about/> (visited on 07/23/2020).
- [257] Cody Underwood. *Robotic Warriors: The Viper*. Military.com. Aug. 23, 2017. URL: <http://www.military.com/video/logistics-and-supplies/military-equipment/robotic-warriors-the-viper/2625125923001> (visited on 06/28/2017).
- [258] Zirong Luo et al. “A reconfigurable hybrid wheel-track mobile robot based on Watt II six-bar linkage”. In: *Mechanism and Machine Theory* 128 (2018), pp. 16–32. ISSN: 0094-114X. DOI: <https://doi.org/10.1016/j.mechmachtheory.2018.04.020>. URL: <http://www.sciencedirect.com/science/article/pii/S0094114X17315227>.
- [259] Dan Laux and Jason Alef. *Tire to Track Transforming System*. PDF file. ISTVS 8th Americas Regional Conference, Detroit, MI, Sept. 12, 2016.

- [260] *Demonstrations of DARPA's Ground-X Vehicle Technologies*. DARPA. June 22, 2018. URL: <https://youtu.be/HrQrJ57J9eE> (visited on 08/07/2018).
- [261] “Queer, Quaint, and Curious: The Peramubulatinig Pedrail”. In: *The New York Times* (Feb. 7, 1904). URL: <https://timesmachine.nytimes.com/timesmachine/1904/02/07/120284033.pdf>.
- [262] Eric Krotkov et al. “The DARPA Robotics Challenge Finals: Results and Perspectives”. In: *Journal of Field Robotics* 34.2 (), pp. 229–240. DOI: 10.1002/rob.21683. eprint: <https://onlinelibrary.wiley.com/doi/pdf/10.1002/rob.21683>. URL: <https://onlinelibrary.wiley.com/doi/abs/10.1002/rob.21683>.
- [263] Erico Guizzo and Evan Ackerman. “How South Korea’s DRC-HUBO Robot Won the DARPA Robotics Challenge”. In: *IEEE Spectrum* (). URL: <https://spectrum.ieee.org/automaton/robotics/humanoids/how-kaist-drc-hubo-won-darpa-robotics-challenge>.
- [264] *Tartan Rescue Team*. URL: <https://www.nrec.ri.cmu.edu/solutions/defense/other-projects/tartan-rescue-team.html> (visited on 09/12/2018).
- [265] *Handle*. Boston Dynamics. 2018. URL: <https://www.bostondynamics.com/handle> (visited on 09/12/2018).
- [266] C. C. Phipps, B. E. Shores, and M. A. Minor. “Design and Quasi-Static Locomotion Analysis of the Rolling Disk Biped Hybrid Robot”. In: *IEEE Transactions on Robotics* 24.6 (Dec. 2008), pp. 1302–1314. ISSN: 1552-3098. DOI: 10.1109/TRO.2008.2007936.
- [267] C.C. Phipps and M. A. Minor. “Introducing the hex-a-ball, a hybrid locomotion terrain adaptive walking and rolling Robot”. English. In: *Proceedings of the 8th International Conference on Climbing and Walking Robots and the Support Technologies for Mobile Machines, CLAWAR 2005*. 2006, pp. 525–532. ISBN: 3540264132. DOI: 10.1007/3-540-26415-9-63.
- [268] Kåre Halverson. *MorpHex, the incredible hexapod robot!* Apr. 15, 2014. URL: <https://youtu.be/yn3FWb-vQQ4> (visited on 09/12/2018).
- [269] K. Togawa, M. Mori, and S. Hirose. “Study on three-dimensional active cord mechanism: development of ACM-R2”. In: *Proceedings. 2000 IEEE/RSJ International Conference on Intelligent Robots and Systems (IROS 2000) (Cat. No.00CH37113)*. Vol. 3. Oct. 2000, 2242–2247 vol.3. DOI: 10.1109/IROS.2000.895302.
- [270] M. Mori and S. Hirose. “Development of active cord mechanism ACM-R3 with agile 3D mobility”. In: *Proceedings 2001 IEEE/RSJ International Conference on Intelligent Robots and Systems. Expanding the Societal Role of Robotics in the the Next Millennium (Cat. No.01CH37180)*. Vol. 3. Oct. 2001, 1552–1557 vol.3. DOI: 10.1109/IROS.2001.977200.
- [271] Jimmy Sastra, Sachin Chitta, and Mark Yim. “Dynamic Rolling for a Modular Loop Robot”. In: *The International Journal of Robotics Research* 28.6 (2009), pp. 758–773. DOI: 10.1177/0278364908099463. eprint: <https://doi.org/10.1177/0278364908099463>. URL: <https://doi.org/10.1177/0278364908099463>.

- [272] A. Castano, W.-M. Shen, and P. Will. “CONRO: towards deployable robots with inter-robot metamorphic capabilities”. English. In: *Autonomous Robots* 8.3 (2000). cited By 156, pp. 309–324. ISSN: 09295593. DOI: 10.1023/A:1008985810481. URL: <https://www2.scopus.com/inward/record.uri?eid=2-s2.0-0034205625&doi=10.1023%2fA%3a1008985810481&partnerID=40&md5=c99419d07436564e7da1fd5da3298fd2>.
- [273] M. Yim, D. G. Duff, and K. D. Roufas. “PolyBot: a modular reconfigurable robot”. In: *Proceedings 2000 ICRA. Millennium Conference. IEEE International Conference on Robotics and Automation. Symposia Proceedings (Cat. No.00CH37065)*. Vol. 1. Apr. 2000, 514–520 vol.1. DOI: 10.1109/ROBOT.2000.844106.
- [274] Daniela Rus and Masette Vona. *Crystalline Robots: Self-reconfiguration with Compressible Unit Modules*. 2001.
- [275] A. Kamimura et al. “Distributed adaptive locomotion by a modular robotic system, M-TRAN II”. In: Jan. 2004, 2370–2377 vol.3. ISBN: 0-7803-8463-6. DOI: 10.1109/IROS.2004.1389763.
- [276] Graham Ryland and Harry Cheng. “Design of iMobot, an Intelligent Reconfigurable Mobile Robot with Novel Locomotion”. In: June 2010, pp. 60–65. DOI: 10.1109/ROBOT.2010.5509359.
- [277] V. Zykov et al. “Evolved and Designed Self-Reproducing Modular Robotics”. In: *Trans. Rob.* 23.2 (Apr. 2007), pp. 308–319. ISSN: 1552-3098. DOI: 10.1109/TRO.2007.894685. URL: <https://doi.org/10.1109/TRO.2007.894685>.
- [278] M.W. Jorgensen, E.H. Ostergaard, and H.H. Lund. “Modular ATRON: Modules for a self-reconfigurable robot”. In: vol. 2. Nov. 2004, 2068–2073 vol.2. DOI: 10.1109/IROS.2004.1389702.
- [279] A. Lyder, R. F. M. Garcia, and K. Stoy. “Mechanical design of odin, an extendable heterogeneous deformable modular robot”. In: *2008 IEEE/RSJ International Conference on Intelligent Robots and Systems*. Sept. 2008, pp. 883–888. DOI: 10.1109/IROS.2008.4650888.
- [280] Eiichi Yoshida et al. “Micro Self-reconfigurable Modular Robot Using Shape Memory Alloy”. In: *Journal of Robotics and Mechatronics* 13.2 (2001), pp. 212–219. DOI: 10.20965/jrm.2001.p0212.
- [281] Kyle Gilpin et al. “Miche: Modular Shape Formation by Self-Disassembly”. In: *The International Journal of Robotics Research* 27.3-4 (2008), pp. 345–372. DOI: 10.1177/0278364907085557. eprint: <https://doi.org/10.1177/0278364907085557>. URL: <https://doi.org/10.1177/0278364907085557>.
- [282] G. Endo and S. Hirose. “Study on Roller-Walker (system integration and basic experiments)”. In: *Proceedings 1999 IEEE International Conference on Robotics and Automation (Cat. No.99CH36288C)*. Vol. 3. 1999, 2032–2037 vol.3.
- [283] Mattracks. *2014 Mattracks Big Game Commercial*. Online video clip. YouTube, Jan. 29, 2014. URL: <https://www.youtube.com/watch?v=6zTxMwYM1tI> (visited on 06/03/2016).
- [284] DARPA Public Affairs. *GXV-T Revs up Research into Nimble, Faster, Smarter Armored Ground Vehicles*. DARPA.mil. U.S. Department of Defense. Apr. 26, 2016. URL: <http://www.darpa.mil/news-events/2016-04-26> (visited on 06/06/2016).

- [285] *SolidWorks*. 2020. URL: <https://www.solidworks.com/> (visited on 06/08/2020).
- [286] *What is Project Chrono*. 2019. URL: <http://projectchrono.org/about/> (visited on 06/08/2020).
- [287] *McMaster-Carr*. 2020. URL: <https://www.mcmaster.com/> (visited on 06/08/2020).
- [288] VEX Robotics. *VersaPlanetary Gearbox*. URL: <https://www.vexrobotics.com/versaplanetary.html> (visited on 07/18/2019).
- [289] *Andy Mark*. 2020. URL: <https://www.andymark.com/> (visited on 06/08/2020).
- [290] *SES 3D Models*. 2020. URL: <http://www.lynxmotion.com/s-5-ses-3d-models.aspx> (visited on 06/08/2020).
- [291] Arduino S.r.l. *Arduino Mega 2560 Rev3*. URL: https://store-usa.arduino.cc/products/arduino-mega-2560-rev3?gclid=CjwKCAjwgqejBhBAEiwAuWHioLqssrM5dqDR2U2SeVh1KUoqBHTGBcBTtozYoeGPd4P6NIL1CtP2eXR0CqBsQAvD_BwE (visited on 05/21/2023).
- [292] RobotShop. *RoboClaw 2x15A, 6-34VDC Regenerative Motor Controller*. 2019. URL: https://www.robotshop.com/en/roboclaw-2x15a-6-34vdc-regenerative-motor-controller.html?gclid=EAIaIQobChMIyq_0pZKK4wIVR0OGCh3q4QcOEAQYAiABEgJocfD_BwE.
- [293] Hao GONG, Jianhua LIU, and Huihua FENG. “Review on anti-loosening methods for threaded fasteners”. In: *Chinese Journal of Aeronautics* 35.2 (2022), pp. 47–61. ISSN: 1000-9361. DOI: <https://doi.org/10.1016/j.cja.2020.12.038>. URL: <https://www.sciencedirect.com/science/article/pii/S1000936120306063>.
- [294] Lily H. Shu and Woodie C. Flowers. “Application of a design-for-remanufacture framework to the selection of product life-cycle fastening and joining methods”. In: *Robotics and Computer-Integrated Manufacturing* 15.3 (1999), pp. 179–190. ISSN: 0736-5845. DOI: [https://doi.org/10.1016/S0736-5845\(98\)00032-5](https://doi.org/10.1016/S0736-5845(98)00032-5). URL: <https://www.sciencedirect.com/science/article/pii/S0736584598000325>.
- [295] K. Terzaghi. *Theoretical Soil Mechanics*. New York: John Wiley and Sons, 1943. URL: <https://onlinelibrary.wiley.com/doi/book/10.1002/9780470172766>.
- [296] Delta-T Devices Ltd. *SM150T Soil Moisture Sensor*. Webpage. URL: <https://www.delta-t.co.uk/product/sm150t-horticulture/>.
- [297] VIVOHOME *High Precision Electronic Digital Refrigerant Charging Weight Scale with Case for HVAC 220LB*. Webpage. URL: https://www.amazon.com/gp/product/B075NPMFGF/ref=ppx_yo_dt_b_asin_title_o05_s00?ie=UTF8&psc=1.
- [298] Deepti Kumari. *A STUDY ON THE EFFECT OF MOISTURE ON STRENGTH CHARACTERISTICS OF RIVER SAND*. Thesis. 2009. URL: <https://core.ac.uk/download/pdf/53187122.pdf>.

- [299] Rui He, Corina Sandu, and Javier E. Osorio. “Systematic tests for study of tire tractive performance on soft soil: Part I – Experimental data collection”. In: *Journal of Terramechanics* 85 (2019), pp. 59–76. ISSN: 0022-4898. DOI: <https://doi.org/10.1016/j.jterra.2019.07.004>. URL: <http://www.sciencedirect.com/science/article/pii/S002248981930103X>.
- [300] M-D Building Products. *SMARTTOOL 60CM (23-5/8in)*. Webpage. URL: <http://mddbbuildingproducts.com/product/smarttool-60cm-23-58/>.
- [301] Howie Choset and Philippe Pignon. “Coverage Path Planning: The Boustrophedon Cellular Decomposition”. In: 1998.
- [302] Jon Louis Bentley. “Programming pearls: algorithm design techniques”. In: *Communications of The ACM* 27 (1984), pp. 865–873.
- [303] Pololu Corporation. *19:1 Metal Gearmotor 37Dx68L mm with 64 CPR Encoder*. 2019. URL: <https://www.pololu.com/product/2822>.
- [304] Lynxmotion. *Lynxmotion Modular Track System*. 2019. URL: <http://www.lynxmotion.com/c-94-modular-track-system.aspx>.
- [305] *E2 Optical Kit Encoder*. 2020. URL: <https://www.usdigital.com/products/encoders/incremental/kit/E2> (visited on 05/21/2020).
- [306] Paul Malchodi. Private Communication. May 11, 2020.
- [307] Shastri Ram. *Semantic Segmentation for Terrain Roughness Estimation Using Data Autolabeled with a Custom Roughness Metric*. Thesis. 2018. URL: https://www.rti.cmu.edu/wp-content/uploads/2018/01/Shastri_Ram_Masters_of_Robotics_Thesis.pdf.